Characterization of Groundwater Flow in the Southeastern San Juan Basin:

Implications for Microbial Origins in the Deep Subsurface

Near Cerro Negro, New Mexico

By

Michelle A. Walvoord

Submitted in Partial Fulfillment of the Requirements for the

Master of Science Degree in Hydrology

New Mexico Institute of Mining and Technology

Socorro, New Mexico

**ABSTRACT**

Recent confirmation of microbial activity in deep (>50 m) subsurface environments has raised many questions concerning the origins of microorganisms in the subsurface, their in situ activities and resultant effects on groundwater geochemistry. The Cerro Negro Microbial Origins Project addressed some of these questions by investigating the present-day microbial activity of a Late Cretaceous 300 m deep sandstone-shale sequence adjacent to a volcanic neck in the southeastern San Juan Basin. The intrusion at Cerro Negro of basaltic magma at 3.39 Ma biologically sterilized a zone around the conduit, which has been subsequently re-colonized as shown by microbial assays. The presence of microbial activity within the thermal aureole supports the hypothesis that groundwater is capable of advecting microorganisms into new subsurface habitats.

The purpose of this study was to determine the present-day groundwater flow pattern and flow rates from the recharge area to Cerro Negro in order to constrain microbial transport rates and nutrient fluxes through the sedimentary layers. Watertable elevation, subsurface geology, $^{14}$C groundwater ages and information provided by a previous groundwater geochemical modeling study were used to develop a numerical groundwater flow model that simulates fluid and heat flow from the Mount Taylor – Mesa Chivato recharge area to Cerro Negro. The finite element cross-sectional model solved a system of coupled steady-state groundwater flow and heat transfer equations for a variable density fluid. The model was calibrated by comparing measured $^{14}$C ages of groundwater samples collected along the flowpath to calculated advective travel times of groundwater between recharge areas and sample well locations. The $^{14}$C age distribution, ranging

from modern to > 40kyr, could be reproduced only when hydraulic conductivity contrasts between lithologic units varied by no more than 2.5 orders of magnitude. This suggests that pervasive fracturing in the aquitards may be causing the hydrologic system to behave closer to isotropic than would be expected for a shale/sandstone sequence.

Groundwater modeling results demonstrate that groundwater flow rates (0.1 to 0.3 m/yr) were adequate to permit relatively rapid microbial re-colonization of the thermal aureole subsequent to the intrusion, and that the flux of limiting nutrients (particularly oxygen and other electron acceptors) by groundwater into the sampled area was relatively large. Modeling results and temperature data indicate a strong upward component of groundwater flow through sedimentary layers from the base of Mesa Chivato to the vicinity of Cerro Negro. Since there is no observable discharge in this region other than springs located just below the mesa, we hypothesize that the upward flux of groundwater reaches the very permeable drainageways containing alluvial valley fill, and then is efficiently drained laterally. Evidence of upward flow and high vertical shale hydraulic conductivities suggest considerable hydraulic connection between lithologic units, which influences the nutrient distribution in the sandstones, and may promote enhanced microbial activity near shale/sandstone interfaces.

## ACKNOWLEGMENTS

Bruce Bjornstad and Dr. Phil Long, as well as Dr. Bruce Hallett (now at Golder Federal

Associates) contributed to the understanding of the local geology of the study area

# TABLE OF CONTENTS

Page

## 3. PREVIOUS WORK COMPLETED ON THE CERRO

## NEGRO PROJECT…………………………………………. 22

## 4. HYDROGEOCHEMICAL AND ISOTOPIC

## CHARACTERIZATION…………………………………………...31

# LIST OF FIGURES

# LIST OF TABLES

# 1. INTRODUCTION

## 1.1. Background and Motivation for Subsurface Microbial Origins Study

Improved subsurface sampling techniques that avoid biological contamination have made it possible to verify that indigenous microorganisms live at depths ranging from tens to thousands of meters below the earth's surface (Ghiorse and Wilson, 1988; Madsen and Ghiorse, 1993; Haldeman *et al*., 1993;  Fredrickson *et al.*, 1991, 1995; Pedersen, 1993; Stevens *et al.*, 1993; Boone *et al.*, 1995).  Physical and chemical properties of the subsurface control the abundance and types of microorganisms present (Kieft *et al*., 1993, 1995; Chapelle, 1993; Madsen and Ghiorse, 1993; Fredrickson *et al*., 1989; Stevens and McKinley, 1995).  However, the question of the origin of these microorganisms remains open.

### 1.1.1.  Origin Theories

Two hypotheses, not mutually exclusive, have been proposed to explain the origins of subsurface microbes.  The in situ survival hypothesis submits that microorganisms have survived within subsurface rocks or sediments since the time of geologic deposition.  In other words, the microbes that are present today are the original inhabitants or their progeny.  The transport hypothesis proposes that subsurface microorganisms have been transported from the surface since the time of sediment deposition (Murphy *et al*., 1992).  The most reasonable mode of microbial transport in the subsurface is through groundwater advection.  Depending on past and present hydrogeological conditions, one

or both of these mechanisms may be responsible for sustaining microbial populations. A study site in which in situ survival or microbial transport can be constrained is necessary in order to test these hypotheses.

### 1.1.2. Sandstone – Shale Interface Theory

McMahon and Chapelle (1991) showed that diffusion of electron donors from fine-grained aquitard sediments into electron acceptor rich coarse-grained aquifers provides an environment near the aquitard/aquifer contact that is favorable to respiratory bacteria. Porewater geochemistries in shale and sandstones often differ. Shale, because of its relatively high organic content, is generally abundant in electron donors, such as organic acids, but limited in electron acceptors. Sandstone porewater is often abundant in electron acceptors such as sulfate, but limited in electron donors. McMahon and Chapelle (1991) have hypothesized that alternating shale and sandstone layers provide contrasts in electron acceptors and donors that are favorable for microbial metabolism and hence encourage high microbial activity near the lithologic interfaces. Sandstone/shale interfaces, which are *theoretically* limited in neither electron donors nor acceptors, should be sites of enhanced microbial activity (Figure 1).
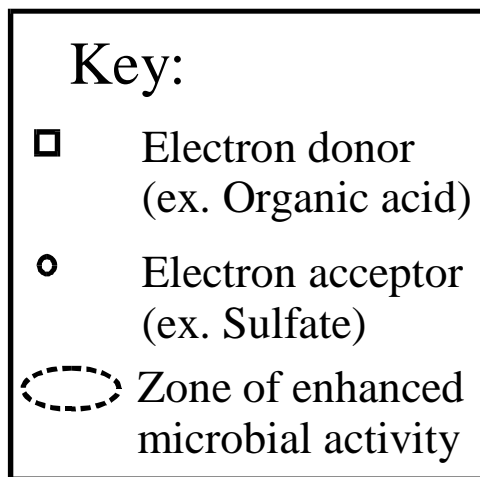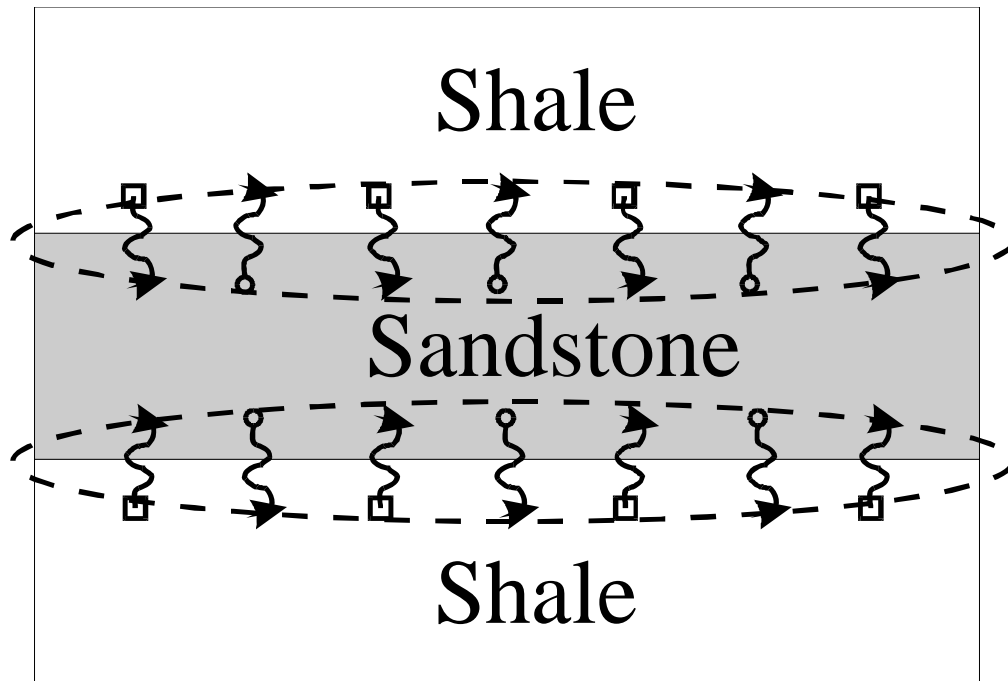
**Figure 1.** Schematic depiction of the shale/sandstone interface hypothesis. Concentration gradients drive the diffusion of electron donors available in shale porewater into the sandstone units, and the diffusion of electron acceptors abundant in sandstone porewater into the shales. (Concept adapted from McMahon and Chapelle 1991).

### 1.1.3. Cerro Negro Site Selection

The site chosen for study under the DOE Subsurface Science Program was a sequence of alternating Cretaceous sandstones and shales in the San Juan Basin of northwestern New Mexico that was intruded by a volcanic neck, Cerro Negro, at 3.39 Ma (Hallett *et al.*, 1997). The heat from volcanism biologically sterilized biologically sterilized sediments around the volcanic conduit. The geologic constraints associated with the volcanic intrusion provided a basis for evaluating the relative contributions of transport and in situ survival to the microbial community structure at this site. A microbial transport origin would be supported if microbes could be found in previously sterilized sediments near the intrusion. Alternatively, if microbes were absent near the intrusion, this would suggest that groundwater flow was not capable of sufficient microbial transport to recolonize the sterilized zone. An in situ survival origin would be supported by the existence of microbes exclusively outside of the paleo-thermal aureole. The study site also enabled examination of microbial abundance and activities at shale/sandstone interfaces.

It was initially expected that the small porethroats of the shales would inhibit transport of microorganisms back into the previously sterilized zone. Such a condition would allow the transport hypothesis to be eliminated as a possible mechanism of survival in this particular setting. Evidence of microbes in the shale units located outside of the paleo-
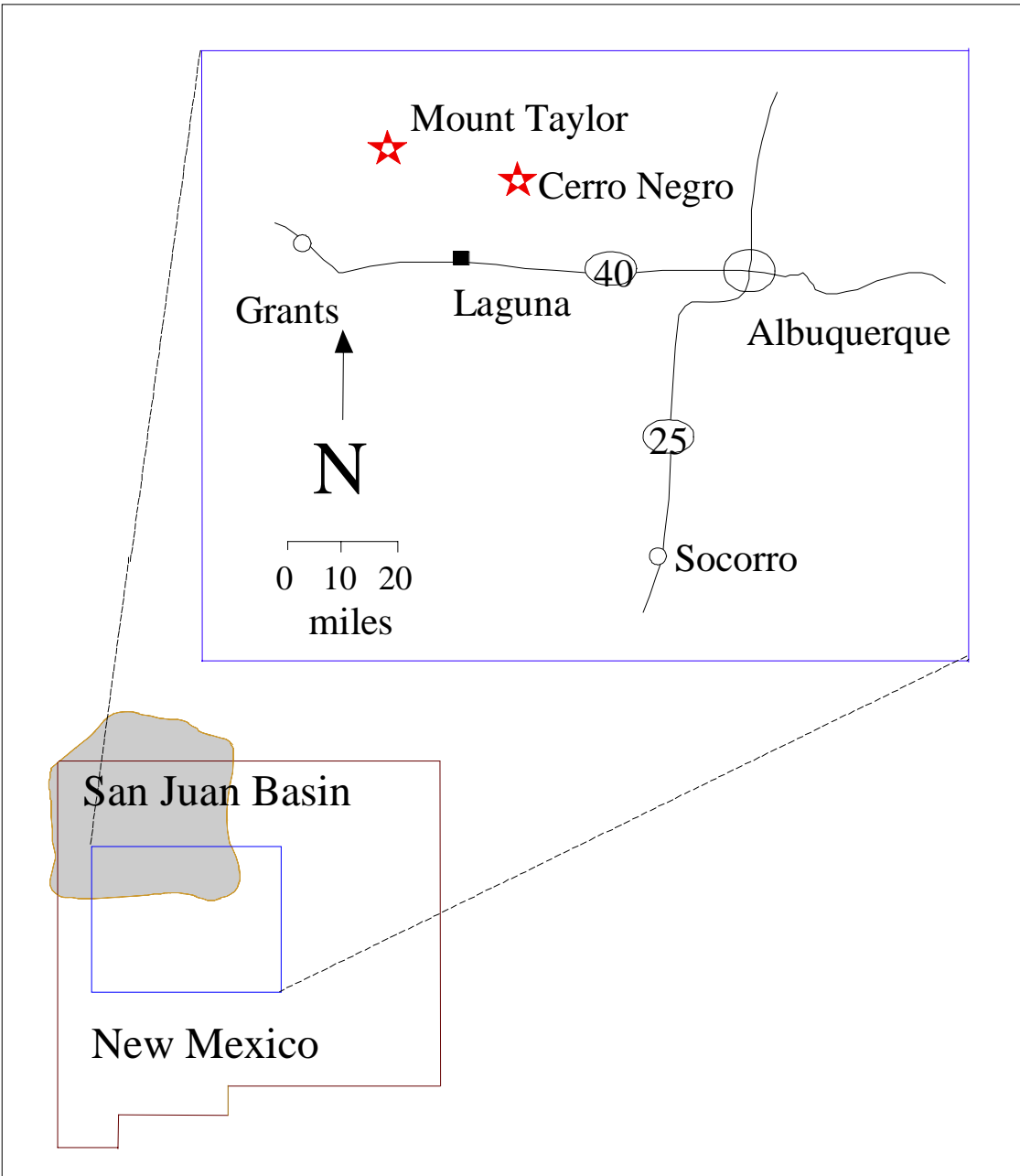
**Figure 2**. Location of study area in northwestern New Mexico.

thermal aureole would suggest that they, or their progeny, are the original inhabitants. However, it is now evident that the shale contains near-vertical fractures that could serve as conduits for relatively rapid advection of microorganisms. This precluded conclusive testing of the in situ hypothesis, since transport could not be ruled out for any region or subset within this particular geologic setting.

The sedimentary package intruded by Cerro Negro is an alternating shale/sandstone sequence. Therefore, the selected study site also enabled examination of microbial abundance and activities at shale/sandstone interfaces.

### 1.2. Purpose of Hydrogeologic Modeling Study

The objective of this study was to provide a hydrologic context for testing the microbial origins hypotheses and for understanding the cross-strata migration of nutrients. Regional and local groundwater flow patterns and flow rates can establish the potential for microbial transport and provide an estimate of nutrient fluxes. A combination of hydrologic, geochemical and microbiologic information is needed for determining the mechanisms controlling vertical nutrient distribution in alternating shale and sandstone layers, since these factors are closely linked.

The regional and local hydrologic regimes were characterized by evaluating water table elevation information and geochemical and isotopic data from groundwater samples in the study area. This information along with available information on aquifer/aquitard

hydraulic properties and subsurface geology were integrated to generate a 2-dimensional finite-element groundwater flow model. The hydrogeologic model served as a tool for better understanding both the regional and the local hydrology of the study site and also provided quantification of groundwater flow rates through specific shale and sandstone layers at various sections of the flow system.

## 2. SITE DESCRIPTION

### 2.1. Site Location

Cerro Negro is a volcanic neck in the southeastern San Juan Basin about 80 km west of Albuquerque, New Mexico (Figure 2).  The study area extends from Mount Taylor, a 3,470 m peak in northwestern New Mexico, to the vicinity of Cerro Negro.  Most field work was concentrated in an area immediately adjacent to the volcanic intrusion, that is located on the Cebolleta Land Grant.

### 2.2. Regional Geology

#### 2.2.1. Structure

The San Juan Basin is a Laramide structural depression located on the eastern margin of the Colorado Plateau that covers approximately 77,000 km$^2$ (Kelley, 1950;  Stone *et al.*, 1983).  Structures that bound the San Juan Basin include the following: the Puerco fault zone bounds the basin on the southeast;   the Nacimiento uplift (a Rocky- Mountain-type uplift that is not part of the Colorado Plateau) bounds the basin on the east; and the uplifts of the Colorado Plateau bound the basin to the south, west, north, and northeast (Woodward and Callender, 1977). Early Cenozoic folding followed by late Cenozoic fracturing and uplift resulted in minor deformation of strata in the southeastern San Juan Basin (Moench and Schlee, 1967).  Asymmetric deformation resulted in a steep northern

limb and a gently dipping southern limb (Woodward and Callender, 1977). Mesozoic sedimentary layers crop out at the basin edges, dipping 2° - 5° toward the structural center of the basin (Green and Pierson, 1977; Stone *et al.*, 1983) (Figure 3). Faults in this area are widely spaced and of small displacement (Moench and Schlee, 1967).

### 2.2.2. Stratigraphy

The stratigraphy of the study area is characterized by a layer-cake sedimentary sequence of alternating sandstones, limestones and shales of Cambrian to Tertiary age (Molenaar, 1977; Stone *et al.*, 1983). The sequence was deposited in fluvial, eolian, lacustrine and marine depositional environments (Green and Pierson, 1977). Figure 4 shows the age-layer sequence of San Juan Basin sediments. The sedimentary package reaches a maximum thickness of 4400 m near the structural center of the basin, and crops out at the edges of the basin (Figure 3), (Stone *et al*., 1983). Cenozoic basalt flows extending from Mount Taylor to Mesa Chivato cap the sedimentary sequence.
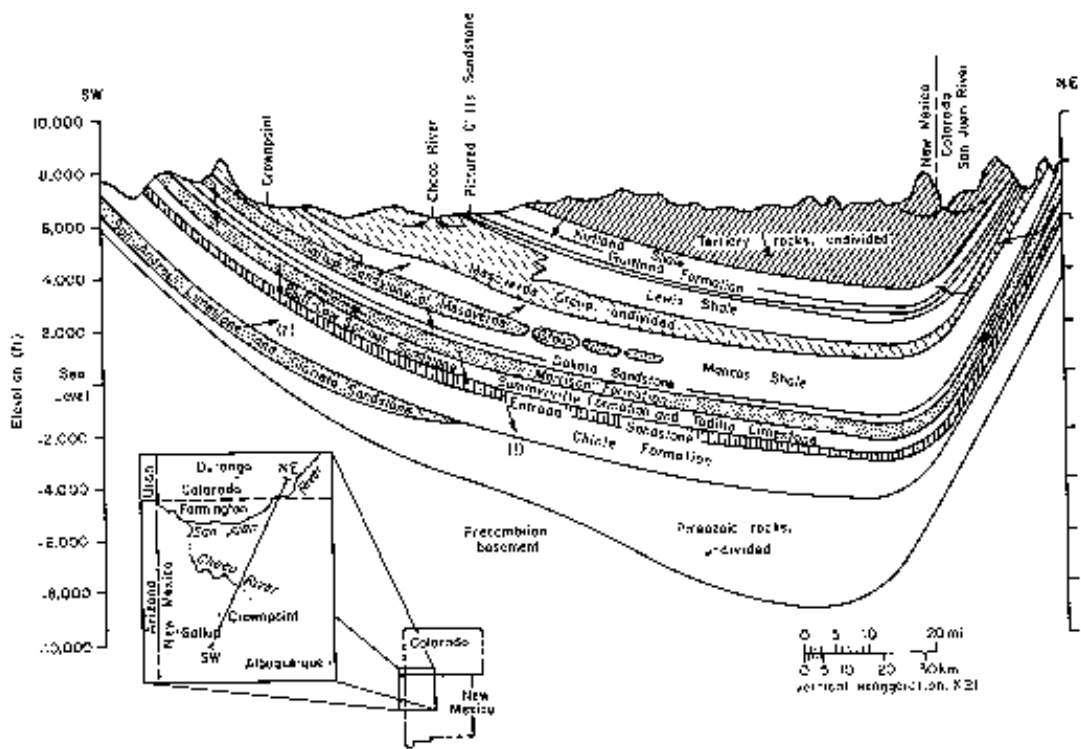
**Figure 3.** Geologic cross-section showing the generalized structure of the San Juan Basin (from Stone *et al*., 1983).
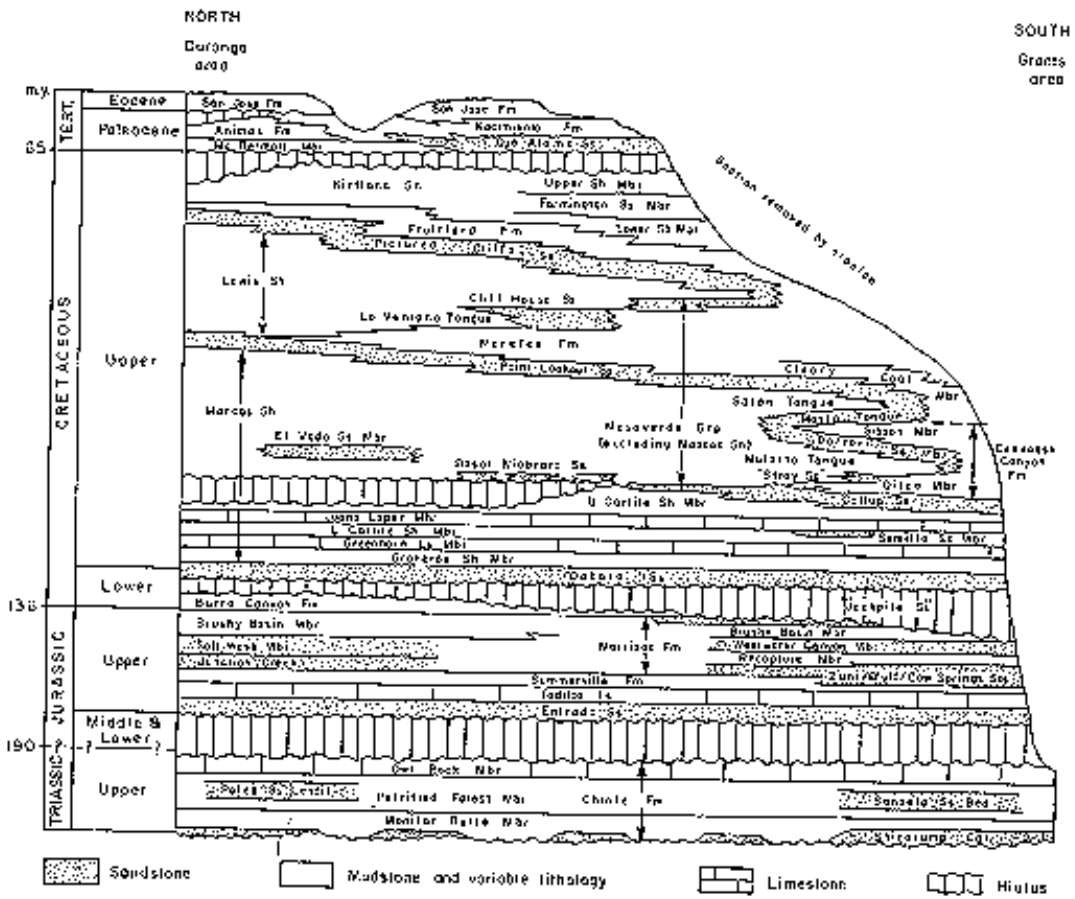
**Figure 4.** Stratigraphy of San Juan Basin sediments (from Stone *et al,*, 1983).

2.3. Local Geology

2.3.1.  Structure

The study area from Mount Taylor to Cerro Negro lies on the southeastern flanks of the
San Juan Basin.  Sedimentary layers in this region show a regional dip of about 2% to the
north-northwest (Schlee and Moench, 1963).

Schlee and Moench (1963) indicate several north to northeast trending normal faults
north of Cerro Negro, although very little displacement has been observed along these
faults.   A fracture-mapping study conducted in the vicinity of Cerro Negro indicated that
fracture frequency increased with distance toward the intrusion (P.E. Long, personal
communication, 1996).

2.3.2.  Stratigraphy

Hydrostratigraphic units of interest for this study consist of alluvium, sandstone, shale
and coal layers, and are continental, marginal-marine and deep-marine in origin (Green
and Pierson, 1977).  Total sediment thickness ranges from about 1450 m beneath Mount
Taylor's basaltic cap to about 1050 m eastward of the base of Mesa Chivato.

The Triassic Chinle Formation is the lower most sedimentary unit in this study area and
is composed of mudstone, sandstone, and limestone (Stone *et al*., 1983).   Paleozoic

sedimentary units underlie the Chinle Formation.

Above the Chinle Formation lies the Jurassic San Raphael Group (Green and Pierson, 1977). These Jurassic deposits in the San Juan Basin are generally eolian and lacustrine in origin (Green and Pierson, 1977). Members of the San Raphael Group present in the study area include the following, in ascending order: the Entrada Sandstone, the Todilto Limestone, the Summerville Formation, and the Bluff / Cow Springs Sandstones. The sandstones were deposited in an eolian environment under arid conditions (Stone *et al*., 1983).

Alternating periods of marine transgression and regression during the Late Jurassic – Late Cretaceous resulted in the deposition of an alternating sandstone/shale sequence (Stone, *et al*., 1983). Molenaar (1977) cites four or five major transgressions and regressions, as well as many minor ones, of a shallow seaway to the northeast during the Late Cretaceous. The Late Jurassic - Late Cretaceous marine sequence present in the study area extends from the Morrison Formation to the Point Lookout Sandstone. Lower shale and siltstone units include members of the late Jurassic Morrison Formation: the Brushy Basin Member and the Recapture Shale Member. The Westwater Canyon Sandstone Member of the Morrison Formation is also late Jurassic in age. Upper shale units, late Cretaceous in age, consist of the main body of the Mancos Shale and tongues of the Mancos shale (in ascending order): the Westwater Arroyo Shale Member, the Clay Mesa Shale Member the Mulatto Tongue, and the Satan Tongue. The Mancos shale comprises the bulk of marine deposits in the San Juan Basin (Molenaar, 1977). Late Cretaceous

sandstone units, in ascending order, include the following members of the Dakota Sandstone (in ascending order): the Oak Canyon Member, the Cubero Sandstone, the Paguate Sandstone and the Two Wells Sandstone.  Above the Dakota Sandstone units lie the following, in ascending order: the Gallup Sandstone, the Dalton Sandstone Member of the Crevasse Canyon Formation, the Hosta Tongue of the Point Lookout Sandstone, and the main body of the Point Lookout Sandstone.  Two coal units of the Crevasse Canyon Formation are also present in the Cretaceous sedimentary package: the Gibson Coal Member and the Dilco Coal Member.

Quaternary deposits in the San Juan Basin include alluvial valley fill and terrace deposits. All drainageways in the San Juan Basin contain alluvial deposits consisting of gravel, sand, silt and clay.  Alluvial deposits in the basin generally do not exceed thicknesses of 40 m (Stone *et al*., 1983).  The valley fill and terrace deposits form a disconformable contact with all underlying units.

### 2.3.3.  Volcanology

The Mount Taylor volcanic field is a part of a broad belt of late Cenozoic volcanism marking the transition between the Rio Grande Rift and the Colorado Plateau.  Volcanoes within the Mount Taylor volcanic field erupted from 4.49 to 2.05 Ma and overlap the 3.73 to 1.57 Ma volcanism observed at Mount Taylor (Hallett *et al*., 1997).

The Cerro Negro neck intruded the Mesozoic sedimentary strata at 3.39 ± 0.02 Ma, (Hallett *et al*., 1997). The elongate dike-like neck is one of the Rio Puerco necks within the Mount Taylor volcanic field. Cerro Negro consists of two plugs, three non-continuous dikes, and minor pyroclastic deposits that erupted through the sedimentary layers. These igneous features trend N5E. The northern peak, the larger of the two plugs, reaches an elevation of 2201 m, with an irregular basal diameter of approximately 38 m. The southern peak located about 122 m south of the larger plug, reaches an elevation of 2147 m, with a basal diameter of 30 m. Both plugs are composed of homogeneous, non-vesicular olivine basalt (Hallett, 1994).

## 2.4. Hydrology

### 2.4.1. Current Flow Regime

In general, groundwater in the San Juan Basin moves toward the basin center from recharge areas along the southern, northeastern, and western basin margins (Stone *et al.,* 1983). However, in the study area, the direction of flow is toward the basin margin due to the topographic high of Mount Taylor and the surrounding Mesa Chivato inward of the basin margin. A contoured water table elevation map was constructed using elevation measurements from 76 wells and 15 springs in the region. The water table configuration indicates that groundwater flow is generally outward from the peak of Mount Taylor. Groundwater moves in an east-southeast direction from the Mount Taylor highland area towards Cerro Negro (Figure 5). The hydraulic gradient is greatest at the edge of Mesa
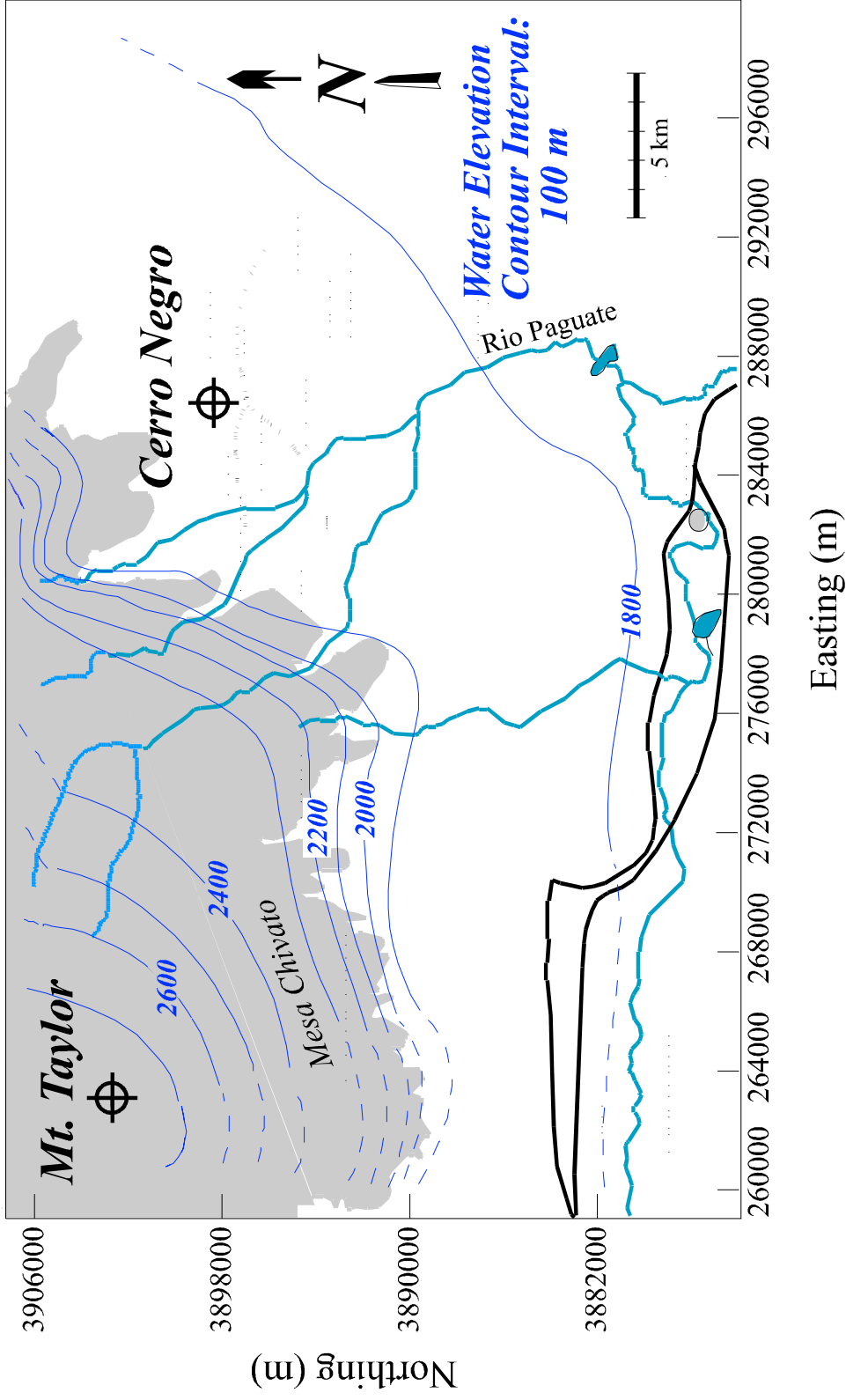
**Figure 5.** Potentiometric surface contour map constructed from available water table level measurements. In general, groundwater flows outward from the peak of Mount Taylor. Shaded area indicates the topotgraphic high of Mount Taylor and the surrounding mesa, Mesa Chivato

16

Chivato and is relatively flat in the vicinity of Cerro Negro. Depth of water varies greatly from >550 m beneath the peak of Mount Taylor to 25-70 m eastward of Mesa Chivato.

Recharge directly from precipitation occurs primarily in the topographically high regions. Runoff may provide another important source of groundwater input. Alluvial valley fill of ephemeral streams may act as a conduit for groundwater infiltration during periods of high precipitation (Brown, 1976). These ephemeral stream channels filled with alluvium are also the principal locations of discharge in some regions of the San Juan Basin (Stone et al., 1983). The alluvial cover usually conceals evidence of discharge, although Brown (1976) reported entire ephemeral stream channels covered with alkali deposits in Kiffen Canyon, NW New Mexico, further supporting the idea that these channels are discharge locations.

### 2.4.2. Hydrostratigraphy

The aquifers in the study region are comprised mainly of sandstone units with some siltstone interbeds. Alluvial deposits also act as aquifers in the region, with hydraulic conductivities >5 orders of magnitude higher than underlying sedimentary units. Shale layers are the major aquitards. Published hydrologic properties associated with each of the units represented in this study are reported in Table 1.

| Unit | Thickness (m) | Porosity (%) | Horizontal Hydraulic Conductivity (m/s) | Vertical Hydraulic Conductivity (m/s) |
|---|---|---|---|---|
| Alluvium | >40 | | $10^{-5} – 10^{-2}$ (5) | |
| Basalt | 0-545 | 10 (1) | $10^{-11} – 10^{-7}$ (1) | |
| Point Lookout Sandstone | 35-40 | 20 (2) | $3.2 \times 10^{-8}$ (5) | |
| Satan Tongue of the Mancos Shale | 5-10 | 12 (1) | | $10^{-13} – 10^{-9}$ (1) |
| Hosta Tongue of the Point Lookout SS | 27-35 | 12 (1) | $3.5 \times 10^{-8}$ (5) | |
| Gibson Coal Member of Crevasse Canyon | 92-118 | 20 (3) | $< 3.2 \times 10^{-7}$ (5) | |
| Dalton Sandstone Mb of Crevasse Canyon | 18-28 | 20 (1) | $3.2 \times 10^{-7}$ (5) | |
| Mulatto Tongue of the Mancos Shale | 68-89 | 12 (1) | | $1-5.9 \times 10^{-8}$ (9) |
| Dilco Coal Mb of Crevasse Canyon | 30-48 | 20 (3) | $< 3.2 \times 10^{-7}$ (5) | |
| Gallup Sandstone | 20-25 | 15 (1) | $9.1 \times 10^{-7}$ (5) | |
| Mancos Shale (main body) | 20-180 | 12 (4) | | $1.0 \times 10^{-10}$ (6) |
| Two Wells SS of the Dakota SS | 13-37 | 15 (4) | $< 1.3 \times 10^{-6}$ (5) $10^{-5} - 10^{-8}$ (7) | |

Parameter values obtained from: (1) *Domenico and Schwartz* [1990];   (2) Craigg [1980];   (3) *Freeze and Cherry* [1979];   (4) core sample measurements, Cheryl D. Gullett, PNNL, personal communication, 1995, (5) transmissivity values in *Stone et al.* [1983], (6) Stephens [1984], (7) Well tests near L-Bar Mine by Hydro-Engineering [1981], (8) SS in Brushy Basin Member by *Risser et al.* [1984], (9) Cl- tracer calculations, *Pegram* [1995], (10) *Ward et al*, [1982].

**Table 1.** Geologic units in the southeastern San Juan Basin and their associated thicknesses and hydraulic properties. SS - Sandstone; Sh - Shale; LS – Limestone; Mb - Member; Fm – Formation.

| Unit | Thickness (m) | Porosity (%) | Horizontal Hydraulic Conductivity (m/s) | Vertical Hydraulic Conductivity (m/s) |
|---|---|---|---|---|
| Whitewater Arroyo Shale of the Mancos Shale | 20-25 | 9 (4) | | $10^{-13} – 10^{-9}$ (1) |
| Paguate Sandstone of the Dakota SS | 20-22 | 8.5 (4) | $< 1.3 \times 10^{-6}$ (5) | |
| Clay Mesa Shale of Mancos Shale | 8-15 | 10 (1) | | $10^{-13} – 10^{-9}$ (1) |
| Cubero SS and Oak Canyon Mb of the Dakota SS | 43-48 | 15 (4) | $< 1.3 \times 10^{-6}$ (5) | |
| Brushy Basin Mb of the Morrison Fm | 52-60 | 10 (1) | $1.2 \times 10^{-6}$ (8) | $10^{-13} – 10^{-9}$ (1) $10^{-12} – 10^{-10}$ (10) |
| Westwater Canyon SS Mb of the Morrison Fm | 62-68 | 20 (1) | $< 2.7 \times 10^{-6}$ (5) $3.2 \times 10^{-7} – 5.8 \times 10^{-6}$ (10) | |
| Recapture Shale Mb of the Morrison Fm | 175-218 | 10 (1) | | $10^{-13} – 10^{-9}$ (1) |
| Bluff – Cow Springs SS, Summerville Fm, Todilto LS, and Entrada SS | 158-163 | 15 (1) | $4.0 \times 10^{-6}$ (5) | |
| Chinle Formation | 330-440 | 12 (1) | $1.9 \times 10^{-8}$ (5) | $10^{-12}$ (10) |

Parameter values obtained from: (1) *Domenico and Schwartz* [1990]; (2) *Craigg* [1980]; (3) *Freeze and Cherry* [1979]; (4) core sample measurements, Cheryl D. Gullett, PNNL, personal communication, 1995, (5) transmissivity values in *Stone et al*. [1983], (6) *Stephens* [1984], (7) Well tests near L-Bar Mine by Hydro-Engineering [1981], (8) SS in Brushy Basin Member by *Risser et al*. [1984], (9) Cl- tracer calculations, *Pegram* [1995], (10) *Ward et al*, [1982].

**Table 1.** (continued) Geologic units in the southeastern San Juan Basin and their associated thicknesses and hydraulic properties. SS - Sandstone; Sh - Shale; LS – Limestone; Mb - Member; Fm – Formation.

### 2.4.3.  Paleo-flow Regime

The scope of the hydrogeologic study was limited to present-day observations and interpretations, due to the minimal data available for paleo-reconstruction.  The current hydrogeologic regime described and modeled as part of this study is probably not entirely reflective of the hydrogeologic flow regime at the time of microbial re-colonization of the thermal aureole around Cerro Negro.  Volcanic activity on Mount Taylor and within the Mount Taylor volcanic field from 4.5 to 1.5 Ma (Hallett *et al.,* 1997;  Perry *et al*., 1990) would have continuously modified the hydrologic regime.  Volcanism would have affected at least three main factors that influence the hydrologic regime: structural controls, topography, and thermal conditions.  Based on the fact that little displacement is observed along faults in the area, it is reasonable to assume that structural control has had little influence on altering the groundwater flow regime.  However, the other two variables, topography and thermal conditions, may have had a profound effect on altering the hydrologic regime in the past 5 million years.  Without completing an extensive reconstruction of the these factors at the time of the Cerro Negro intrusion through the present, it is impossible to precisely characterize the paleohydrology.

Prior to 4.5 Ma, (the onset of Mount Taylor volcanism), the groundwater flow direction in the vicinity of Cerro Negro was probably to the northwest, toward the structural center of the San Juan Basin.  The rationale behind that supposition stems from the present observation that groundwater in the San Juan Basin flows toward the center on the regional scale (Stone *et al*., 1983).  As volcanism on Mount Taylor proceeded, significant

topographic relief was created and a localized flow field presumably developed. The newly created topography established a groundwater flow pattern radiating from Mount Taylor, similar to that presently observed although initially more subdued. It is likely that the groundwater flow pattern in the study area existent when Cerro Negro intruded, 3.39 Ma, was relatively similar to the current pattern, although flow rates may have differed by an order of magnitude or more. As volcanism continued and topographic relief (and consequently, water table relief) of Mount Taylor and Mesa Chivato increased, the hydraulic gradient would have also increased. It is probable that groundwater flow rates were at a maximum shortly after the last major volcanic events occurred, about 1.5 Ma, and have gradually decreased due to continued erosion that has reduced the topographic relief and consequently, the hydraulic gradient.

Yet another unconstrained parameter influencing the paleo-flow regime is climate change. Variation in the amount of precipitation and evapotranspiration through time has undoubtedly had an effect on the regional hydraulic gradient and consequently, on the flow rates through the sedimentary layers. A shift to a more arid climate in the Holocene in the San Juan Basin (Phillips *et al.,* 1986; Stute *et al*., 1995) has probably lowered water table elevations and effectively subdued the water table configuration resulting in lower groundwater flow rates. However, based on the extreme topographic control of the Mount Taylor/ Mesa Chivato on recharge, groundwater flow patterns have probably not varied appreciably in response to Quaternary climate change.

# 3. PREVIOUS WORK COMPLETED ON THE CERRO NEGRO PROJECT

Investigation at the Cerro Negro site began at the end of summer 1994. Field methods included subsurface drilling, sediment and groundwater sample collection, field geology characterization, fracture mapping and temperature profiling. Laboratory methods included geochemical, isotopic, petrographic, geothermochronological and microbiological analyses on sediment samples and geochemical and isotopic analyses on groundwater samples. Analyses completed by various investigators under the Cerro Negro Microbial Origins Project are listed in Appendix A.

## 3.1. Drilling Effort

Boreholes were drilled using a rotary method similar to that described by Colwell *et al.* (1992), and cores were collected for microbiological, lithologic, geochemical and isotopic analyses from two locations near Cerro Negro (Figure 6). A brief description of lithologic characteristics and depositional environment for each unit encountered in drilling is given in Table 2. The first drilling location, 1200 m southwest of the main plug, was intended to be far enough away from the volcanic neck that the strata would have been unaffected by the heat from volcanism. Two vertical boreholes (CNV and CNV-R) were drilled at this location reaching depths of 205.2 m and 232.5 m. Another borehole (CNA-R) was drilled 450 m southwest of the intrusion at an approximately 30° angle (ending at about a 45° angle) toward the intrusive body and reached a depth of 297 m. This borehole was intended to sample along the thermal gradient through
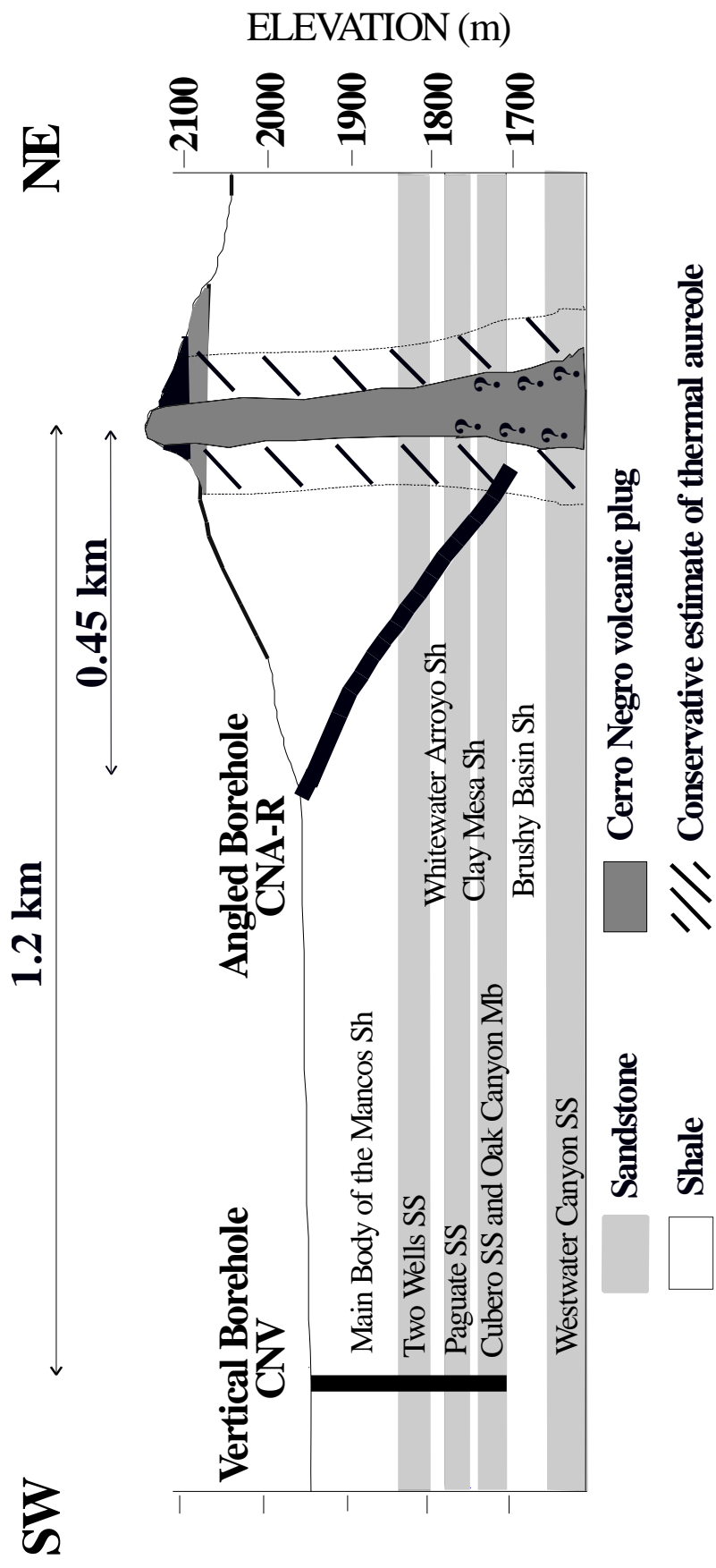
**Figure 6.** Schematic depiction of drilling completed near the Cerro Negro volcanic neck.

| Unit | Depositional environment | Lithology | Degree of sorting | Calcite cementation |
|---|---|---|---|---|
| Mancos Shale | Marine, transgressive; on or near edge of continental shelf | Mudstone/ claystone | Very well-sorted | Moderate – strong |
| Two Wells Sandstone | Marine, regressive; off-shore, shallow-water marine shelf | Fine to very fine-grained sandstone | Very well-sorted | Moderate – strong |
| Whitewater Arroyo Shale | Marine, transgressive; shallow-water marine shelf | Mudstone/ claystone/ siltstone | Well- sorted | Moderate-strong |
| Paguate Sandstone | Marine, regressive; open-marine shelf and nearshore | Sandstone/ mudstone | Very well-sorted | Weak –strong |
| Clay Mesa Shale | Marine, transgressive; open-marine shelf and nearshore | Siltstone/ mudstone/ claystone | Very well-sorted | Moderate |
| Cubero Sandstone | Marine, regressive; deeper-shallower nearshore | Medium-grained quartz sandstone | Very well-sorted, coarsening upward | Weak – moderate |
| Oak Canyon Member | Terrestrial and marine; (drilled section represents only upper marine, transgressive unit – open-marine to nearshore) | Sandstone, some mudstone | Very well-sorted | Moderate |
| Morrison Formation | Terrestrial, braided-stream | Sandstone, siltstone | Moderately sorted | Moderate |

**Table 2.** Depositional environment and lithologic description of geologic units encountered in the CNV and CNA-R boreholes.

the paleo-thermal aureole produced by the intrusion, while intersecting both shale and sandstone strata. The angled borehole did not intersect the main body of the plug but did penetrate four small (< 1m diameter) basaltic dikes suggesting that the main intrusive body was close.

## 3.2. Microbiology Sampling Strategy

Core samples were collected with disinfected spoon samplers. Immediately after coring and retrieval within disinfected Lexan liners, cores were transferred into an argon-filled glove box. Subcores were collected using aspetic techniques (Fredrickson and Phelps, 1992) from the interior of the rock cores in order to avoid possible contamination from the core periphery. Solute tracers (bromide and a prefluorinated hydrocarbon) and a particulate tracer (carboxlated, fluorescent, 1μm-diameter microbeads) were used in drilling fluids, as described by Phelps *et al.* (1989), Colwell *et al.* (1992), and McKinley and Colwell (1996) to detect contamination in samples collected for microbial analysis. The criterion for subcore acceptance was a minimum 1000-fold decrease in concentrations of tracers between parings and subcore. Existence of higher amounts of tracers in the subcore indicated possible contamination from drilling fluid. Sixty-five samples were taken from the cores for microbial analysis. 18 samples were taken from shale units and 47 were taken from sandstone units.

## 3.3. Microbiological Analyses

Evidence of microbial activity ($^{14}$C acetate mineralization and $^{35}$S sulfate reduction) was detected throughout both boreholes (Fredrickson *et al.*, 1997) (Figure 7). The methodologies used for measuring $^{14}$C-labeled acetate microbial mineralization and $^{35}$S
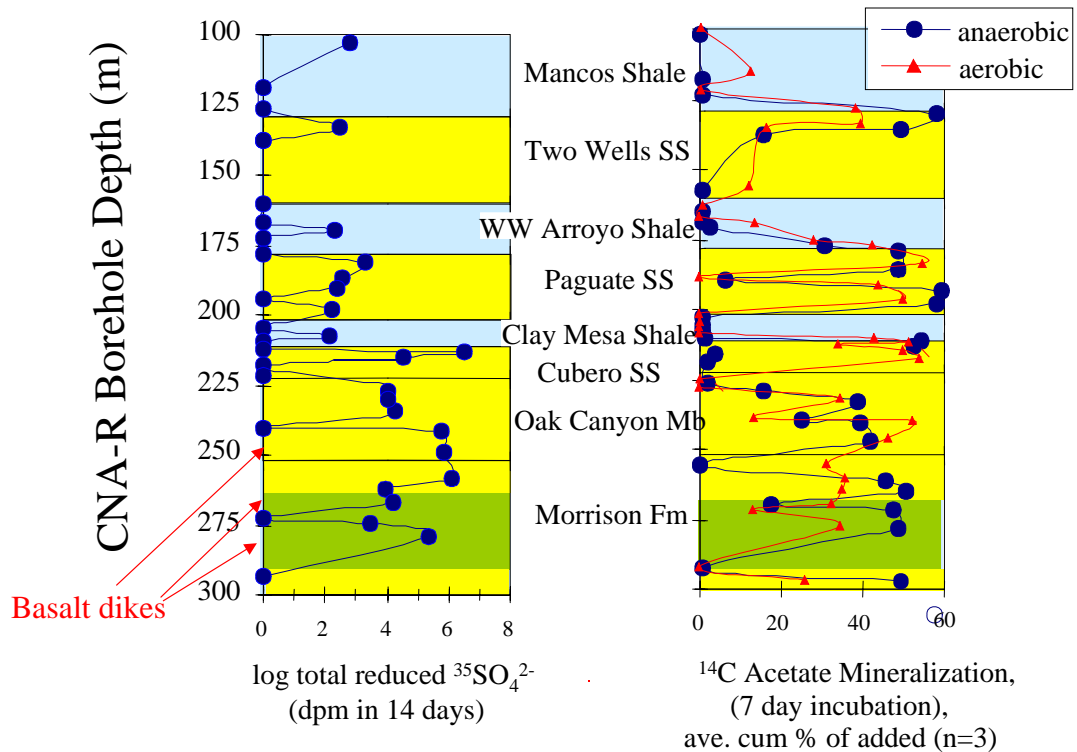
**Figure 7.** Microbial activity measurements (total reduced $^{35}SO_4^{2-}$ and $^{14}C$ mineralization) with depth in the CNA-R borehole. The locations of basalt stringers are noted. Sandstone units are yellow. Siltstone unit is in green. Shale units are blue. In general, higher activities were observed near the shale/sandstone interfaces. Total reduced $^{35}SO_4^{2-}$ and $^{14}C$ mineralization measurements (not shown here) taken from the vertical borehole showed similar trends although activities, in general, were lower.

sulfate reduction are provided in Appendix B. Although microbial activity was not detected in all samples, measurable activities were detected in samples located immediately adjacent to basaltic stringers. There were no trend in microbial activities with increasing proximity to the intrusion. The major pattern observed was increased microbial activity near the shale/sandstone interfaces. Also, the frequency of samples with detectable microbial activities, as well as their magnitude, was higher in the sandstones than in the shales.

Contrary to original expectations, microbial activity was detected in some shale samples collected near the intrusion, suggesting the importance of microbial transport through fractures. Fredrickson *et al*., (1997) found little-to-no microbial activity in intact, unfractured shale samples and high rates in material with a significant fraction of porethroat diameters >0.2 μm, which emphasized that porethroat size has an important influence on microbial survival.

### 3.4. Paleothermometry Study

Investigation of the origins hypotheses at the Cerro Negro site was based on the assumption that sediments near the volcanic neck were heated to sufficient temperatures to kill all microorganisms. A generally accepted upper limit for microbial survival in the deep subsurface is approximately 110°C (Stetter *et al.,* 1990), although some microbiologists speculate that the actual upper limit may be closer to 150°C (Deming and Baross, 1993). Many independent paleothermometry analyses were completed, using

samples from the angled and vertical (control) boreholes, to constrain the thermal history of the sediments surrounding the intrusion. Despite this effort, the paleothermal regime was not well-constrained. The results from illite/smectite ratios, sterane ratios, and fluid inclusions suggested that paleotemperatures of >90°C did not persist for any significant length of time on a geologic scale (Gao *et al*., 1995). Such temperatures (75-90°C) are on par with temperatures the Cretaceous sediment package would have attained under typical geothermal conditions at its estimated maximum burial depth (Molenaar, 1983). Thus, no evidence of a heating event was observed. In contrast, vitrinite reflectance data indicated that paleotemperatures reached 200°C in both the angled borehole (CNA-R) as well as the vertical borehole (CNV) (Gao *et al.,* 1995). Also, fission track analyses on zircons and apatite in the sandstones showed evidence of a prior heating event in samples located up to 50 m away from the main intrusive body. A precise time-temperature history could not be obtained due to the sparsness and poor quality of reworked apatite and zircon grains (see Appendix C). The apparent discrepancy in the paleothermometry data may be explained by the variation in time sensitivity among the measured paleothermometers. Vitinite reflectance does not require as lengthy sustained periods of heating to record a thermal pulse as do the other paleothermometers. Therefore, one explanation for the apparent discrepancy in the paleothermometry data is that the volcanic intrusion produced a relatively short thermal pulse that was rapidly dissipated. It is reasonable that the heat generated by the intrusion was transferred proportionally more through forced convection in the sandstones and conduction in the shales. Convection is a more efficient heat transfer process. A significant amount of heat transfer by convection would serve to expand the spatial extent of thermal alteration

(especially in the sandstones) and decrease the duration of the heating event, as compared to a conduction-only heat transfer.  In the proposed convection-dominated  scenario, the duration of the heating event may not suffice to alter the thermal signatures of many paleothermal indicators.

### 3.5.  Groundwater Geochemical and Isotopic Study

Groundwater samples were collected from 11 wells (Figure 8) from the recharge area to the vicinity of Cerro Negro and analyzed for ion chemistry, dissolved carbon (inorganic and organic), iron redox species, $^{14}C$, $\delta^{13}C$, $\delta^{18}O$, $\delta D$, and tritium as part of the study by Pegram (1995).  Sampled wells included available domestic, irrigation and livestock wells, and the vertical borehole drilled as part of this study.  Well information is provided in Table 3.   Description of methods, results and identification of the dominant geochemical processes using geochemical modeling are presented in detail in Pegram (1995) and briefly summarized in the following section of this paper.

| Sample name | Date sampled | UTM Coordinates Easting (m) | Northing (m) | Surface Elevation (m) | Water table Elevation (m) | Depth Interval (m bgs) | Screened Unit |
|---|---|---|---|---|---|---|---|
| Presbyterian | 10-94 | 275625 | 3895975 | 2328.7 | NA | NA | Pt. Lookout SS |
| Elkins | 10-94 | 275725 | 3895975 | 2359.7 | 2334.1 | 25.6-36.0 | Pt. Lookout SS |
| Bibo | 10-94 | 281429 | 3895320 | 1938.5 | 1879 | 126.5-137.2 | PaguateSs |
| Seboyeta | 10-94 | 282401 | 3898401 | 1969.0 | 1870 | 207.3-231.6 | Cubero Ss |
| Moquino | 10-94 | 284088 | 3894708 | 1891.9 | 1830.9 | 118.9-167.6 | Westwater Ss |
| CNV-W2 | 7-94 | 285438 | 3897475 | 1937.0 | 1875.4 | 139.0-144.8 | Two Wells Ss |
| CNV-W3 | 7-94 | 285438 | 3897475 | 1937.0 | 1875.4 | 194.0-199.3 | Cubero Ss |
| CNV-W5 | 7-94 | 285438 | 3897475 | 1937.0 | 1875.4 | 159.0-164.2 | Paguate Ss |
| MW-64 | 5-94 | 386500 | 3896415 | 1895.8 | 1865.9 | 45.2-57.4 | Two Wells Ss |
| MW-65 | 5-94 | 386500 | 3896750 | 1912.7 | 1866.7 | 65.7-78.5 | Two Wells Ss |
| MW-60 | 5-94 | 286650 | 3896575 | 1902.0 | 1864.5 | 51.8-64.0 | Two Wells Ss |
| MW-68 | 5-94 | 286875 | 3896975 | 1933.1 | 1865.5 | 88.3-100.5 | Two Wells Ss |
| L-Bar | 10-94 | 288339 | 3896638 | 1875.7 | 1860 | NA | Morrison Fm |

bgs = below ground surface; NA = information not available
**Table 3.**  Sampled well information.
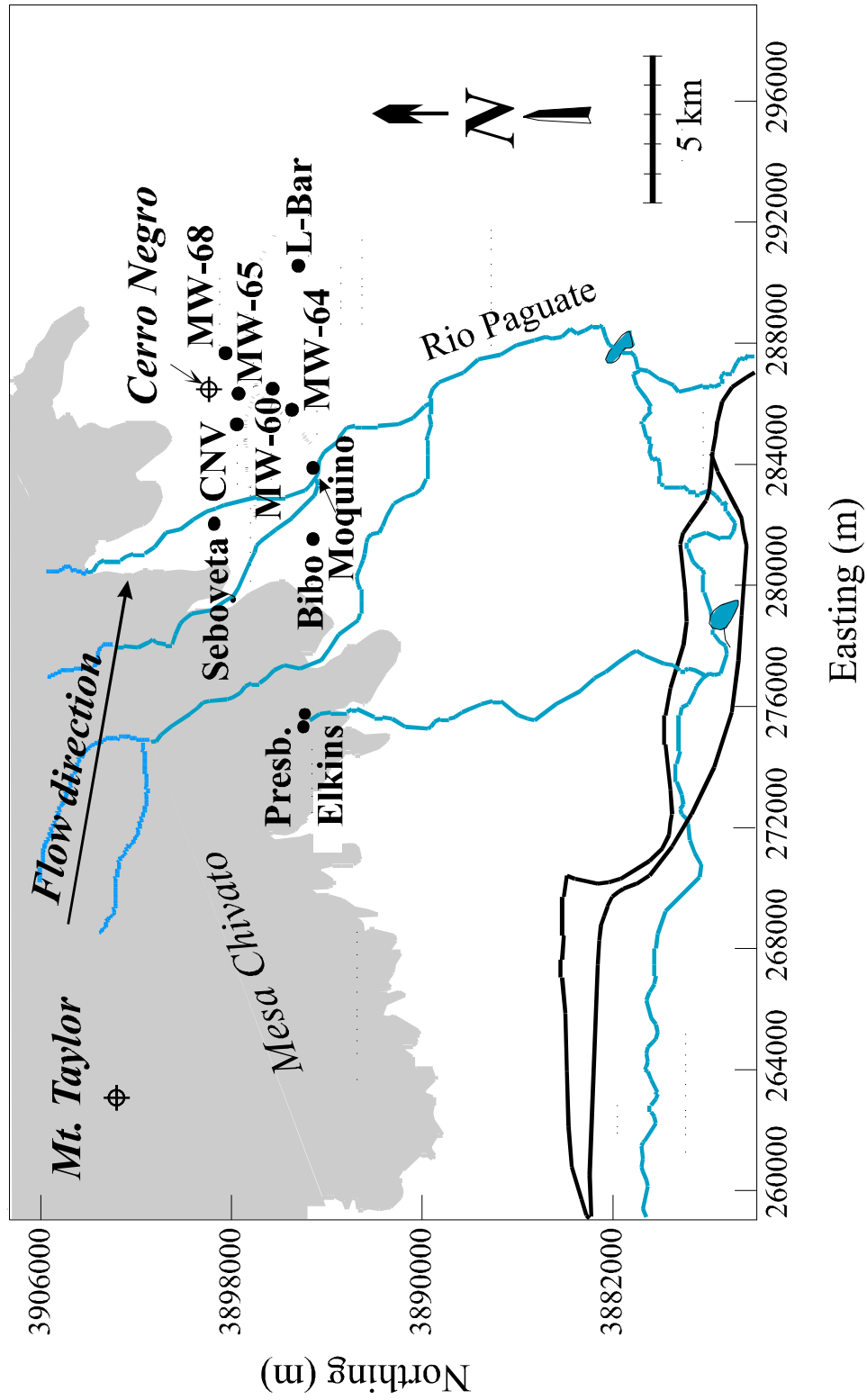
**Figure 8.** Location of wells used in Pegram's (1995) groundwater isotopic and geochemical study.

# 4.  GROUNDWATER CHARACTERIZATION

Table 4 provides a summary of geochemical and isotopic data from groundwater samples collected from wells indicated in Figure 8 (Pegram, 1995).

## 4.1.  Geochemical Modeling

Pegram (1995) used the isotopic and geochemical model NETPATH (Plummer *et al.*, 1994), which simulates thermodynamically-constrained mass transfers of solutes, to elucidate the geochemical evolution of the groundwater and to calculate groundwater ages for each sample from the corresponding DIC, $^{14}C$ activity and $\delta^{13}C$ values. The geochemistry and isotopic signature of the sample collected from the Presbyterian well was assumed to be representative of "initial" or recharge water and was compared to the water chemistry of each sample collected from downgradient wells.   For detailed descriptions of the geochemical modeling procedure and results, refer to Pegram, 1995.

In general, the NETPATH model indicated that calcite is the main source of carbon along groundwater flowpaths.  Precipitation of dolomite is a minor sink for carbon (except in two cases where small amounts dissolve).  The dissolution of large amounts of calcite forces precipitation of dolomite and gypsum (in most cases).  Ion exchange between $Ca^{2+}$ and $Na^+$ provides the driving force for calcium dissolution.  Ion exchange removes calcium and forces calcite in the aquifer matrix to dissolve (Pegram, 1995)

| Well | Presbyterian | Elkins | Bibo | Seboyeta | Moquino | CNV-W2 |
|---|---|---|---|---|---|---|
| Date sampled | 10/27/94 | 10/27/94 | 10/5/94 | 10/5/94 | 10/5/94 | 7/17/94 |
| Temp (C) | 12.48 | 16.02 | 19.74 | 22.9 | 17.7 | 20* |
| DO (mg/L) | 6.87 | 5.91 | 0.62 | 0 | 0.05 | 0.2 |
| Cond. (mS/cm) | 0.17 | 0.132 | 0.839 | 0.311 | 0.604 | 0.93 |
| pH (log units) | 7.27 | 7.81 | 8.05 | 7.94 | 8.59 | 8.26 |
| Eh (mV) | 395 | 229 | 273 | -25 | -8 | 282 |
| | | | | | | |
| F | 0.17 | 0.19 | 1.03 | 0.23 | 1.57 | 1.85 |
| Cl | 2.73 | 2.96 | 15 | 7.75 | 4.07 | 13.88 |
| $NO_2$ | <0.01 | <0.01 | <0.03 | <0.03 | <0.03 | <0.03 |
| Br | 0.05 | 0.03 | <0.02 | 0.03 | <0.02 | 0.06 |
| $NO_3$ | 0.86 | 1.21 | 0.22 | 0.12 | <0.02 | 1.27 |
| $PO_4$ | 0.23 | 0.17 | <0.06 | <0.06 | <0.06 | <0.03 |
| $SO_3$ | <0.05 | <0.05 | <0.05 | <0.05 | <0.05 | <0.05 |
| $SO_4$ | 2.34 | 2.06 | 163.2 | 22.97 | <0.05 | 225.59 |
| OX | <0.09 | <0.09 | <0.07 | <0.07 | <0.07 | <0.07 |
| $HCO_3$** | 119.8 | 91.68 | 362.38 | 213.53 | 393.7 | 464.48 |
| | | | | | | |
| Zn | 0.096 | 0.05 | 0.058 | 0.022 | 0.08 | 0.18 |
| Ba | 0.038 | 0.018 | 0.078 | 0.096 | 0.046 | Nd |
| B | <0.0066 | <0.0066 | 0.096 | <0.0066 | 0.126 | 0.33 |
| Si | 23.42 | 23.492 | 8.468 | 9.412 | 4.408 | 5.616 |
| Mn | 0.002 | 0.002 | 0.006 | 0.002 | 0.008 | 0.005 |
| Fe | 0.008 | 0.242 | 0.042 | 0.008 | 0.086 | 0.57 |
| Mg | 6.418 | 5.2 | 4.734 | 3.232 | 2.294 | 1.345 |
| Al | 0.042 | 0.026 | 0.034 | 0.034 | <0.015 | Nd |
| Sr | 0.104 | 0.082 | 0.576 | 0.374 | 0.296 | 0.185 |
| Ca | 16.132 | 13.668 | 12.78 | 8.468 | 4.314 | 3.335 |
| Na | 10.644 | 9.072 | 192.48 | 68.172 | 172.84 | 307 |
| Li | 0.004 | 0.004 | 0.044 | 0.022 | 0.038 | <0.06 |
| K | 3.848 | 3.546 | 2.722 | 2.012 | 1.394 | 6.37 |
| $Fe^{3+}$, lab | Nd | <0.04 | <0.04 | <0.04 | <0.04 | 0.11 |
| $Fe^{2+}$, lab | Nd | <0.1 | <0.1 | <0.1 | <0.1 | 0.46 |
| Fe(tot), lab | Nd | 0 | 0 | 0 | 0 | 0.57 |
| | | | | | | |
| DIC (ppm) | 23.6 | 18.1 | 71.7 | 42.2 | 78.9 | 92.9 |
| DOC (ppm) | 0.78 | 0.67 | 0.66 | 0.75 | 0.71 | 5.29 |
| | | | | | | |
| $\delta^{13}C$ (‰) | -13.969 | -13.279 | -8.669 | -11.317 | -7.085 | -4.43 |
| $^{14}C$ (pmc) | 73.33+/-0.48 | 56.45+/-0.39 | 17.84+/-0.27 | 23.96+/-0.29 | 4.61+/-0.29 | 52.29+/-0.37 |
| $\delta^{18}O$ (‰) | -10.90 | -11.00 | -11.55 | -11.30 | -11.50 | -11.20 |
| $\delta D$ (‰) | -91.8 | -94.5 | -94.5 | -89.38 | -93.87 | -98.6 |
| Tritium (TU) | <0.8 | 0.9 | <0.8 | <0.8 | <0.8 | <0.8 |
| $\delta^{34}S\ SO_4$ (‰) | Nd | Nd | -12.15 | -2.25 | -6.35 | -22.09 |

KEY: **nd** – not determined; **\*** - estimated from data on nearby monitoring wells; **\*\*** - calculated from DIC and pH

**Table 4.** Geochemical analyses. Units in mg/L unless otherwise specified. (Pegram, 1995)

| Well | CNV-W3 | CNV-W5 | MW-64 | MW-65 | MW-60 | MW-68 | L-Bar |
|---|---|---|---|---|---|---|---|
| Date sampled | 7/25/94 | 7/31/94 | 5/20/94 | 5/20/94 | 5/20/94 | 5/20/94 | 10/5/94 |
| Temp (C) | 20* | 20* | 19* | 20* | 19* | 19* | 18.41 |
| DO (mg/L) | 0.18 | 0.01 | nd | nd | nd | Nd | 2.39 |
| Cond. (mS/cm) | 0.99 | 1.53 | nd | nd | nd | Nd | 1.074 |
| PH (log units) | 8.17 | 8.46 | 7.9* | 7.8* | 8.1* | 8.1* | 8.26 |
| Eh (mV) | 231 | 233 | nd | nd | nd | Nd | 103 |
| | | | | | | | |
| F | 1.38 | 4.53 | 1.53 | 1.81 | 1.84 | 1.71 | 2.15 |
| Cl | 5.25 | 11.16 | 34.21 | 305.43 | 42.64 | 61.42 | 15.12 |
| $NO_2$ | <0.03 | <0.03 | <0.01 | <0.01 | <0.01 | <0.01 | <0.03 |
| Br | 0.29 | 0.3 | 0.11 | 0.041 | 0.13 | 0.2 | 0.08 |
| $NO_3$ | 0.08 | 0.07 | 0.39 | 0.04 | <0.01 | 0.04 | 0.31 |
| $PO_4$ | <0.03 | <0.06 | <0.02 | <0.02 | <0.02 | <0.02 | <0.06 |
| $SO_3$ | <0.05 | <0.05 | nd | nd | nd | Nd | <0.05 |
| $SO_4$ | 80.76 | 370.42 | 409.36 | 260.25 | 588.92 | 1131.81 | 236.24 |
| OX | <0.07 | <0.07 | <0.06 | <0.06 | <0.06 | <0.06 | <0.07 |
| $HCO_3$** | 585.8 | 535.89 | 653.48 | 664.11 | 746.01 | 612.67 | 482.11 |
| | | | | | | | |
| Zn | 0.165 | 0.065 | nd | nd | nd | Nd | 0.028 |
| Ba | nd | Nd | nd | nd | nd | Nd | 0.02 |
| B | 0.34 | 0.655 | nd | nd | nd | Nd | 0.222 |
| Si | 4.965 | 3.96 | 7.11 | 7.525 | 7.575 | 10.145 | 4.712 |
| Mn | 0.03 | 0.005 | 0.01 | 0.035 | 0.02 | 0.01 | 0.006 |
| Fe | 0.95 | 0 | <0.012 | 0.06 | <0.012 | 0.725 | 0.034 |
| Mg | 0.77 | 6.61 | 2.825 | 9.77 | 2.825 | 4.47 | 1.322 |
| Al | nd | Nd | nd | nd | nd | Nd | 0.02 |
| Sr | 0.22 | 0.565 | nd | nd | nd | Nd | 0.228 |
| Ca | 4.98 | 17.425 | 7.97 | 10.06 | 7.97 | 12.995 | 3.626 |
| Na | 247.2 | 355.1 | 568.34 | 527.12 | 568.34 | 724.3 | 289.24 |
| Li | 0.105 | 0.09 | nd | nd | nd | Nd | 0.054 |
| K | 2.17 | 1.705 | 3.36 | 4.095 | 3.36 | 4.3 | 1.704 |
| $Fe^{3+}$, lab | 0.14 | <0.07 | <0.13 | <0.13 | <0.13 | 0.14 | <0.04 |
| $Fe^{2+}$, lab | 0.81 | <0.04 | <0.07 | <0.07 | <0.07 | 0.36 | <0.1 |
| Fe(tot), lab | 0.95 | 0 | 0 | 0 | 0 | 0.5 | 0 |
| | | | | | | | |
| DIC (ppm) | 116.1 | 106.9 | 129.1 | 131.1 | 147.7 | 121.3 | 95.7 |
| DOC (ppm) | 1.84 | 13.85 | nd | nd | nd | Nd | 0.86 |
| | | | | | | | |
| $\delta\ ^{13}C\ (\%_o)$ | -3.08 | -3.6 | -5.65 | -6.84 | -5.04 | -4.67 | -5.986 |
| $^{14}C$ (pmc) | 0.74+/- 0.30 | 0.28+/- 0.60 | -0.02+/- 0.30 | -0.05+/- 0.30 | -0.14+/- 0.31 | -0.41+/- 0.30 | -0.14+/- 0.30 |
| $\delta\ ^{18}O\ (\%_o)$ | -11.20 | Nd | -11.90 | -11.60 | -12.80 | -12.70 | -12.60 |
| $\delta\ D\ (\%_o)$ | -100.34 | -88.5 | -97.88 | -89.02 | -105.42 | -105.39 | -105.47 |
| Tritium (TU) | <0.8 | <0.8 | <0.8 | <0.8 | <0.8 | <0.8 | <0.8 |
| $\delta\ ^{34}S\ SO_4\ (\%_o)$ | -9.95 | -8.78 | -16.61 | -14.55 | -18.3 | -19.18 | -8.89 |

KEY:  **nd** – not determined;  **\*** - data from nearby monitoring wells;  **\*\*** - calculated from DIC and pH

**Table 4 (continued).**  Geochemical and isotopic analyses.  Units in mg/L unless otherwise specified.  (Pegram, 1995).

## 4.2. Stable Isotopes

A local meteoric water line, $\delta D = 8 \; \delta^{18}O + 12.5$, is representative of modern precipitation in northwestern New Mexico [*Vuataz and Goff*, 1986]. All modern samples analyzed in this study plot below and to the right of the local and global meteoric water lines indicating that precipitation has experienced evaporation prior to infiltration into the groundwater system. An interesting observation is that, in general, the younger (Holocene age) samples are 1-2 ‰ enriched in $\delta^{18}O$ and up to 14 ‰ enriched in $\delta D$ relative to older (Pleistocene age) samples. These relative differences in stable isotope composition correspond to about a 3°C cooler recharge temperature for older waters. Such a trend is consistent with southwestern U.S. climate change studies that indicate a wetter, colder (5°-7°C lower than present) climate in the Pleistocene [*Phillips et al.*, 1986; Stute *et al.*, 1995] although the magnitude of the calculated temperature change is less. It is important to note that altitude effects may have also affected the relative differences in isotopic composition between the collected groundwater samples if there was significant variation in recharge elevations. However, it is difficult to distinguish between the effects of climate change and recharge elevation differences on isotopic composition.

## 4.3. Carbon Isotopes

The $^{13}C$ ratio increased downgradient from approximately -14 ‰ to -3 ‰, paralleling the increase in dissolved organic carbon. Just prior to recharge, soilwater normally has a $\delta^{13}C$ value in equilibrium with that of soil $CO_2$, approximately -20 ‰. Dissolution of carbonate minerals, with heavier $\delta^{13}C$ values, was most likely responsible for the enrichment in $\delta^{13}C$ in the direction of flow. Carbonate samples (fossil shell, concretion, cement, and vein) in the study area show a large range of isotopic compositions from +2.2 ‰ to –11.8 ‰ [*Gao et al.*, 1995].

Carbon-14 activity decreased with distance from Mount Taylor, reaching nearly zero at the Cerro Negro vertical borehole and the L-Bar monitoring wells. Carbon-14 activity in the CNV-W2 sample was anomalously high (52.29 ± 0.37 pmc). This sample was taken at the water table from the Two Wells Sandstone in the Cerro Negro vertical borehole. Samples, CNV-W3 and CNV-W5, collected below CNV-W2 in the same borehole yielded much older corrected $^{14}C$ ages ( > 20,000 years). The high $^{14}C$ activity in CNV-W2 probably resulted from vertical recharge from the surface, which introduced young water into the top of the aquifer in this area. Considering that groundwater collected from below the Two Wells Sandstone in the CNV borehole showed no signature of modern precipitation, it is likely that vertical recharge from the surface was not a significant component of groundwater near Cerro Negro, and therefore was neglected for groundwater modeling purposes.

## 4.4. Radiocarbon Dating

In the study completed by Pegram (1995), the hydrologic system was considered to be closed with respect to carbon. The $^{14}$C activity and geochemistry of the sample taken from the Presbyterian well was considered to be representative of local recharge water. Sources and sinks of carbon, such as incongruent and congruent dissolution of carbonate minerals, affect the $^{14}$C signal by adding old carbon with no $^{14}$C or preferentially precipitating the heavier isotope which causes the sample to appear falsely old. Therefore, the measured $^{14}$C activities in downgradient wells were adjusted using NETPATH to remove all $^{14}$C effects resulting from processes other than radioactive decay. The decay equation was then applied to calculate an apparent age for groundwater in each downgradient groundwater sample given the NETPATH-corrected $^{14}$C activity, the initial $^{14}$C activity ($A_0$), and the half-life of $^{14}$C (5730 years). For comparison, a simple carbonate dissolution model was used to correct $^{14}$C activities. In this model, $^{14}$C measured values are multiplied by the ratio between the DIC concentration in the initial well and the sum of the DIC concentrations in the initial and final wells to calculate a corrected $^{14}$C activity. Radiocarbon ages calculated using the simple carbonate dissolution model were virtually identical to the ages predicted by the more elaborate NETPATH model. This implies that the carbonate geochemistry of the Cerro Negro groundwater flow system is not complicated and that microbial influence on geochemistry and isotopic signatures is relatively small. If there were major sources of inorganic carbon other than carbonate rocks (such as oxidation of methane or microbial respiration) the isotopic and chemical data used to constrain the NETPATH model would

be unlikely to produce the same groundwater ages as the simple carbonate dissolution calculations. Table 5 lists ^{14}C groundwater ages obtained from applying 1) the simple dissolution model and 2) the NETPATH model to correct for sources and sinks of carbon. The ages range from approximately 2,200 years at the Bibo well to >38,000 years at the MW-68 well. The ages uniformly increase with distance from the initial well. NETPATH calculates a negative age for the CNV-W2 sample, because the corrected ^{14}C activity in that sample is greater than the ^{14}C activity in the recharge well. This indicates much younger water in the CNV-W2 sample relative to the initial well, probably resulting from vertical recharge through fractures near Cerro Negro.

| Well | Simple Dissolution Model Corrected $^{14}$C age (yr) | NETPATH Corrected $^{14}$C Age (yr) | Distance from Recharge Area (km) |
|---|---|---|---|
| Presbyterian | 0 | modern | NA |
| Elkins | 4,360 | modern | NA |
| Bibo | 2,570 | $2,180 \pm 120$ | 5.8 |
| Seboyeta | 4,440 | $3,630 \pm 100$ | 6.0 |
| Moquino | 12,900 | $12,200 \pm 500$ | 8.4 |
| CNV-W2 | "negative" age | $-9300 \pm 60$ | 9.3 |
| CNV-W3 | 25,200 | $24,000 \pm 2,800$ | 9.3 |
| CNV-W5 | 33,500 | $33,500 \pm 9,500$ | 9.3 |
| MW-64 | $> 32000$ | $> 31,500$ | 10.1 |
| MW-65 | $> 32800$ | $> 32,800$ | 10.2 |
| MW-60 | $> 35000$ | $> 34,500$ | 10.4 |
| MW-68 | $> 40,200$ | $> 39,900$ | 10.7 |
| L-Bar | $> 39,100$ | $> 38,300$ | 12.9 |

**Table 5.** Corrected ^{14}C groundwater ages calculated using a simple dissolution mass balance and the NETPATH model (from Pegram, 1995).

## 5. HYDROGEOLOGIC MODELING

In attempts to understand better and quantify the present-day hydrogeologic flow regime, a cross-sectional finite element groundwater flow model was developed to simulate fluid and heat flow from Mount Taylor to Cerro Negro.

### 5.1. Conceptual Groundwater Flow Model

In constructing a numerical groundwater flow model, it is crucial to have a reasonable idea of flow conditions and the important mechanisms driving flow *a priori*. Understanding the fundamentals of fluid and heat flow in similar geologic settings is the first step in ascertaining the flow conditions in the region to be modeled. Since the study region lies near the edge of the San Juan Basin, it was useful to apply the general concepts of fluid and heat flow in sedimentary basins to formulate the conceptual model of flow in the study region.

#### 5.1.1. Fluid Flow

##### 5.1.1.1. Mechanisms Driving Fluid Flow in Sedimentary Basins

Subsurface fluid migration within sedimentary basins is driven by a number of mechanisms including gradients in topography, sedimentation and compaction, fluid density variations, and seismogenic pumping (Figure 9), (Person *et al*., 1996).

Topography-driven

Compaction-driven

X

X

X

X

X

X

X

X

X

X

X

X

X

X

X

X

Seismogenic Pumping

Key:

| | |
|---|---|
| ☰ | Low permeability sediment |
| ◦ ◦ | High permeability sediment |
| X X | Crytalline Basement Rock |
| ➤ | Fluid Flow Direction |
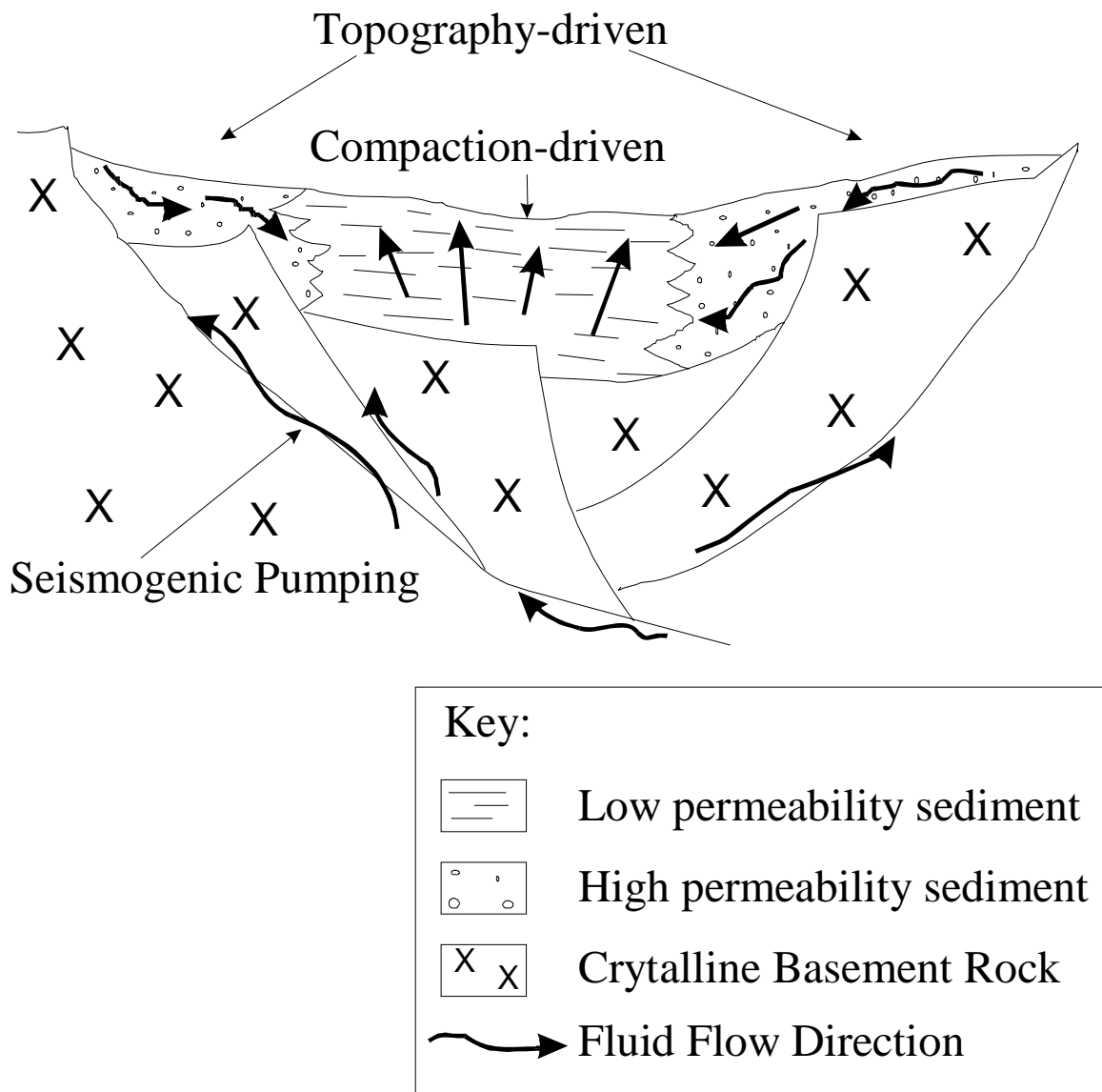
**Figure 9.** Mechanisms driving fluid flow including topography, compaction and seismogenic pumping. (modified from Person *et al*., 1996)

Topography-driven flow is induced by elevation changes in the water table. In tectonically stable areas, the water table surface tends to be a subdued replica of the land surface. Consequently, flow is directed from areas of high topography to areas of low topography. Compaction-driven flow is induced by mechanical loading of sediment and may control fluid flow in thick sedimentary packages that contain low permeability units. Density-driven flow arises from fluid density gradients produced by temperature or compositional variations or phase changes in fluids. For example, deep fluids may be heated, becoming less dense, and forced upward when buoyant forces exceed viscous forces. It is proposed, but not widely accepted, that free convective cells may result in deep systems consisting of highly permeable material (Deming, 1992). Criticism of this phenomenon emphasizes that the high permeabilities required for free convection ($>10^{-15}$ $m^2$) are probably quite rare at deep depths on a large scale. Seismogenic pumping, episodic fluid flow due to permeability and pressure changes along fault zones, may be an important mechanism driving fluid flow in tectonically active settings (Sibson, 1994).

### 5.1.1.2. Mechanisms Driving Fluid Flow in the Study Area

Topography is expected to have the greatest influence on controlling fluid flow in the study area due to the significant change in groundwater level elevation from Mount Taylor to the base of Mesa Chivato. The total change in water elevation from the peak of Mount Taylor to Cerro Negro is about 1000 m over a distance of 22 km which imposes a large hydraulic head gradient that is at a maximum near the slope of the Mesa Chivato (about 15 km from the peak of Mount Taylor) and at a minimum east of Cerro Negro

where there is little change in land surface elevation and also water table elevation.

Compaction and fluid density instabilities significant enough to affect drive fluid flow are generally confined to central regions of sedimentary basins where the sedimentary package is thickest. Since the study area is located near the margin of the San Juan Basin where the sedimentary package is considerably thinner than the central basin, compaction-driven flow and density-driven flow are probably not significant factors influencing the fluid flow regime.

Seismogenic pumping effects are confined to regions of seismic activity. The study area is located in a presently tectonically stable region. Therefore, seismogenic pumping is probably not a viable mechanism driving fluid flow in the study area currently, but may have influenced flow during periods of volcanism 4.5 Ma – 1.5 Ma.

### 5.1.1.3. Groundwater Flow Patterns

Mount Taylor and the surrounding Mesa Chivato are dramatic topographic highs in the southeastern San Juan Basin. Based on the regional geomorphology and the supposition that topography is the main mechanism of fluid flow, it is expected that Mount Taylor and the surrounding  Mesa Chivato are regional recharge areas and that the area below the base of the mesa and discharge occurs at some distance from the mesa. There are no obvious discharge points (lakes, gaining streams, ect..) other than relatively low volume springs located at various places at the edge of Mesa Chivato where the basalt flows

terminate. The Rio Puerco, a potential discharge point, is located 35 km east of Cerro Negro.

The water table elevation contour map indicates a quasi-radial groundwater flow pattern, with the highest water table elevation below the peak of Mount Taylor (Figure 5). Of course, this conceptual model is a simplified version of the actual groundwater flow regime, but presuming a strong topographic control of fluid flow, we can assume that groundwater flow is essentially 2-dimensional from the peak of Mount Taylor to Cerro Negro. The flow regime can therefore be represented in a numerical model as a vertical cross-section perpendicular to water table equipotentials from the peak of Mount Taylor in the direction of Cerro Negro.

### 5.1.2. Heat Flow

Another important transport process in the subsurface, strongly coupled with fluid flow, is heat flow. Heat flow originating from the inside the Earth averages about 62 mW/m$^2$ through the continents and 100 and mW/m$^2$ through the ocean (Vacquier, 1991) and may be transferred in the lithosphere to the groundwater surface through conduction and convection.

#### 5.1.2.1. Modes of Heat Transfer in the Subsurface

Conductive heat transfer, an enthalpy exchange resulting from Brownian (molecular)

motion within solid and liquid phases, is the predominant mode of heat transfer in the lithosphere. Conduction prevails in tectonically stable settings and in conditions of low groundwater flow. Convective heat transfer involves an energy exchange between a surface and an adjacent fluid. Convection becomes an important mechanism of heat transfer in the subsurface if a strong component of vertical flow exists (Person *et al.*, 1996).

### 5.1.2.2. Modes of Heat Transfer in the Study Area

In general, the subsurface thermal regime in the study area is expected to be dominantly conductive, considering the present stable geologic setting. However, advection may play a substantial role in subsurface heat transfer in areas of strong recharge and strong discharge where vertical fluid flow predominates. Areas near the top of Mount Taylor and the base of Mesa Chivato are the most probable regions to be affected by convective heat transfer, since recharge and discharge are strongest in those regions, respectively.

### 5.1.2.3. Heat Flow Patterns

A pattern of parallel horizontal isotherms is representative of a purely conductive thermal regime (Figure 10). Deviation from this pattern indicates that convection may play a role in the transfer of heat in the subsurface. Downward advection depresses the isotherms by introducing cool meteoric water (Figure 10). Upward advection uplifts the isotherms by bringing the deep geothermally heated groundwater up towards the surface

# Conductive thermal regime
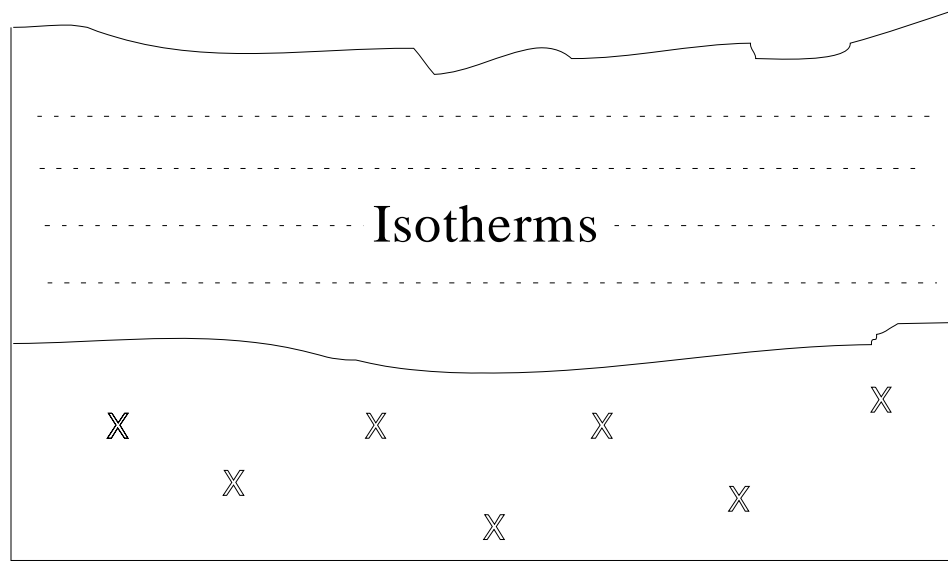
Isotherms

# Convective  thermal regime
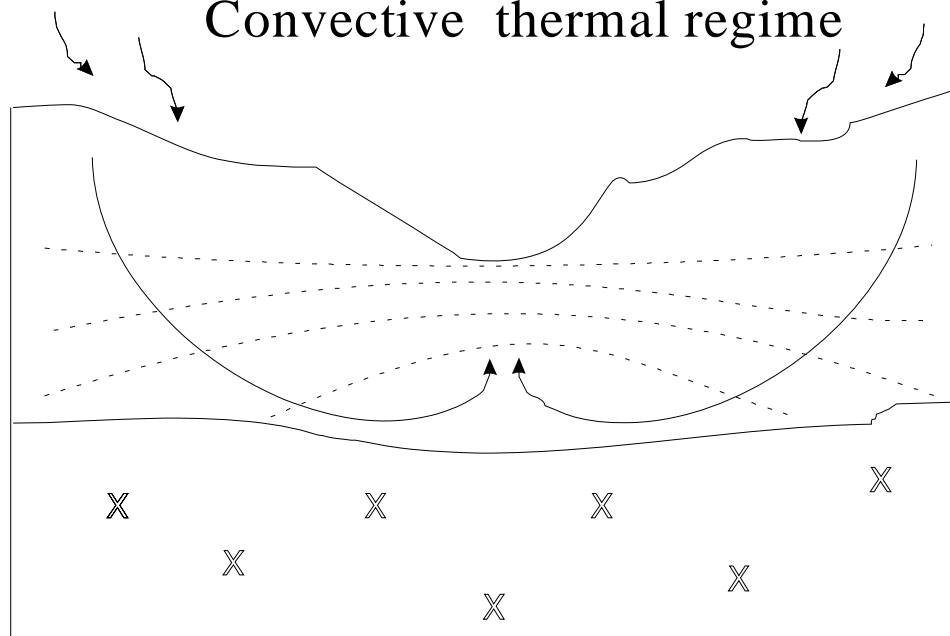
Fluid flow

Isotherms

**Figure 10.**  Schematic depiction of idealized subsurface thermal regimes dominated by conductive heat transfer (top) and influenced by convective heat transfer (bottom).

### 5.1.3. Simplifying Assumptions

Numerical model precision may be limited either by the capacity of the model or by the quantity and quality of data and observations. In representing a real flow regime with mathematical and numerical models, simplifying assumptions are applied for reasons related to these limitations. Some assumptions may be mandatory to conform to the capabilities of existing numerical codes. Simplification may also be the best approach when detail potentially accommodated by the model exceeds detail that can be measured or observed from the study site. Assumptions may be applied to simplify the problem, both conceptually and computationally, provided that the accuracy of the model is not sacrificed.

### 5.1.3.1. General Simplifying Assumptions

General simplifying assumptions that define the basis of the conceptual model of fluid and heat flow in the southeastern San Juan Basin include the following:

1. The fluid is pure water – no compositional variation.

2. The rock layer sequence can be adequately represented as a saturated porous medium.

3. The specific discharge vector obeys the continuity equation and Darcy's law, which expresses the sum of forces acting on the fluid per unit volume of the fluid.

4. Advection is the dominant mechanism for mass transport.

5. The thermal conductivity and specific heat capacities of the fluid are constant.

6. The fluid and the medium are in thermal equilibrium.

7. The medium is incompressible.

8. The groundwater flow system is in steady state. The water table elevation does not vary with time.

9. Individual rock layers are homogeneous and anisotropic. Preferential fluid flow through fractures, if present, can be adequately represented by increasing the hydraulic conductivity value of the unit relative to a value for the unfractured matrix.

In this system, the last two stated assumptions probably have the greatest implications for the accuracy of the model solution. The water table configuration has certainly undergone changes within the residence time of groundwater in the system (refer back to section 2.4.3.). Recall the measured corrected radiocarbon ages of >40,000 kyr in the vicinity of Cerro Negro. The steady-state assumption is a limitation to the model that should be considered when assessing model results. Also, assuming lateral uniformity of hydraulic characteristics presents limitations to the model. There is lateral variation in the hydraulic parameters in each layer for several reasons. Most of the sedimentary units

were deposited during periods of marine transgression and regression (Stone *et al.,* 1983) which presumably caused gradation and tonguing in the lithology. In addition to lithologic heterogeneity which has a somewhat random distribution, a systematic lateral variation is present due to the progressively decreasing amount of overlying rock material with distance away from Mount Taylor. The overlying rock material serves to compress the rock and reduce the fracture aperture widths, which will tend to decrease the porosity, hydraulic conductivity and thermal conductivity of the bulk rock (Nelson, 1994). Since the model does not account for lateral variation within a layer, the set of constant hydraulic properties prescribed for each hydrostratigraphic unit represent laterally averaged values. Another inexactitude of the model results from addressing fracture flow simply by increasing the bulk permeability of a fractured layer in an equivalent continuun approach rather than representing matrix and fracture flow separately, as in a dual porosity or dual permeability approach. This simplification is generally acceptable when analyzing the groundwater flow regime at the regional scale, provided that fracture aperture width is relatively small and displacement is negligible, as it is in this case. Neglecting fracture flow in the model, however, prohibits detailed interpretation of intra- and inter- layer fluid flow at the smaller scale.

### 5.1.3.2. Simplifying Assumptions Relating to Boundary Conditions

Simplifying assumptions specific to the assigned boundary conditions of the model include the following:

1. The peak of Mount Taylor represents a groundwater divide.

2. The presumed 2-dimensional pattern of groundwater flow from Mount Taylor to Cerro Negro allows for representation of the flow regime as a cross-section taken from the peak of Mount Taylor and projected outward perpendicular to the hydraulic gradient.

3. Fluid flux into or out of the Paleozoic layers that lies beneath the Cretaceous sediment is negligible relative to fluid flux within the overlying sedimentary layers.

4. Lateral heat fluxes are negligible around 12 km east of Cerro Negro.

5. The temperature of the fluid at the water table is constant over time.

6. The temperature of the fluid at the water table can be reasonably estimated by factoring in the mean annual air temperature at a known elevation, local adiabatic lapse rate, spatial variation in thickness of the vadose zone, and vadose zone geothermal gradient. A uniform vadose zone geothermal gradient is an additional assumption. (Calculation methods are explicated in Appendix D).

7. The basal heat flux is uniform and constant within the study region.

## 5.2. Mathematical Model

### 5.2.1. Governing Equations

The model solves a system of coupled steady-state groundwater flow, stream function, and heat transfer equations for a variable density fluid described by Bear (1972), Smith and Chapman (1983) and Senger and Fogg (1990) and summarized in Appendix E.

### 5.2.2. Equivalent Fresh Water Heads

This model assumes that the fluid composition is pure water, but that the fluid density varies in response to changes in pressure and temperature. Since this is a relatively deep groundwater flow system with relatively high basal temperatures, the density of the fluid will decrease with depth, which may affect, to a small degree, the flow regime. The expression for the fluid potential as an equivalent fresh water head is introduced in order to allow spatial variability of the fluid density:

$$h = \frac{p}{\rho_0 g} + z$$

(Refer to Appendix C for symbol notation.)

### 5.2.3. Stream Function

The stream function, $\psi$, is a fluid flux potential derived from Darcy's law. The stream function is related to specific discharge (q) through the following equations (Bear, 1972):

$$q_x = -\frac{\partial \varphi}{\partial z}$$

$$and$$

$$q_z = \frac{\partial \varphi}{\partial x}$$

(Refer to Appendix C for symbol notation.)

Connecting equal stream function values establishes a streamline. The difference in $\Psi$ values corresponds to the specific discharge between these stream lines (Senger and Fogg, 1990). The stream function is useful to apply when representing variable-density groundwater, because the single-valued function does not depend on the properties of the fluid involved (De Josselin de Jong, 1960).

### 5.2.4. Equations of State

Equations of state were required to characterize the temperature and pressure dependence of fluid properties, i. e. fully coupled groundwater flow and heat transfer. Kestin *et al.* (1986) describe the equations of state which relate fluid density and viscosity to fluid pressure and temperature.

$$\rho = \rho(P,T)$$

$$\mu = \mu(P,T)$$

## 5.3. Numerical Model

The results from the geochemical modeling and available hydrogeologic information were integrated to develop a numerical groundwater flow model capable of simulating 2-dimensional fluid and heat flow from the peak of Mount Taylor to Cerro Negro. Equivalent fresh water heads, temperatures, and stream functions were solved using triangular elements which employ linear basis functions. The model simulation was calibrated by running a series of simulations, varying the conductivities of hydrostratigraphic units to produce the best match of observed radiocarbon groundwater ages and computed groundwater ages.

### 5.3.1. Location of Model Cross-section

The 35 km cross-section chosen extends from the peak of Mount Taylor to approximately 12 km beyond the Cerro Negro volcanic neck, approximately parallel to the west-northwest to east-southeast groundwater direction (Figure 11). Cross-sectional model thickness ranges from approximately 2000 m in the west to 1000 m in the east. Sedimentary units considered in the model include the Triassic Chinle Formation up through the Cretaceous Point Lookout Sandstone (Figure 12). Also represented in the model are the basalts and andesites at the top of Mount Taylor. Because the Cerro Negro volcanic neck is very small relative to the scale of the cross-section, the intrusion is not represented in the model.
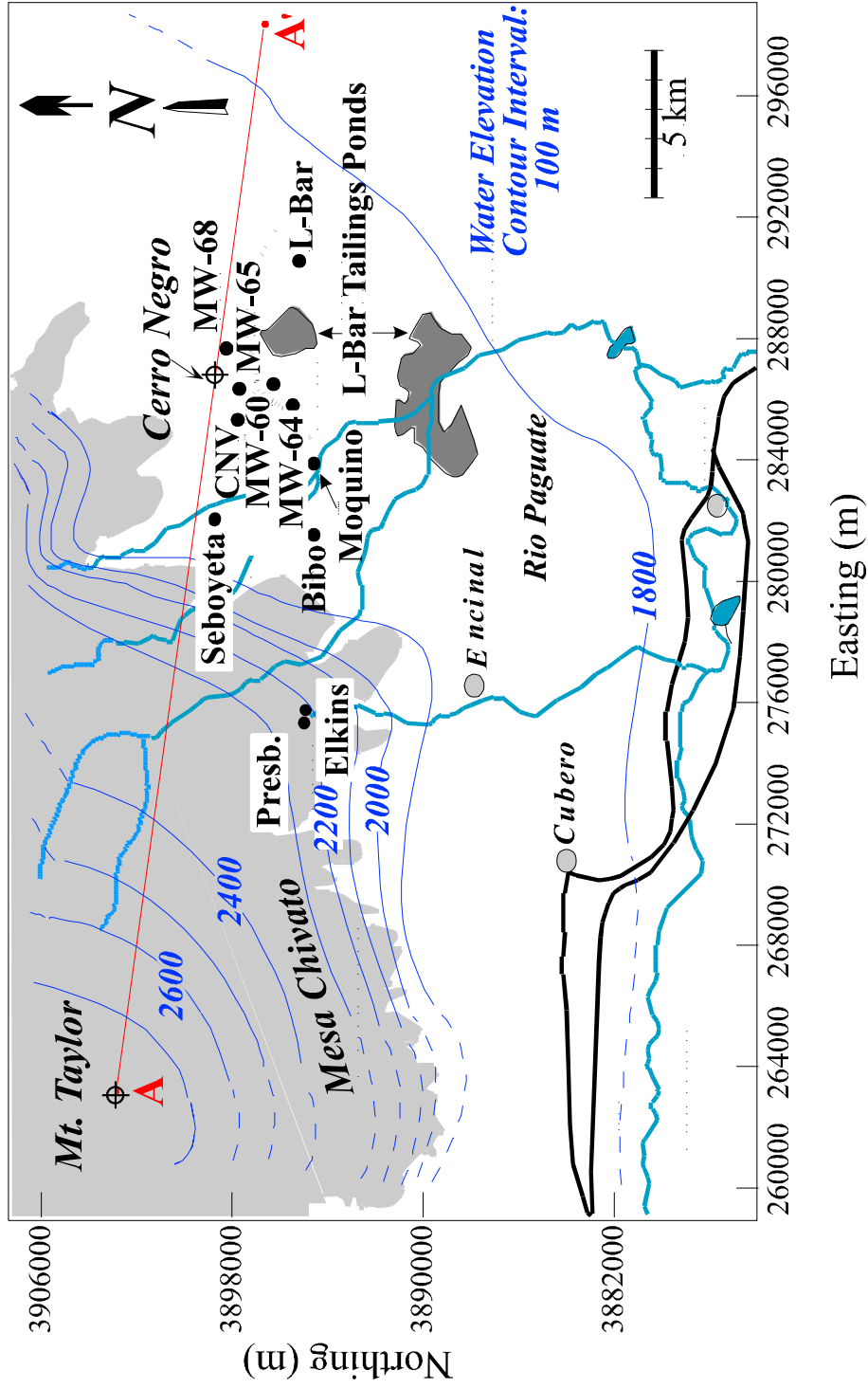
**Figure 11.** Map indicating cross-section A – A' used in numerical model, taken parallel to the groundwater flow direction. [14]C sample locations are also shown.

# A A'



**Legend:**
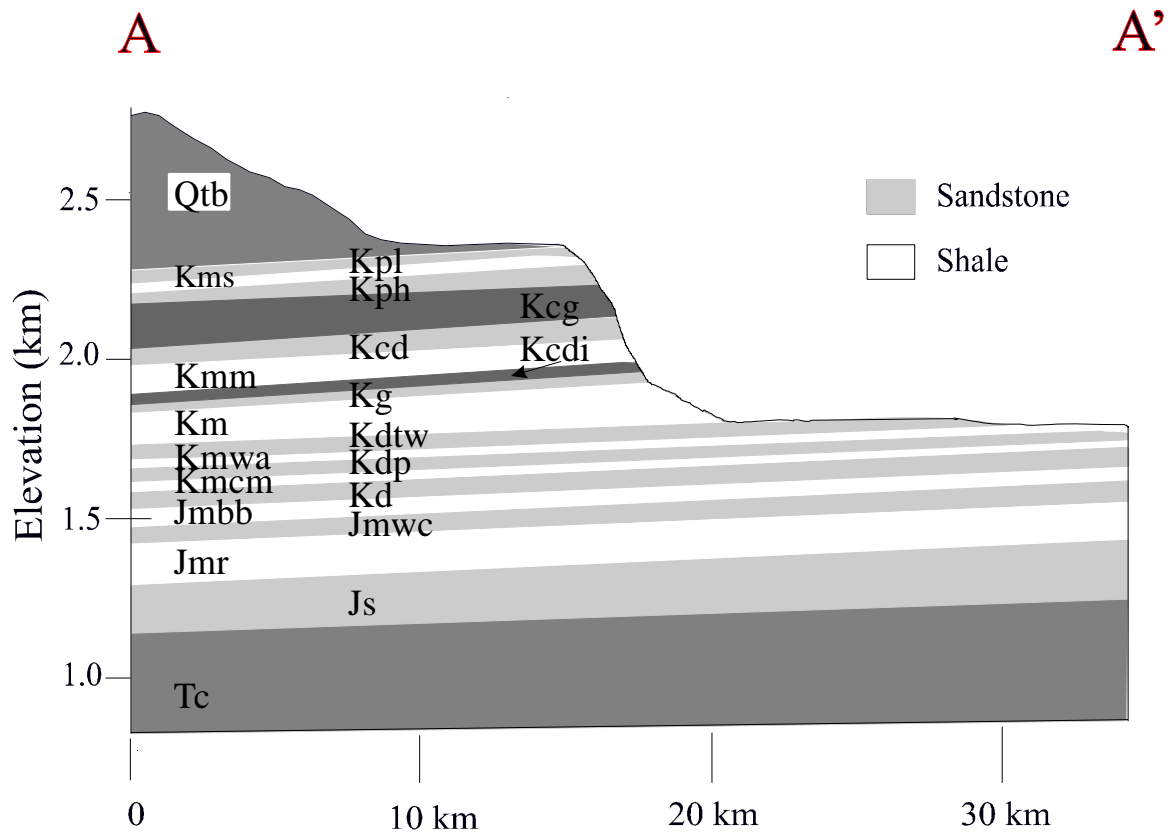
- Qtb — Basalt undifferentiated
- Kpl — Point Lookout Sandstone
- Kms — Satan Tongue of the Mancos Shale
- Kph — Hosta Tongue of the Point Lookout SS
- Kcg — Gibson Coal Member
- Kcd — Dalton Sandstone
- Kmm — Mulatto Tongue of Mancos Sh
- Kcdi — Dilco Coal Mb of Crevasse Canyon
- Kg — Gallup Sandstone
- Km — Mancos Shale (main body)
- Kdtw — Two Wells Sandstone
- Kmwa — Whitewater Arroyo Shale
- Kdp — Paguate Sandstone
- Kmcm — Clay Mesa Shale
- Kd — Cubero Sandstone and Oak Canyon Mb
- Jmbb — Brushy Basin Shale Member
- Jmwc — Westwater Canyon Sandstone Member
- Jmr — Recapture Shale
- Js — Bluff-Cow Springs SS, Summerville Fm, Todilto Limestone, and Entrada SS
- Tc — Chinle Formation

Figure 12. Hydrogeologic cross-section A – A', used in groundwater flow model. Only the saturated zone is represented in this illustration and in the model.

53

### 5.3.2.  Boundary Conditions


#### 5.3.2.1.  Groundwater Flow Boundary Conditions


The top boundary of the cross-sectional model constitutes a specified head equal to the water table elevation (Figure 13).  Prescribed no-flow along the lower boundary is reasonable due to the large permeability contrast between the sedimentary rocks and underlying Paleozoic sediment.  To the west, the vertical no-flow boundary represents the groundwater divide beneath the top of Mount Taylor.  The eastern boundary was assumed to be far enough away from Cerro Negro to have little effect on the model solution in the area of interest.  Initially, the eastern boundary was set as a no flow, and later modified to an open boundary for heads and stream functions to assess the effects and sensitivity of the boundary.  The open condition is iterative, since the imposed stream function boundary is calculated from the darcy fluxes (described in Senger and Fogg, 1990).
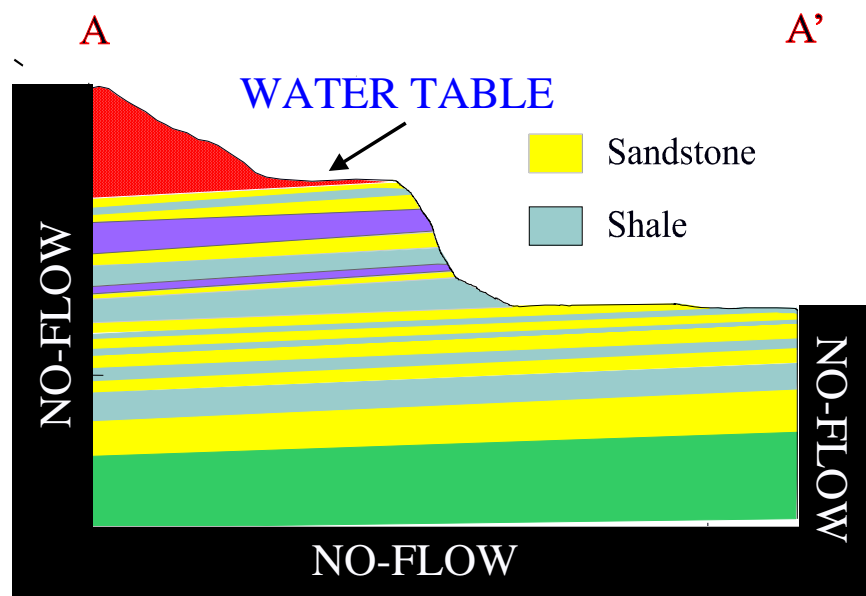


**Figure 13**.  Schematic of numerical model fluid flow boundary conditions.

Based on data from Reiter *et al.* (1975) in the San Juan Basin, a relatively high basal heat

flow of 100 mW/m$^2$ was prescribed.  For comparison, average terrestrial heat flow value

through the continents is 60 mW/m$^2$ (Vacquier, 1991).  The top thermal boundary is a

non-uniform specified temperature that was calculated for each surface node based on the

local atmospheric lapse rate of -5.3 °C/km (Gabin and Lesperance, 1976;  Kunkel, 1984),

the vadose zone thickness, and an average vadose zone geothermal gradient of 70 °C/km.

Calculations are provided in Appendix D.  Due to the dramatic increase in vadose zone

thickness toward the peak of Mount Taylor, the calculated water table temperature

actually increases with elevation, counter to the lapse rate trend.  The side boundaries are

no-flow heat boundaries, represented as insulated walls (Figure 14).
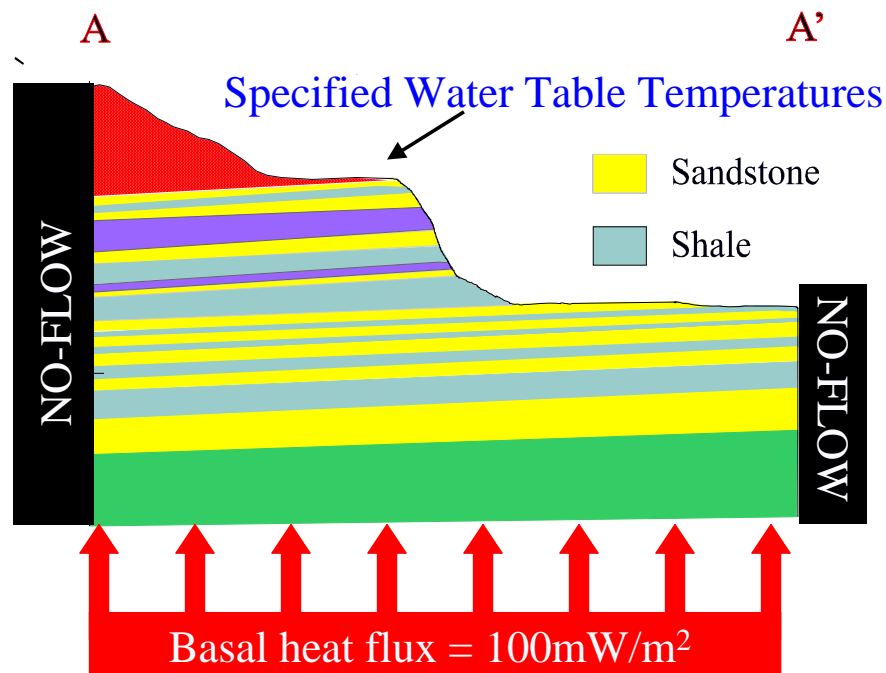


Figure 14.  Schematic of numerical model heat flow boundary conditions.

### 5.3.3. Hydrostratigraphic Units

Hydrostratigraphic units were chosen based on sedimentary layers which have similar hydraulic properties. The cross-section consists of 20 discrete aquifers and aquitards including sandstone, shale, coal, basalt, and clayey siltstone. Layers range in thickness from 5 m to 440 m. Thickness variations within individual layer are present, but are difficult to detect at the scale of the cross-section illustrated in Figure 12. Because triangular elements are used, variable thicknesses are effectively represented in the model. Poor well control on the western most side of the cross-section precluded certainty of any upward bowing of sedimentary layering from Mount Taylor volcanic intrusions, and was therefore neglected. This uncertainty may have affected model results in the recharge area, but probably not significantly in the area of most interest to this study, near Cerro Negro.

### 5.3.4. Input Parameters

#### 5.3.4.1. Fluid Properties

Fluid properties including heat capacity and thermal conductivity were assigned typical values and held constant. Although heat capacity and thermal conductivity vary slightly with changes in temperature, the effects are assumed to be negligible at this scale. Constant values of 4187 J kg$^{-1}$ K$^{-1}$ and 0.63 W m$^{-1}$ K$^{-1}$ were assigned for the heat capacity and thermal conductivity of water, respectively.

## 5.3.4.2. Rock Properties

Rock properties were assigned to each individual rock layer. These properties include porosity, hydraulic conductivity, anisotropy, bed angle, thermal conductivity, and heat capacity. Porosity values, obtained from available data (Craigg, 1990; Gullett, personal communication, 1995) and generic values for given lithologies (Domenico and Schwartz, 1990; Freeze and Cherry, 1979), range from 9% – 20% (Table 1). Hydraulic conductivities range from $1.0 \times 10^{-6}$ m/s to $1 \times 10^{-10}$ m/s based on published values (Stone *et al.*, 1983, Risser *et al.*, 1984, Hydro-Engineering, 1981, and Stephens, 1983) and typical values for given lithologies (Domenico and Schwartz, 1990). In general, the sandstone units were considered to be anisotropic with horizontal hydraulic conductivities exceeding vertical hydraulic conductivities by 1 order of magnitude. The shale units were considered to be isotropic. A uniform rock matrix thermal conductivity of 2.5 W m$^{-1}$ K$^{-1}$ was prescribed for all units for most model simulations. The model computes bulk thermal conductivity values ($\lambda_{bulk}$) for each unit using the equation:

$$\lambda_{bulk} = \lambda_{rock}(1-\theta) + \lambda_{fluid}(\theta)$$

where $\lambda$ = thermal conductivity, and $\theta$ = porosity.

To test the sensitivity of the model to rock thermal conductivity input, rock layers were

assigned different thermal conductivity values, shown below, based on typical values for their lithology (de Marsily, 1986).

| Lithology | Thermal Conductivity (W m$^{-1}$ K$^{-1}$) |
|---|---|
| Sandstone | 2.47 |
| Shale | 2.07 |
| Coal | 0.29 |
| Basalt | 1.95 |

Model simulations run with uniform and with non-uniform specified rock thermal conductivities produced virtually identical results, suggesting that the model is not very sensitive to thermal conductivity spatial variability within the accepted range of values.

### 5.3.5.  Finite Element Mesh

A finite element mesh generator was used to discretize the grid used for this hydrogeologic model.  Mesh generation required the input of spatial coordinates of geologic unit interfaces and the boundaries of the entire modeled domain.  The resulting numerical mesh consists of 3016 nodal vertices and 5748 triangular elements (Figure 15). Elements range in size and are smallest in the area near Cerro Negro.  Each element is accommodated entirely within a specific hydrostratigraphic unit, so that it contains the specified hydraulic properties of the unit.
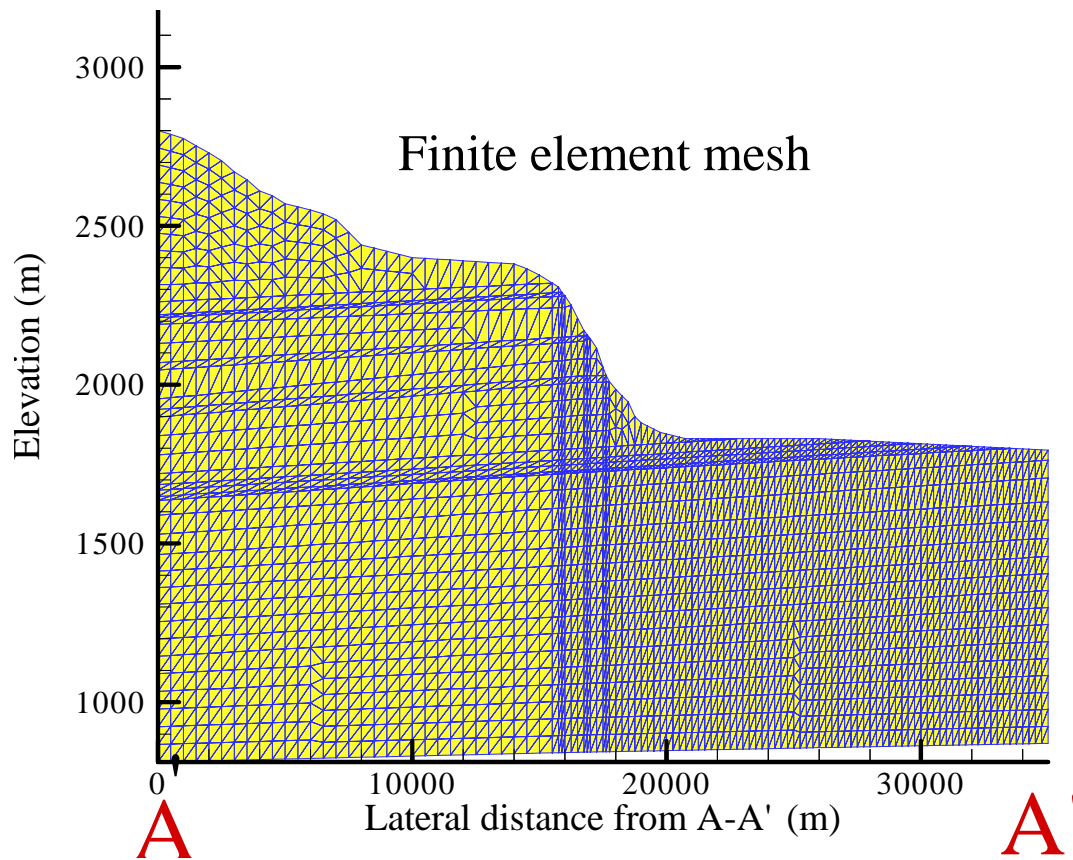
**Figure 15**. Finite element mesh used in numerical model.

### 5.3.6.  Finite Element Method

The governing equations are solved for at the nodal vertices of the triangular elements using the fluid and rock properties associated with each element.   The unknown variables, including hydraulic head (h), stream function ($\Psi$), and temperature (T) are approximated for each element using the polynomial function:

$$unknown\ variable(x,z) = a + bx + cz,$$

$$where,\ x,z = spatial\ coordinates,$$

$$and\ a,b,c = polynomial\ fit\ coefficients\ that\ are\ unique\ for\ each\ element.$$

### 5.3.7.  Model Calibration

The corrected ^{14}C ages of 13 groundwater samples (locations shown in Figure 11) represented in the cross-section were used for model calibration.   Corrected ^{14}C ages correspond to the residence time of groundwater at the location of sample collection. These groundwater ages were compared with model-calculated groundwater travel times, using reverse particle tracking, for numerous model simulations.   Calibration involved running an extensive series of simulations, varying the hydraulic conductivities of the hydrostratigraphic units represented in the model within reasonable range of reported or typical values, to produce the best match of measured ^{14}C groundwater ages and corresponding model-calculated travel times.

5.3.7.1. Reverse Particle Tracking

A reverse particle tracking algorithm, described by Taylor and Person (1998) was used to determine the advective travel times of groundwater between recharge areas and sample well locations. The model delineates the pathways from $^{14}$C locations backward, at a uniform time step size of 5 years, to their respective points of recharge at the water table (Figure 14). The computed travel time for the discrete water package to reach the water table corresponds to the approximate groundwater age, assuming that advection is the dominant mechanism for isotope mass transport. Analysis by Phillips *et al.* (1989) indicated that macrodispersion did not exert a significant influence on the $^{14}$C distribution in the central San Juan Basin. Accordingly, this study assumes that dispersion is negligible compared to advection.

5.3.7.2. Model-Predicted and Measured Groundwater Age Comparison

Measured groundwater ages were compared with model-computed travel times for numerous simulations using variable hydraulic conductivities, both vertical and horizontal, until a good match of observed and computed data was achieved (Table 6, Figure 17). One exception to the fit is the modern $^{14}$C groundwater age from CNV-2 collected at the water table. This young $^{14}$C age presumably reflects local recharge through fractures in the vadose zone which is not accounted for in the model. Model-predicted ages range from 200 yr for the Presbyterian well sample to 62 kyr for the L-Bar
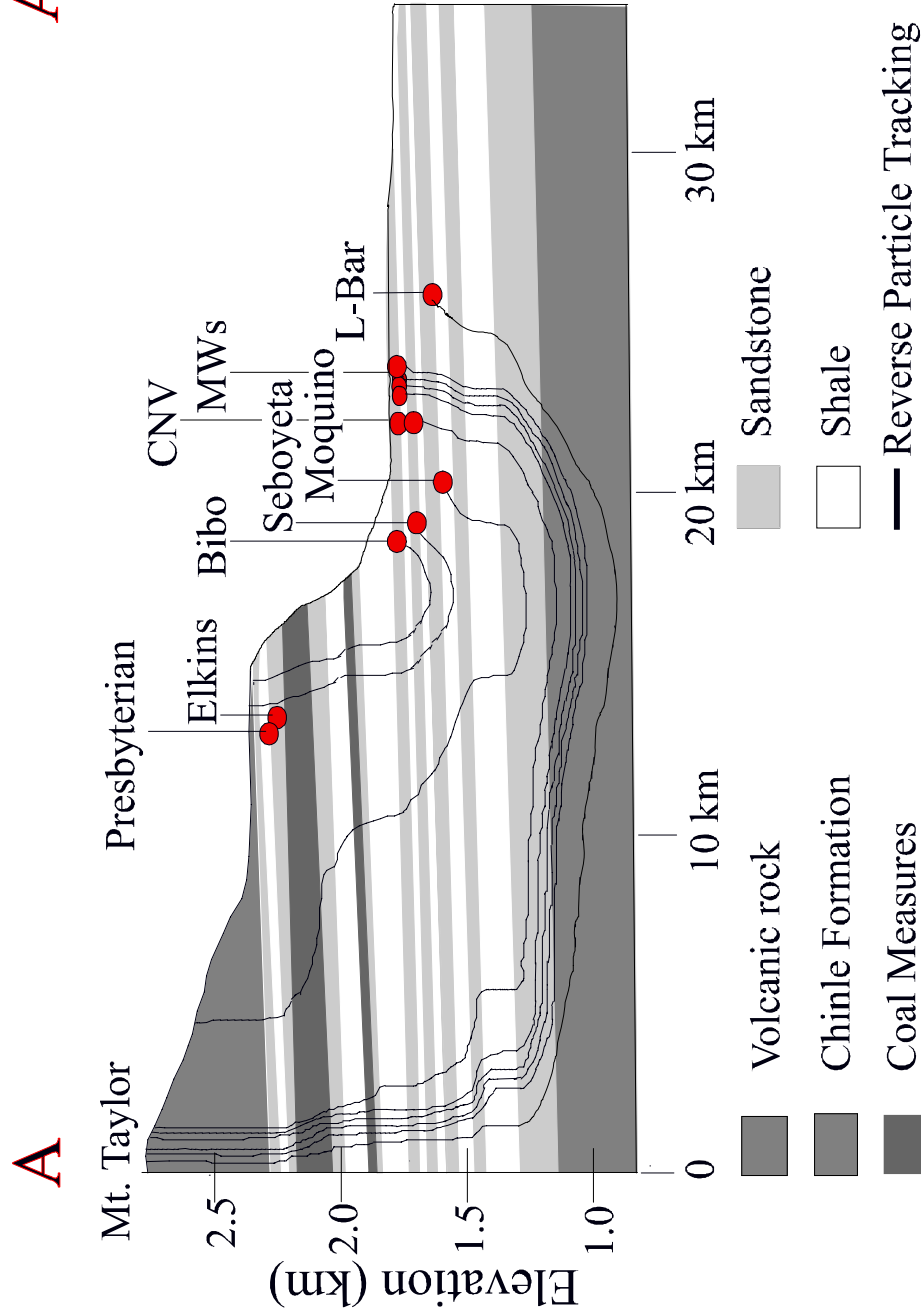
**Figure 16.** Groundwater flow pathlines obtained from the reverse particle-tracking procedure in the numerical model. Initial particle positions are at $^{14}$C sample locations. Final particle locations are at the water table.

| Well | Simple Dissolution Model Corrected $^{14}$C Age (yr) | NETPATH Corrected $^{14}$C Age (yr) | Hydrogeologic Model Calculated Age (yr) |
|---|---|---|---|
| Presbyterian | 0 | Modern | 195 |
| Elkins | 4,360 | Modern | 205 |
| Bibo | 2,570 | $2,180 \pm 120$ | 2,415 |
| Seboyeta | 4,440 | $3,630 \pm 100$ | 3,355 |
| Moquino | 12,900 | $12,200 \pm 500$ | 19,160 |
| CNV-W2 | "negative" age | $-9,300 \pm 60$ | 24,700 |
| CNV-W3 | 25,200 | $24,000 \pm 2,800$ | 24,650 |
| CNV-W5 | 33,500 | $33,500 \pm 9,500$ | 24,675 |
| MW-64 | > 32,000 | > 31,500 | 30,620 |
| MW-65 | > 32,800 | > 32,800 | 33,110 |
| MW-60 | > 35,000 | > 34,500 | 36,175 |
| MW-68 | > 40,200 | > 39,900 | 39,670 |
| L-Bar | > 39,100 | > 38,300 | 63,000 |

**Table 6.** Corrected $^{14}$C groundwater ages calculated from measured $^{14}$C activity in groundwater samples using a simple dissolution mass balance and the NETPATH model, and ages simulated by the reverse particle-tracking model.
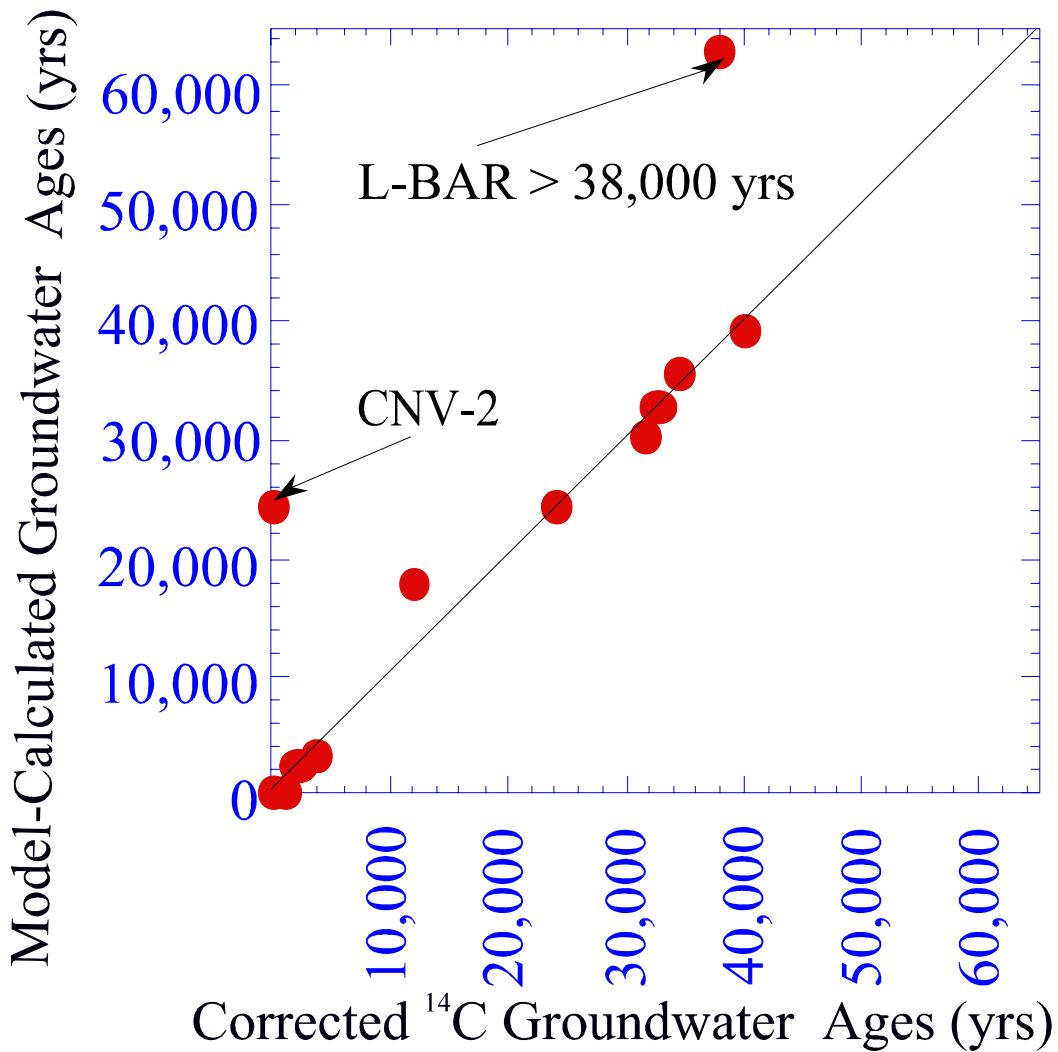
**Figure 17.** Graphical comparison of measured $^{14}C$ groundwater ages and model-calculated groundwater ages.

well sample compared with $^{14}C$ measured ages of 0 to > 38 kyr. Radiocarbon ages given for the MW monitoring wells, L-Bar and CNV-5 represent only minimum age constraints, due to the limits of $^{14}C$ dating. Therefore, minimum $^{14}C$ age limits are consistent with model-computed ages for wells in the L-Bar region.

5.4. Groundwater Flow Model Solution

### 5.4.1. Hydraulic Conductivities

The set of hydraulic conductivities that produced the best-fit run generally agree with published conductivity data, (Stone *et al.*, 1983, Risser *et al.,* 1984, Hydro-Engineering, 1981) obtained from pump tests, drawdown observations, and slug tests, as well as typical values for given lithologies (Table 7, Figures 17 & 18).  Pump test, slug test and drawdown data collected near L-Bar (located on the eastern side of the model cross-section) yielded hydraulic conductivity values ranging from $5.6 \times 10^{-5}$ m/s to $3.5 \times 10^{-8}$ m/s for the Two Wells sandstone aquifer (Hydro-Engineering, 1981).  The calibrated model uses a horizontal conductivity value of $2.2 \times 10^{-7}$ m/s from the Two Wells aquifer. Similar parity is observed in the other sandstone units.  The hydraulic conductivities obtained from the model calibration exercise represent average values of each layer over the extent of the cross-section.

The calibrated model yielded vertical hydraulic conductivity values of approximately $6 \times 10^{-9}$ m/s for shale units.  These values are rather high for shales (Neuzil, 1994). Fracturing due to volcanic activity and stresses from erosional unloading in the study area are most likely responsible for the high vertical conductivity of the Mancos Shale.  The model does not directly account for preferential flow through fractures but addressed enhanced flow by incorporating  higher bulk vertical hydraulic conductivities.  Stephens

| Unit | Kx (m/s) | Kz (m/s) | Kx used in model (m/s) | Kz Used in model (m/s) |
|---|---|---|---|---|
| Basalt | $10^{-11} - 10^{-7}$ (1) | | $3.2 \times 10^{-9}$ | $3.2 \times 10^{-9}$ |
| Point Lookout Sandstone | $3.2 \times 10^{-8}$ (2) | | $5.1 \times 10^{-8}$ | $5.1 \times 10^{-8}$ |
| Satan Tongue of Mancos Shale | | $10^{-13} - 10^{-9}$ (1) | $5.9 \times 10^{-9}$ | $5.9 \times 10^{-9}$ |
| Hosta Tongue of Point Lookout SS | $3.5 \times 10^{-8}$ (2) | | $5.1 \times 10^{-7}$ | $5.1 \times 10^{-8}$ |
| Gibson Coal Member of Crevasse Canyon | $< 3.2 \times 10^{-7}$ (2) | | $1.6 \times 10^{-7}$ | $1.6 \times 10^{-8}$ |
| Dalton Sandstone Mb of Crevasse Canyon | $3.2 \times 10^{-7}$ (2) | | $5.1 \times 10^{-7}$ | $5.1 \times 10^{-8}$ |
| Mulatto Tongue of Mancos Sh | | $10^{-13} - 10^{-9}$ (1) | $5.9 \times 10^{-9}$ | $5.9 \times 10^{-9}$ |
| Dilco Coal Mb of Crevasse Canyon | $< 3.2 \times 10^{-7}$ (2) | | $1.0 \times 10^{-7}$ | $1.0 \times 10^{-8}$ |
| Gallup Sandstone | $9.1 \times 10^{-7}$ (2) | | $1.9 \times 10^{-7}$ | $3.2 \times 10^{-8}$ |
| Mancos Shale (main body) | | $1.0 \times 10^{-10}$ (3) <br> $1- 6 \times 10^{-8}$ (4) | $5.9 \times 10^{-9}$ | $5.9 \times 10^{-9}$ |
| Two Wells Sandstone of Dakota SS | $< 1.3 \times 10^{-6}$ (2) <br> $10^{-5} - 10^{-8}$ (5) | | $2.2 \times 10^{-7}$ | $2.2 \times 10^{-8}$ |
| Whitewater Arroyo Sh of Mancos Sh | | $10^{-13} - 10^{-9}$ (1) | $5.9 \times 10^{-9}$ | $5.9 \times 10^{-9}$ |
| Paguate Sandstone of the Dakota SS | $< 1.3 \times 10^{-6}$ (2) | | $2.1 \times 10^{-7}$ | $2.1 \times 10^{-8}$ |
| Clay Mesa Shale of Mancos Shale | | $10^{-13} - 10^{-9}$ (1) | $5.9 \times 10^{-9}$ | $5.9 \times 10^{-9}$ |
| Cubero SS and Oak Canyon Mb of the Dakota SS | $< 1.3 \times 10^{-6}$ (2) | | $2.1 \times 10^{-7}$ | $2.1 \times 10^{-8}$ |
| Brushy Basin Mb of Morrison Fm | $1.2 \times 10^{-6}$ (6) | | $1.0 \times 10^{-7}$ | $1.0 \times 10^{-8}$ |
| Westwater Canyon SS Mb of Morrison Fm | $< 2.7 \times 10^{-6}$ (2) | | $4.8 \times 10^{-7}$ | $4.8 \times 10^{-8}$ |
| Recapture Shale Mb of Morrison Fm | | $10^{-13} - 10^{-9}$ (1) | $5.9 \times 10^{-9}$ | $5.9 \times 10^{-9}$ |
| Bluff - Cow Springs SS, Summerville Fm, Todilto LS, and Entrada SS | $4.0 \times 10^{-6}$ (2) | | $3.2 \times 10^{-7}$ | $3.2 \times 10^{-8}$ |
| Chinle Formation | $1.9 \times 10^{-8}$ (2) | | $6.3 \times 10^{-8}$ | $6.3 \times 10^{-9}$ |

Above data from: (1) *Domenico and Schwartz* [1990], (2) Conductivity values calculated from transmissivity values given in *Stone et al.* [1983], (3) *Stephens* [1984], (4) Cl- tracer calculations, *Pegram* [1995], (5) Well tests near L-Bar Mine by Hydro-Engineering [1981], (6) SS in Brushy Basin Member by *Risser et al.* [1984].

Key: Ss – Sandstone; Sh – Shale; Ls – Limestone; Mb – Member; Fm – Formation; Kx – Horizontal hydraulic conductivity; Kz – Vertical hydraulic conductivity.

**Table 7.** Comparison of published and calibrated model hydraulic conductivity values for each of the hydrostratigraphic units represented in the regional groundwater flow model, ordered from the top of the model package (basalt) to the bottom (Chinle Formation).

**Horizontal Hydraulic Conductivity Value Comparison**
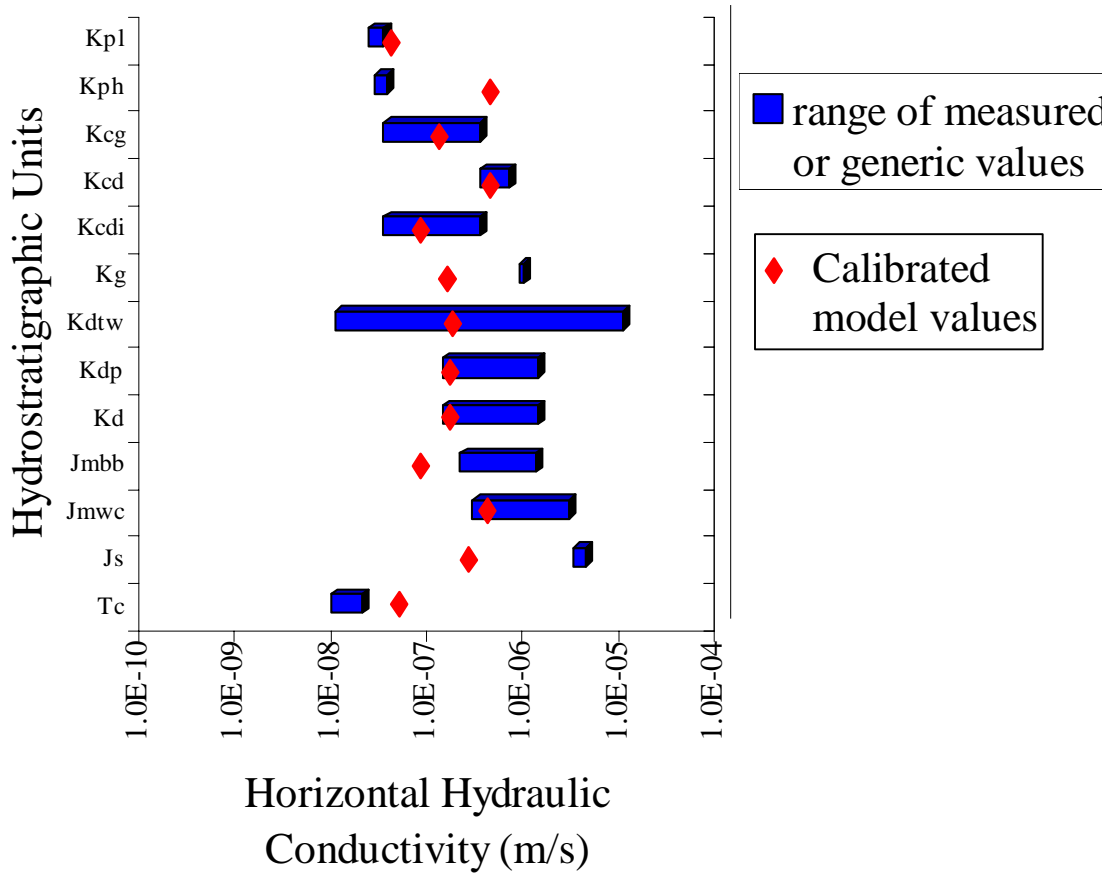
| | |
|---|---|
| Kpl | Point Lookout Sandstone |
| Kph | Hosta Tongue of the Point Lookout SS |
| Kcg | Gibson Coal Member |
| Kcd | Dalton Sandstone |
| Kcdi | Dilco Coal Mb of Crevasse Canyon |
| Kg | Gallup Sandstone |
| Kdtw | Two Wells Sandstone |

| | |
|---|---|
| Kdp | Paguate Sandstone |
| Kd | Cubero Sandstone and Oak Canyon Mb |
| Jmbb | Sandstone in Brushy Basin Mb |
| Jmwc | Westwater Canyon Sandstone Member |
| Js | Bluff-Cow Springs SS, Summerville Fm, Todilto LS, and Entrada SS |
| Tc | Chinle Formation |

**Figure 18.** Comparison between measured or generic values (or ranges of values) of horizontal hydraulic conductivity and those obtained through model calibration for sandstones and coal units.

**Figure 19.** Comparison of the generic range of values of vertical hydraulic conductivity for shales, locally measured field values, and those obtained through model calibration for shales units.

(1983) reported a Mancos Shale vertical hydraulic conductivity of $1.0 \times 10^{-10}$ m/s near Prewitt, New Mexico, northwest of the study site. This value is probably representative of the unfractured shale matrix. In contrast, estimates of $1 \times 10^{-8}$ m/s - $6 \times 10^{-8}$ m/s were obtained using as a tracer chloride from a nearby mine tailings pond (Pegram, 1995).

The 5 m high L-Bar Tailings pond, lined with sodium-chloride-treated clay was emplaced on top of the Mancos Shale from 1976 to 1982. Vertical leakage through the 39.6 m of Mancos Shale caused a pulse of high concentration chloride to reach the top of the underlying Two Wells Sandstone three years after tailings were first ponded. Based on the 3 year travel time, an average porosity of 12 %, and a vertical gradient of 0.85 (Pegram, 1995), the chloride tracer pulse yielded a vertical seepage velocity of $4.2 \times 10^{-7}$ m/s and a vertical hydraulic conductivity of $5.9 \times 10^{-8}$ m/s. Taking into account the area of the pond and the estimated volume of contaminated groundwater in three years time, the chloride mass balance method yielded a vertical seepage of $7.2 \times 10^{-8}$ m/s and a vertical hydraulic conductivity of $1.0 \times 10^{-8}$ m/s. The values obtained using chloride as a tracer, especially the chloride pulse method, are probably more representative of preferential flow through vertical fractures. Vertical hydraulic conductivities of the shales used in the calibrated model, $5.9 \times 10^{-9}$ m/s, represent an average of preferential flow through fractures and matrix flow.

### 5.4.2. Hydraulic Heads

Hydraulic head equipotentials calculated by the numerical model are shown on the model cross-section (Figure 20). Head contour curvature at the peak of Mount Taylor and at the top of Mesa Chivato indicates a downward component to the east-southeast lateral hydraulic gradient. Head contour curvature 20 km from the peak of Mount Taylor indicates an upward component to the hydraulic gradient.
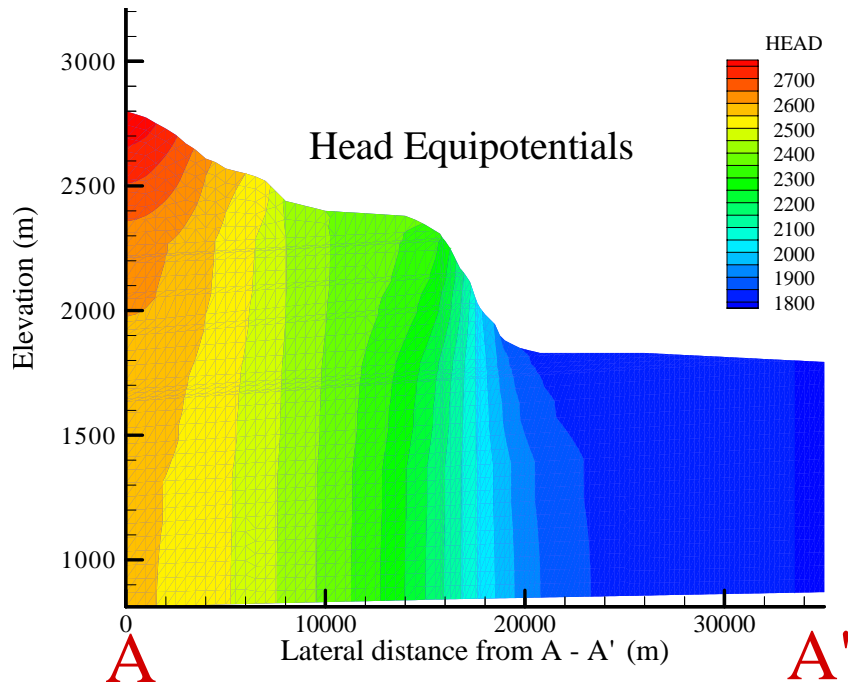
**Figure 20.** Computed heads calculated by the calibrated numerical model.

### 5.4.3. Fluid Flow Regime

Stream function equipotentials (streamlines) calculated by the model are shown on the model cross-section (Figure 21). Streamlines generally follow the hydraulic head gradient: flow occurs from west to east and is directed downward between Mount Taylor and Mesa Chivato and upward eastward of the mesa. Due mainly to the vertical exaggeration of the cross-section illustration, streamlines do not always appear perpendicular to head equipotentials (from Figure 20). If the cross-section were depicted true-to-scale, head equipotentials and streamlines would be nearly perpendicular. The effects of lithologic anisotropy present in this scenario impart some deviation of the flow direction from the hydraulic gradient in favor of the principle direction of highest hydraulic conductivity, which is horizontal in this case.

Streamlines that are more closely spaced delineate regions of greater flux. As indicated by the model-generated contour plot of stream functions on the cross-section, the greatest groundwater fluxes are observed near the base of Mesa Chivato. Figure 20 shows that areas of highest flux include the areas around Mesa Chivato, both at the top and at the base. Fluxes decrease dramatically with increasing distance eastward of the mesa.
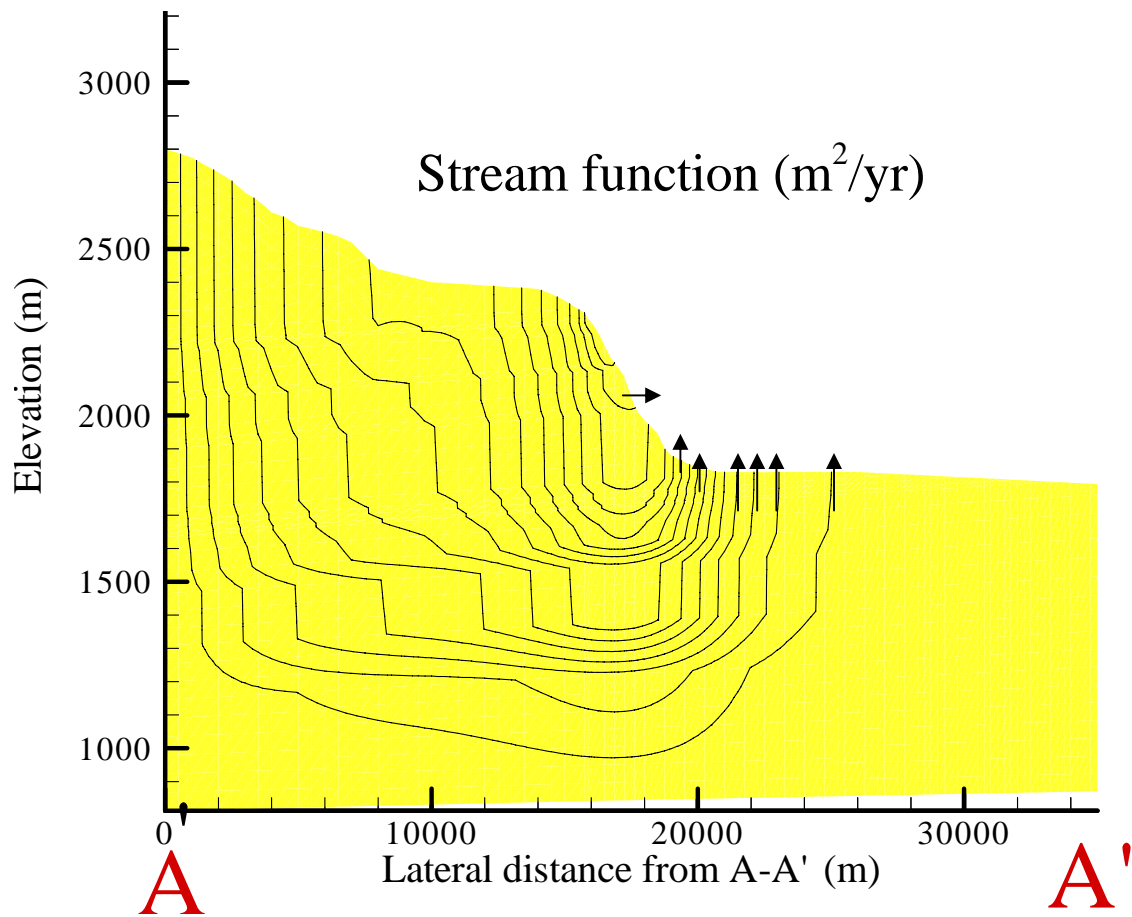
**Figure 21**. Computed streamlines calculated by the calibrated numerical model.

Temperature contours (Figure 22) indicate advective redistribution of heat in the recharge and discharge areas. The enthalpy redistribution results in a very low geothermal gradient in the recharge area and a high geothermal gradient in the discharge area. Descending cool fluids in the recharge area reduce groundwater temperatures as illustrated by depressed isotherms on the model cross-section beneath Mount Taylor. Ascending fluids advect geothermal heat toward the surface and thus uplift the isotherms in the discharge area (on the east side of the cross-section). High heat fluxes of up to 125 mW/m$^2$ are predicted by the model in areas of groundwater discharge. In contrast, low heat fluxes, of $< 25$ mW/m$^2$ are predicted in recharge areas.
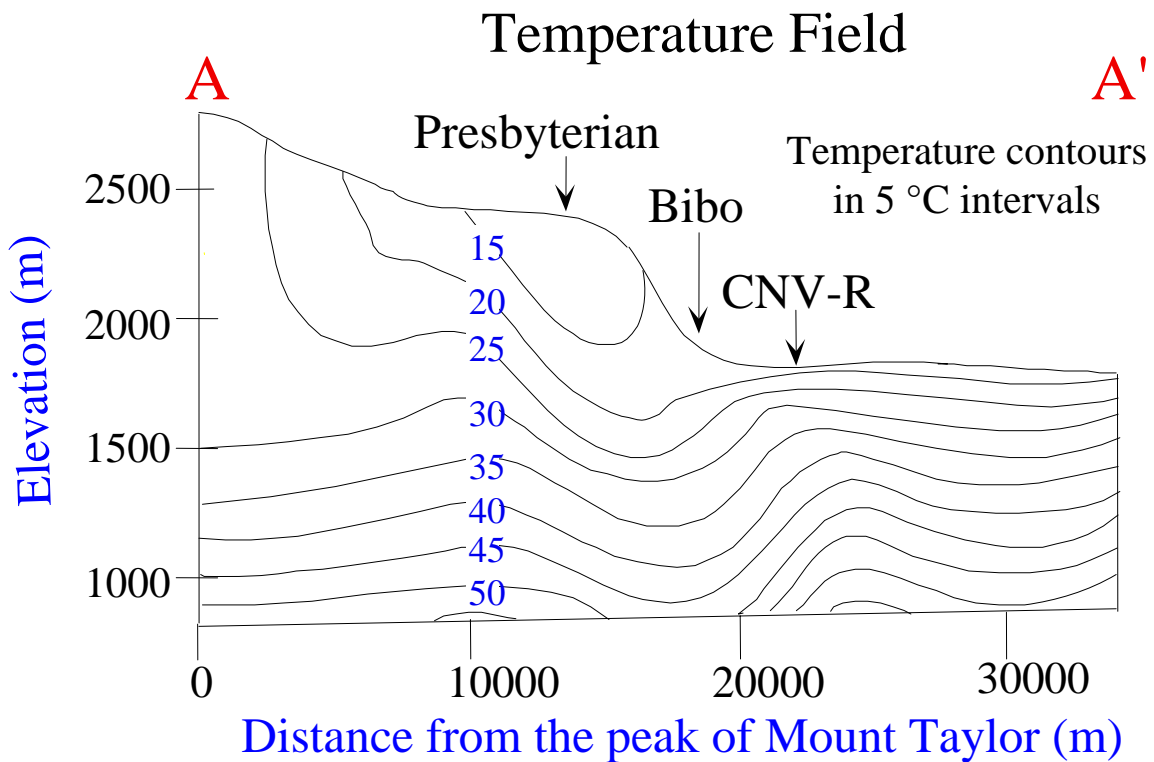


**Figure 22.** Computed temperature field calculated by the calibrated flow model.

73

5.5. Model Verification

Fluid flow and heat flow are closely coupled transport phenomena. Due to this strong coupling, the validity of the groundwater flow model could be tested by comparing groundwater temperatures measured in the field to the model-predicted temperatures at corresponding locations and depths.

Reiter (1974) presents a deep temperature profile in the general study area. Reiter completed a detailed geothermal analysis on several wells in the San Juan Basin including the 340 m deep well at Bibo. Reiter estimated a terrestrial heat flow of 108 mW/m$^2$ and a geothermal gradient of 34°C/km at Bibo, compared to the model prediction of 98 mW/m$^2$ and 31°C/km, respectively.

We measured a 40 m temperature profile from the vertical borehole drilled near Cerro Negro (CNV-R) as part of this study. A detailed description of methodology and raw data measurements are provided in Appendix F. The measured geothermal gradient at CNV-R was 56°C/km, compared to the model prediction of 44°C/km. It is quite possible that the high geothermal gradient measured at CNV-R is biased on the high side resulting from surface temperature effects. A deeper temperature profile would have secured a higher confidence level in the gradient measurement but would have required more sophisticated mechanical equipment for lowering and raising the probe. Regardless, the geothermal gradient near Cerro Negro is significantly higher than typical conductive geothermal gradients on the stable continent, suggesting upward advective heat transport.

The temperature profiles from Bibo (Reiter, 1974) and CNV-R agree well with the model-calculated depth temperature distributions for corresponding localities (Figure 23). For comparison, a model-computed temperature profile taken from the Presbyterian well is included in Figure 23. (The shallow depth of the Presbyterian well precluded temperature profiling field measurements). The Presbyterian well is located in the recharge zone and has a below-average model-calculated heat flow value and thermal gradient. In contrast, the Bibo and CNV-R wells, are located in the discharge zone; therefore, above-average heat flow values and thermal gradients are observed. The model-predicted stream functions indicate that water discharging near CNV-R should have circulated much deeper in the system and therefore acquired and transported greater amounts of heat than the fluid discharging at Bibo. These model predictions are consistent with the measured temperature data. The favorable comparison between the measured temperature profiles and the model predicted temperature profiles supports the accuracy of the model.
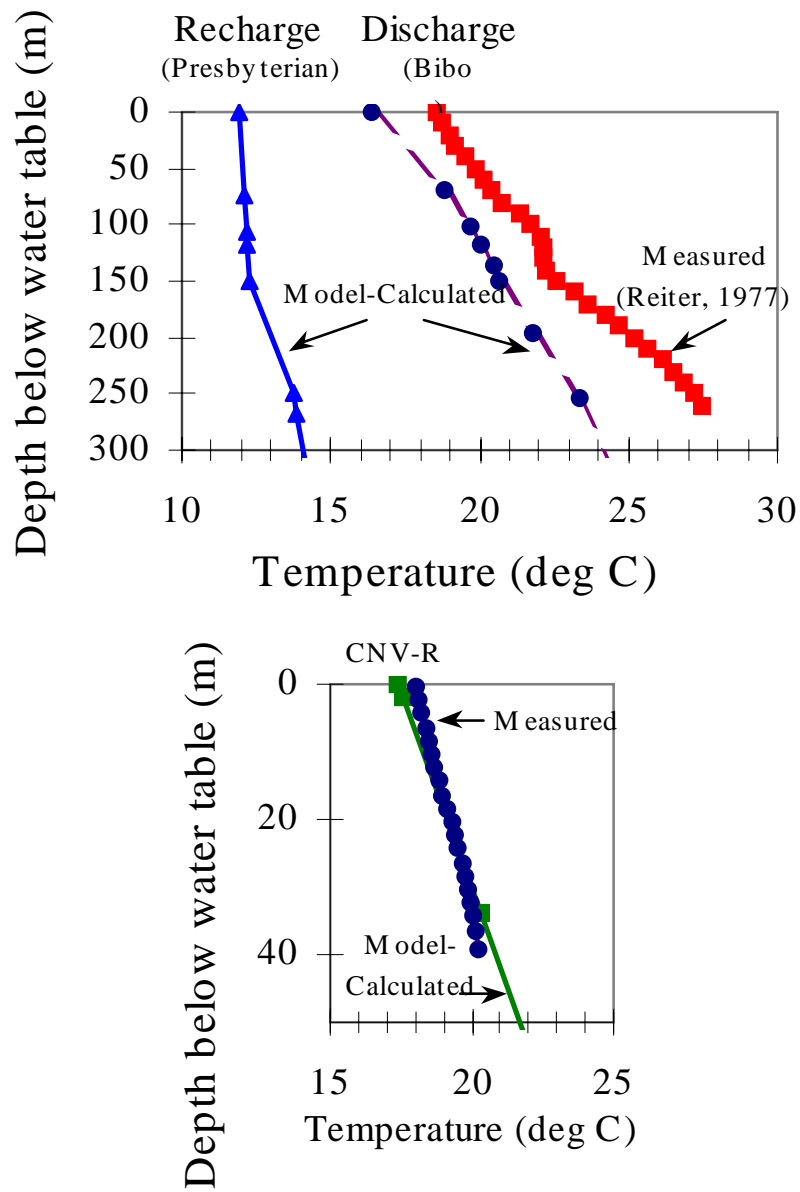
**Figure 23.** Measured and model-calculate temperature profiles from wells located along the A-A' cross-section in the discharge zone and recharge zone for comparison.

# 6.  ANALYSIS OF HYDROGEOLOGIC MODELING

## 6.1.  Regional Groundwater Flow Regime

### 6.1.1.  Groundwater Flow Pattern

Model-predicted streamlines (Figure 21) corroborate the *a priori* conception that topography is the main mechanism dominating the hydrogeologic regime.  The principal flow direction is from west-northwest to east-southeast (from A to A' along the model cross-section).  The groundwater is recharged between the top of Mount Taylor and the top of Mesa Chivato.  Flow is generally directed downward, until it reaches the deflection point coincident with the slope associated with Mesa Chivato (18 - 19 km from the peak of Mount Taylor) and then is directed upward.  Discharge is focused at the base of Mesa Chivato where low volume springs are observed in the field.  The model solution also predicts discharge in the topographically low region eastward of the mesa, including the area around Cerro Negro.  There is no obvious indication of discharge in this area where the water table is 40 - 60 m below ground surface.  The discrepancy between the model prediction and field observations led to further investigation of model boundary conditions and hydraulic parameters.  We performed numerous simulations to test alternative conceptual models that might explain this aspect of the flow system.

### 6.1.1.1.  Effect of Eastern Boundary Condition

To assess the influence of the imposed eastern boundary condition on the model flow solution, the boundary was changed from a no flow condition to an open boundary for heads and stream functions.  Using the hydraulic conductivities obtained from the original $^{14}$C data calibration, the flow solutions attained when no-flow and open conditions were imposed on the eastern boundary were nearly identical.  Of 105 stream functions, only 3 crossed the eastern boundary.  This suggests that the eastern boundary has little effect on the model solution when the hydraulic conductivity contrast between units does not exceed 2.5 orders of magnitude.  As will be demonstrated in section 6.1.1.3., the eastern boundary imposes greater influence on the model solution when the hydraulic conductivity contrast between units is increased above 2.5 orders of magnitude.

### 6.1.1.2.  Effect of Water Table Configuration

To assess the influence of the water table configuration on the model flow solution, a more gently sloping water table was imposed.  The flow solution was affected only slightly.  Groundwater flow patterns were similar, but flow rates varied somewhat. Model-predicted ages for the Bibo, Seboyeta and Moquino wells were higher than measured $^{14}$C ages, and model-predicted ages for the downgradient wells were lower than measured $^{14}$C ages.

6.1.1.3.  Effect of Increased Macroanisotropy


The contrast in hydraulic conductivity between units was increased by one to three orders of magnitude to assess the effect of macroanisotropy on the flow solution for an open eastern boundary condition.  The flow pattern was affected dramatically.  As the anisotropy between units increased, horizontal flow became dominant over upward flow in the region east of Mesa Chivato.  Increasingly high anisotropic parameterization focused more of the flow out out of the eastern boundary of the model.  Figure 24 shows the groundwater flow pattern generated when hydraulic conductivity contrasts between shales and sandstones were about 3 to 4 orders magnitude.


Reverse particle-tracking results for these simulations gave very small calculated age ranges between wells near the base of Mesa Chivato and wells near Cerro Negro, contrary to measured ^{14}C data.  Numerous simulations were conducted using various combinations of hydraulic conductivities.  No simulations came close to reproducing the ^{14}C measured ages when the macroanisotropy was increased beyond 2.5 orders of magnitude.  Table 8a lists the hydraulic conductivities used to produce the model solution illustrated in Figure 24.  Table 8b compares model-calculated and observed ages for this solution.  The solution produced a poor match to observed groundwater ages, but was the best fit run for simulations that generated flow out of the eastern boundary of the model.  Also, the model simulations in which flow was directed out of the eastern boundary poorly reproduced observed temperature profiles;   model-calculated temperature gradients were lower than observed, indicative of a conductive thermal profile.
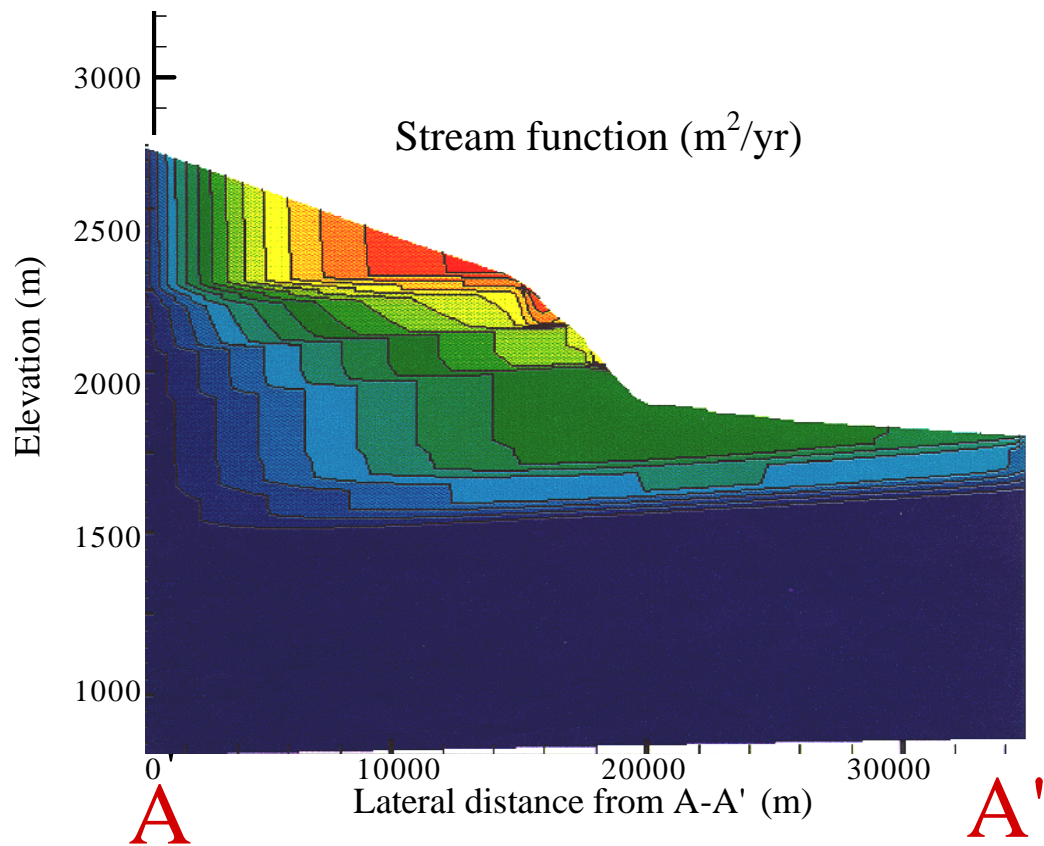
**Figure 24.** Model-calculated stream functions for increased anisotropic parameterization. Hydraulic conductivites used for this solution are given in the following table (8a).

| Unit | Kx used in model (m/s) | Kz used in model (m/s) |
|---|---|---|
| Basalt | $9.5 \times 10^{-9}$ | $9.5 \times 10^{-9}$ |
| Point Lookout Sandstone | $1.3 \times 10^{-6}$ | $1.3 \times 10^{-7}$ |
| Satan Tongue of Mancos Shale | $9.5 \times 10^{-11}$ | $9.5 \times 10^{-11}$ |
| Hosta Tongue of Point Lookout SS | $1.3 \times 10^{-6}$ | $1.3 \times 10^{-7}$ |
| Gibson Coal Member of Crevasse | $1.6 \times 10^{-7}$ | $1.6 \times 10^{-8}$ |
| Dalton Sandstone Mb of Crevasse Canyon | $1.3 \times 10^{-6}$ | $1.3 \times 10^{-7}$ |
| Mulatto Tongue of Mancos Sh | $9.5 \times 10^{-11}$ | $9.5 \times 10^{-11}$ |
| Dilco Coal Mb of Crevasse Canyon | $1.0 \times 10^{-7}$ | $1.0 \times 10^{-8}$ |
| Gallup Sandstone | $1.3 \times 10^{-6}$ | $1.3 \times 10^{-7}$ |
| Mancos Shale (main body) | $9.5 \times 10^{-11}$ | $9.5 \times 10^{-11}$ |
| Two Wells Sandstone of Dakota SS | $3.2 \times 10^{-7}$ | $3.2 \times 10^{-8}$ |
| Whitewater Arroyo Sh of Mancos Sh | $9.5 \times 10^{-11}$ | $9.5 \times 10^{-11}$ |
| Paguate Sandstone of the Dakota SS | $1.6 \times 10^{-7}$ | $1.6 \times 10^{-8}$ |
| Clay Mesa Shale of Mancos Shale | $9.5 \times 10^{-11}$ | $9.5 \times 10^{-11}$ |
| Cubero SS and Oak Canyon Mb of | $3.2 \times 10^{-6}$ | $3.2 \times 10^{-7}$ |
| Brushy Basin Mb of Morrison Fm | $1.0 \times 10^{-8}$ | $1.0 \times 10^{-8}$ |
| Westwater Canyon SS Mb of Morrison Fm | $3.2 \times 10^{-6}$ | $3.2 \times 10^{-7}$ |
| Recapture Shale Mb of Morrison Fm | $9.5 \times 10^{-11}$ | $9.5 \times 10^{-11}$ |
| Bluff - Cow Springs SS, Summerville Fm, Todilto LS, and Entrada SS | $3.2 \times 10^{-7}$ | $3.2 \times 10^{-8}$ |
| Chinle Formation | $6.3 \times 10^{-9}$ | $6.3 \times 10^{-10}$ |

**Table 8a.**

| Well | Corrected [14]C Age (yr) | Model-Calculated Age (yr) |
|---|---|---|
| Presbyterian | Modern | 200 |
| Elkins | Modern | 700 |
| Bibo | $2.180 \pm 120$ | 16,000 |
| Seboyeta | $3.630 \pm 100$ | 26,000 |
| Moquino | $12.200 \pm 500$ | 26,000 |
| CNV-W2 | $-9.300 \pm 60$ | 31,000 |
| CNV-W3 | $24.000 \pm 2.800$ | 36,000 |
| CNV-W5 | $33.500 \pm 9.500$ | 37,000 |
| MW-64 | $> 31,500$ | 37,000 |
| MW-65 | $> 32,800$ | 34,000 |
| MW-60 | $> 34,500$ | 34,000 |
| MW-68 | $> 39,900$ | 26,000 |
| L-Bar | $> 38,300$ | 31,000 |

**Table 8b.**

**Table 8.** a) Hydraulic conductivities used in the model to produce flow regime illustrated in Figure 24. b) Model-calculated ages as compared with ^{14}C ages.

6.1.1.4. Summary of Sensitivity Analyses

Modeling results from the above modifications led us to believe that the original calibrated solution closely approximates the actual hydrogeology of the southeastern San Juan Basin. One notable feature of the $^{14}$C ages is that although the Bibo and Seboyeta wells are located just 3-7 km upgradient from Cerro Negro and the eastern wells, they have much younger $^{14}$C ages (2-4 kyr vs. >20 kyr). The observed wide $^{14}$C age distribution could only be reproduced numerically if the groundwater from the Bibo and Seboyeta locations experienced shorter flowpaths than groundwater from the downgradient wells. This implies that groundwater in aquifers near Cerro Negro must have moved much deeper in the system in order to have long residence times relative to groundwater near Mesa Chivato. Such a groundwater flow pattern, and thus a good match of observed and model-calculated ages, could only be realized when the anisotropy of the entire modeled domain was less than 2.5 orders of magnitude. The model solution of upward flow in a region in which there is no observable discharge other than springs located just below the mesa can be rationalized if we consider the role of highly permeable alluvial valley fill. The hydraulic conductivity of the alluvium is >5 orders of magnitude higher than underlying sediments (Stone *et al.,* 1983), and alluvial channels have been cited as principal locations of discharge in some areas of the San Juan Basin (Brown, 1976; Stone *et al.,* 1983). We hypothesize that alluvial valley fill similarly accomodates discharge in the flat region east of Mesa Chivato included in the model. The upward flux of groundwater reaches the very permeable drainageways containing alluvial valley fill, and efficiently drains laterally. Based on sensitivity modeling results

(particularly the inability to match observed and model-predicted groundwater ages for > 2.5 orders of magnitude macroanistropy), hydraulic and thermal evidence (presented in sections 6.2 and 6.3 respectively) of an upward gradient in the region, and a plausible phenomenon for accomodating discharge in the vicinity of Cerro Negro, we assume the original calibrated model solution to be the most reasonable.

### 6.1.2. Groundwater Flow Rates

Model-calculated groundwater flow velocities vary about 2 orders of magnitude from Mesa Chivato to the L-Bar discharge zone east of Cerro Negro. Table 9 provides a summary of model-calculated average groundwater flow velocities through the aquifers and aquitards of interest in this study in 3 distinct zones of the regional flow system: 1) the Mesa Chivato recharge area 2) Bibo – Cerro Negro discharge area, 3) Cerro Negro – L-Bar discharge area. Flow rates decrease with increasing distance from Mount Taylor due to the considerably subdued topographic gradient, and consequently lower hydraulic gradient. It is important to point out that flow rates determined from $^{14}$C data (travel times) and the horizontal distance between sample locations would underpredict groundwater flow rates. The $^{14}$C method assumes that a straight line horizontal distance is representative of the flowpath and ignores any vertical movement along the pathway (Note that the model illustrations are vertically exaggerated, so the model-described flowpath lengths are not longer than horizontal distances to the degree that the illustrations suggest). Furthermore, as the groundwater flow model demonstrates, samples collected from wells at the base of Mesa Chivato have been subjected to shorter flowpaths than samples collected from the wells around Cerro Negro which presumably were recharged at higher elevations on Mount Taylor. Flow rates determined from the hydrogeologic model do account for both the 2-dimensionality in the flowpaths and the variance in flowpath distances.

| Geologic Unit | Seepage Velocity Recharge Area (m/yr) | Seepage Velocity Bibo–Cerro Negro (m/yr) | Seepage Velocity Cerro Negro-L-Bar (m/yr) |
|---|---|---|---|
| Two Wells SS | 3.90 | 0.29 | 0.07 - 0.09 |
| Whitewater Arroyo Sh | 0.62 (v*) | 0.24 – 0.26 (v*) | 0.06 (v*) |
| Paguate SS | 2.93 – 3.69 | 0.16 – 0.19 | 0.05 |
| Clay Mesa Shale | 0.64 (v*) | 0.20 - 0.22 (v*) | 0.03 |
| Cubero/Oak Canyon Mb | 4.26 – 5.92 | 0.21 | 0.11 |

**KEY:** v* = vertical flow rate (all other values are horizontal flow rates)

**Table 9.**  Summary of the average groundwater flow rates determined from calibrated groundwater flow model.

6.2. Groundwater Flow Regime Near Cerro Negro

6.2.1. Groundwater Flow Pattern

Cerro Negro is located within the regional discharge zone. In the vicinity of Cerro Negro, groundwater flow has a strong upward component through sandstone and shale layers. Hydraulic head data from wells in the L-Bar mine tailings region corroborates the model solution of an upward gradient in the region. For example, the hydraulic head in a deep well (bottom of well = 867 m), L-Bar 2, is 1897 m ( about 2 meters below ground surface), whereas more shallow wells in the same region have hydraulic heads ranging from 1829 – 1849 m. Table 10 shows hydraulic head data from wells in the model-predicted discharge area ranging in depth.

| Well | Surface Elevation | Elevation of Bottom of Well | Head | Projected location on cross-section from A | Projected on A-A' from |
|------|------|------|------|------|------|
| | (m) | (m) | (m) | (km) | |
| 3 | 1899 | 1709 | 1850 | 20.8 | 2.85 km south |
| 10 | 1894 | 1787 | 1833 | 20.4 | 3.85 km south |
| Pueblo t-3 | 1907 | 1765 | 1884 | 20.2 | 6.25 km south |
| PL | 1895 | 1778 | 1844 | 21.6 | 6.60 km south |
| P.S.2 | 1876 | 1857 | 1877 | 21.4 | 7.30 km south |
| L-Bar 2 | 1900 | 867 | 1896.8 | 25.5 | 1.80 km south |
| LJ 205 | 1877 | 1718 | 1848.9 | 26.15 | 1.30 km south |
| LBR | 1855 | 1790 | 1835.8 | 27.7 | 2.95 km south |
| Anaconda 1 | 1878 | 1759 | 1828.8 | 26.9 | 2.35 km south |

**Table 10.** Hydraulic head data from wells in the model-predicted discharge area.

### 6.2.2. Groundwater Flow Rates

Average flow rates near Cerro Negro in the rock layers that were drilled for this study range from about 0.1 – 0.3 m/yr (Table 9).  The model-predicted vertical seepage velocities through the shale units are on the order of 0.20 – 0.26 m/yr  near Cerro Negro. It is likely that vertical fractures in the shale units are responsible in part for the relatively high vertical flow rates.

### 6.3.  Thermal Regime Near Cerro Negro

An above average geothermal gradient is observed below and to the east of Mesa Chivato, including the vicinity of Cerro Negro.  The most reasonable explanation for such high subsurface heat flow in this geologic setting is that deep-heated groundwater  is transporting heat towards the surface.  Conductive heat flow alone would not be able to produce such a high geothermal gradient.  Upward advective flow, perhaps enhanced by the presence of near vertical fractures in the aquitards, is required to account for the high geothermal gradient measured in the study area.

# 7.  IMPLICATIONS FOR ORIGINS OF SUBSURFACE MICROORGANISMS

## 7.1.  Microbial Transport

Evidence of microorganisms was detected in many samples collected at the Cerro Negro site, including some positioned near the volcanic intrusion, indicating that microbes were able to re-populate a previously sterile zone within the past 3 million years.  The most probable mechanism of microbial re-colonization is through advective groundwater transport.  Hydrogeologic modeling results obtained from this study further support groundwater microbial transport as the agent responsible for the re-colonization of these rocks, particularly the sandstones.  Considerable groundwater has flowed through the thermal aureole within the 3 million years since neck emplacement. Groundwater flow velocities calculated by hydrogeologic modeling permit relatively rapid transport of microbes back into the zone sterilized at the time of intrusion.  Using highly conservative values of a 0.1 m/yr average flow rate, a 100 meter thermal aureole radius, the entire sterilized zone (200 meter diameter) could have been recolonized within 2,000 years after the intrusive body cooled if microbes are transported at approximately the same rate as groundwater advection.  Given a time period of 3 million years, microbial retardation during advection would have had to exceed a linear retardation factor of 1500 to prevent repopulation of the thermal aureole.  Although the sorption characteristics of microbes are not currently well-constrained, such a high degree of retardation, linear or non-linear, is unlikely.  The estimate of rapid recolonization is consistent with the absence of any

remnant pattern in microbiology reflecting past heating; i.e., there is no gradational trend of decreasing microbial activity with proximity to the volcanic neck.

## 7.2. Microbial In Situ Survival

Contrary to original expectations, microbial activity was detected in some shale samples collected near the intrusion.  It was initially believed that the small porethroats of the shales would inhibit transport of microorganisms back into the previously sterilized zone. In that case, the original inhabitants hypothesis would be supported by the existence of microbes in shale located outside of the previously sterilized zone.  However, it is now evident that the shale contains vertical fractures, especially prevalent near the main volcanic plug, that could serve as conduits for relatively rapid advection of microorganisms and provide increased pore space for microbial growth.  Fredrickson *et al*. (1997) found little or no microbial activity in intact, unfractured shale samples and high rates of microbial activity in material with a significant fraction of porethroat diameters >0.2 µm.  Calculations using chloride mass balance methods (at the L-Bar tailings pond described in Pegram, 1995 and briefly mentioned in section 5.4.1. of this document) and hydrogeologic modeling results indicate relatively high vertical flow rates through the main body and interbeds of the Mancos Shale confirming the importance of fracture flow.  Consequently, the Cerro Negro Microbial Origins study was not able to provide conclusive evidence concerning the in situ survival origin of subsurface microorganisms in these strata, since no lithologic unit was effectively "closed" to potential microbial transport subsequent to sediment deposition.

# 8. IMPLICATIONS FOR THE SHALE/ SANDSTONE INTERFACE HYPOTHESIS

Both physical and chemical parameters likely control the vertical distribution of microbial activity within a shale/sandstone sequence.  An important physical parameter influencing microbial distribution in the subsurface is porethroat size.  Minimal microbial activity measured in the shales, particularly where fracturing is absent, probably results from the significantly smaller porethroats which inhibit microbial growth and transport (Fredrickson *et a*l., 1997).  An important chemical parameter influencing microbial distribution is porewater geochemistry, which is governed largely by lithology.  Shale, because of its relatively high organic content, is generally abundant in elecron donors such as organic acids, and sandstone is often abundant in electron acceptors such as sulfate.  McMahon and Chapelle (1991) showed that diffusion of organic acids from fine-grained aquitard sediments into electron acceptor-rich coarse-grained aquifers provided an environment near the aquitard/aquifer contact that was favorable to respiratory bacteria.  Within the 200-300 m deep package of Cretaceous shale and sandstone layers, some of the highest rates of microbial activity were measured in the upper portion of sandstone units near the shale interfaces (Fredrickson *et al*., 1997).  Krumholz *et al*. (1997) also detected increased sulfate reduction activity in shale-sandstone interfaces in the vicinity of Cerro Negro.  However, the irregularities in the microbial activity pattern within the sandstone units are not explained by the 1-dimensional nutrient diffusion hyptohesis put forth by McMahon and Chapelle (1991). The complexity of both the nutrient distribution and the hydrologic regime probably contribute to these patterns, and

preclude a simple explanation of solute-transport-controlled microbial distribution. The distribution of sulfate, probably the most important electron acceptor in this case, is not clearly correlated with lithology (McKinley, unpublished data, 1996). The strong upward flow in the vicinity of Cerro Negro, indicated by hydrogeologic modeling, should enhance the transport of nutrients out of the shale layers. The amount of nutrient leaching with upward flow, however, may be reduced due to significant water flux through shale fractures. Diffusion across shale/sandstone interfaces is also likely to be a significant mechanism for the cross-stratigraphic migration of organic nutrients. Detailed explanation of the formation-scale nutrient transport and biochemical reactions is beyond the scope of this investigation, but our results do demonstrate that strong vertical hydraulic gradients and multi-porosity create a much more complex transport/reaction scenario than the simple one-dimensional diffusion-controlled model envisioned for the interface hypothesis.

## 9. CONCLUSIONS

Hydrogeologic modeling has been used to characterize present-day groundwater flow patterns and flow rates in the southeastern San Juan Basin, New Mexico. Detailed hydrologic characterization was important in analyzing microbial data obtained from 200-300 meter deep cores, since groundwater provides both a means of transport and nutrient supply for microorganisms. A cross-sectional groundwater flow model taken from the peak of Mount Taylor (the regional topographic high) to 35 km east-southeast parallel to flow, was calibrated using reaction path-corrected $^{14}C$ groundwater dates from 13 groundwater samples. Reverse particle tracking was used to compare measured $^{14}C$ ages with computed travel times. Numerous simulations were run for various hydraulic conductivities of alternating sandstone and shale units in order to produce the best match of observed and computed groundwater ages. Model sensitivity analyses indicated that a contrast in hydraulic conductivity of less than 2.5 orders of magnitude between hydrostratigraphic units was required to reproduce the $^{14}C$ dates, emphasizing the role of vertical fractures in the shale units. The model-predicted thermal regime solution agreed well with available temperature profile data. The calibrated model solution showed a strong component upward flow in the vicinity of Cerro Negro where groundwater flow rates ranged from 0.1 – 0.3 m/yr. Although the region around Cerro Negro does not display obvious surface expressions of discharge (other than low volume springs at the base of Mesa Chivato), several lines of evidence support the model solution indicating upward flow in the area. These include deep well potentiometric data indicating an upward head gradient and above-average measured geothermal gradients that can best be

explained by upward advective heat flow. Furthermore, it is quite probable that the upward flux of groundwater is being accomadated in the shallow subsurface through highly permeable alluvial-filled channels that laterally conduct flow.

The synthesis of microbiological, geochemical and hydrogeologic data obtained from research completed under the Cerro Negro Microbial Origins Project confirms that groundwater plays an important role in the distribution of microorganisms in subsurface environments by providing a medium for the transport of cells and nutrients for maintaining microbial populations. Microbes have succeeded in re-colonizing a sterilized zone following the emplacement of a volcanic intrusion at 3.39 Ma. Based on calculated groundwater flow rates in the vicinity of the volcanic neck, relatively rapid re-colonization (on the order of $> 0.1$ m/yr subsequent to intrusion and dissipation of most of the associated heat) was possible through microbial transport in groundwater. Groundwater flow rates provide an upper limit for microbial re-colonization rates. The actual timing of re-colonization would depend on 1) the extent of the thermal aureole, 2) the cooling history of the intrusion and affected sediments, and 3) the sorptive properties of microorganisms. Currently, these factors are not well-constrained. However, even assuming highly conservative estimates of these parameters, calculated groundwater velocities far surpass rates required to permit microbial re-colonization within the past 3 million years.

Present-day microbial activity shows no indication of the paleothermal gradient imposed by the volcanic intrusion 3.39 Ma. This homogeneity is consistent with the relatively

high flow rates determined from geochemical and hydrogeological modeling that would have resulted in repeated flushing of the thermal aureole. In hindsight, it is recognized that a similar study conducted at a much more recently sterilized zone might have produced results in which the paleothermal signature was preserved in the microbial data (i.e., partial re-colonization of the thermal aureole could be observed). Ideally, effective microbial transport properties could be then determined.

The increased microbial activity observed at several sandstone/ shale interfaces in the Cerro Negro boreholes supports a modified version of the interface theory proposed by McMahon and Chapelle (1991). The strong component of upward advection in the study area serves to enhance the transport of dissolved organic matter into the sandstones. Downward diffusion of organic acids from the shale matrix into the sandstones is probably also important. This study illustrates the complexities of nutrient release, transport, and consumption in subsurface environments. Quantification will require a detailed understanding of both subsurface biogeochemistry and groundwater flow regimes.

# REFERENCES

Bear, J., *Dynamics of Fluids in Porous Media*, Elsevier, New York, 1972.

Brown, D. R. *Hydrogeology and water resources of the Aztec Quadrangle, San Juan County, New Mexico*, unpublished Geology Master's Thesis, 174 pp., New Mexico Institute of Mining and Technology, Socorro, NM, 1976.

Chapelle, F. H., *Ground-Water Microbiology and Geochemistry*, John Wiley & Sons, New York, 424 pp., 1993.

Chapelle, F. H. and  P. B. McMahon, Geochemistry of dissolved inorganic carbon in a coastal plain aquifer. 1. Sulfate from confining beds as an oxidant in microbial $CO_2$ production.  *J. Hydrol.*, *127*, 85-108, 1991.

Colwell, F. S., G. J. Stormberg, T. J. Phelps, S. A. Birnbaum, J. McKinley, S. A. Rawson, C. Veverka, S. Goodwin, P. E. Long, B. F. Russell, T. Garland, D. Thompson, P. Skinner, and S. Grover,  Innovative techniques for collection of saturated and unsaturated subsurface basalts and sediments for microbiological characterization.  *J. Microbiol. Methods  15*, 279-292, 1992.

Craigg, S. D., W. L. Dam, J. M. Kernodle, and G. W. Levings, Hydrogeology of the Dakota Sandstone in the San Juan structural basin, New Mexico, Colorado, Arizona and Utah, *U. S. Geol. Surv. Hydrol. Invest. Atlas HA-720-I,* 1989.

De Josselin de Jong, G., Singularity distributions for the analysis of multiple fluid flow through porous media, *J. Geophys. Res.*, *65*, 3739-3758, 1960.

de Marsily, G., Quantitative Hydrogeology, 440 pp., Academic, San Diego, CA, 1986.

Deming, D., Catastrophic release of heat and fluid flow in the continental crust, *Geology*, *20*, 83-86, 1992.

Deming, J.W., and J. A. Baross, Deep-sea smokers: Windows to the subsurface biosphere?, *Geochim. Cosmochim. Acta*, *57*, 3219-3230, 1993.

Domenico, P. A., and F. W. Schwartz, *Physical and Chemical Hydrogeology*, 824 pp., John Wiley & Sons, New York, pp. 26, 65, 1990.

Evans, D. G. and J. P. Raffensperger, On the Stream Function for Variable-Density Groundwater Flow, *Water Resour. Res., 28,* 2141-2145, 1992.

Fogg, G. E. and R. K. Senger, Automatic generation of flow nets with conventional groundwater modeling algorithms, *Groundwater, 23,* 336 – 344, 1985.

Freeze, R. A., and J. A. Cherry, *Groundwater,* Prentice-Hall, Inc., New Jersey, 604 pp., 1979.

Fredrickson. J. K., T. T. Garland, R. J. Hicks, J. M. Thomas, S. W. Li, and S. M. McFadden, Lithotrophic and heterotrophic bacteria in deep subsurface sediments and their relation to sediment properties, *Geomicrobiol. J.*, *7*, 53-66, 1989.

Fredrickson, J. K., D. L. Balkwill, J. M. Zachara, S. W. Li, F. J. Brockman, and M. A. Simmons, Physiological diversity and distributions of heterotrophic bacteria in deep Cretaceous sediments of the Atlantic coastal plain, *Appl. Environ. Microbiol.*, *57*, 402-411, 1991.

Fredrickson, J. K., and T. J. Phelps, Subsurface drilling and sampling, in *Manual of Environmental Microbiology*, edited by C. J. Hurst, G. R. Knudsen, M. J., McInerney, L. D. Stetzenbach, and M. V. Walter, pp. 526–540, American Society for Microbiology, Washington, D. C., 1996.

Fredrickson, J. K., J. P. McKinley, B. N. Bjornstad, P. E. Long, D. B. Ringelberg, D. C. White, L. R. Krumholz, J. M. Suflita, F. S. Colwell, R. M. Lehman, T. J. Phelps, and T. C. Onstott, Pore-size constraints on the activity and survival of subsurface bacteria in a late Cretaceous shale-sandstone sequence, northwestern New Mexico, *Geomicrobiol. J., 14,* 183-202, 1997.

Gabin, V. L. and L. E. Lesperance, *New Mexico climatalogical data: Precipitation, temperature, evaporation and wind: Monthly and annual means 1850-1975*, pp. 422-436, W. K. Summers and Associates, Socorro, New Mexico, 1977.

Gao, G., Long, P.E., Hallett, R.B., Riciputi, L., Pratt, L.M., Feigenson, M., Diagenesis and Thermal Regime of the Dakota-Mancos Sandstone/Shale Sequence: Constraints on the Investigation of Subsurface Bacteria, unpublished manuscript, 14 pp., 1995.

Ghiorse, W. C., and J. T. Wilson, Microbial ecology of the terrestrial subsurface, *Adv. Appl. Microbiol.*, 33, 107-172, 1988.

Green, M. W. and C. T. Pierson, A summary of the stratigraphy and depositional environments of Jurassic and related rocks in the San Juan Basin, Arizona, Colorado, and New Mexico, *New Mexico Geol. Soc., Guidebook 28th Field Conference*, pp. 147-152, 1977.

Green, P.F., A new look at statistics in fission track dating, *Nucl. Tracks, 5*, 77-86, 1981.

Green, P.F., On the thermo-tectonic evolution of Northern England: evidence from fission track analyses, *Geol. Mag., 123*, 493-506, 1986.

Haldeman, D. L., P. S. Amy, D. Ringelberg, and D. C. White, Characterization of microbiology within a 21 $m^3$ section of rock from the deep subsurface, *Microb. Ecol.*, *26*, 145-159, 1993.

Hallett, R.B., Geologic and hydrologic summary of Cerro Negro, Golder Federal Services, Los Alamos, NM, 15 pp., 1994.

Hallett, R.B., P. R. Kyle, and W. C. McIntosh, Paleomagnetic and $^{40}Ar/^{39}Ar$ age constraints on the chronologic evolution of the Rio Puerco volcanic necks and Mesa Prieta, west-central New Mexico: Implications for transition zone magmatism, *Geol. Soc. Am. Bull.*, *109*, 95-106, 1997.

Hydro-Engineering, Ground-water hydrology near the L-Bar tailings reservoir, prepared for Sohio Western Mining Company by Hydro-Engineering, Casper, Wyoming, 1981.

Kelley, V. C., Regional structure of the Sand Juan Basin: New Mexico Geological Society, Guidebook 1st Field Conference, 101-108, 1950.

Kernodle, J. M., G. W. Levings, S. D. Craigg, and W. L. Dam, Hydrogeology of the Gallup Sandstone in the San Juan structural basin, New Mexico, Colorado, Arizona and Utah, *U.S. Geol. Surv. Hydrol. Invest. Atlas HA-720-H*, 2 sheets, 1989.

Kestin, J., H. E. Khalifa, and R. J. Correia, Tables of the dynamic and kinematic viscosity of aqueous NaCl solutions in the temperature range 20-150°C and the pressure range 0.1-35 MPa, *J. Phys. Chem. Ref. Data, 10*, 71-87, 1981.

Kieft, T. L., Dwarf cells in soil and subsurface terrestrial environments, in *Non-culturable Microorganisms in the Environment*, edited by R. R. Colwell, and D. J. Grimes, Chapman & Hall, New York, 1997 (in press).

Kieft, T. L., J. K. Fredrickson, J. P. McKinley, B. N. Bjornstad, S. A. Rawson, T. J. Phelps, F. J. Brockman, and S. M. Pfiffner, Microbiological comparisons within and across contiguous lacustrine, paleosol, and fluvial subsurface sediments, *Appl. Environ. Microbiol.*, *61*, 749-757, 1995.

Krumholz, L. R., J. P. McKinley, G. A. Ulrich, and J. M. Suflita, Confined subsurface microbial communities in Cretaceous rock, *Nature, 386,* 64-66, 1997.

Kunkel, K. E., *Temperature and Precipitation Summaries for Selected New Mexico Locations,* New Mexico Depart. of Agriculture document, 190 pp., 1984.

Madsen, E. L., and W. C. Ghiorse, Ground water microbiology: subsurface ecosystems processes, in Aquatic Microbiology: An Ecological Approach, edited by T. Ford, pp. 167-213, Blackwell Scientific Pub. Inc., Cambridge, MA, 1993.

McKinley, J. P., and F. S. Colwell, Application of perfluorocarbon tracers to microbial sampling in subsurface environments using mud-rotary and air-rotary drilling techniques, *J. Microb. Methods, 26*, 1-9, 1996.

McMahon, P. B. and F. H. Chapelle, Microbial production of organic acids in aquitard sediments and its role in aquifer geochemistry, *Nature*, *349*, 233-235, 1991.

Moench, R. H., and J. S. Schlee, Geologic quadrangle map of the Seboyeta Quadrangle, New Mexico, *U.S. Geol. Surv. Map GQ-207*, 1963.

Molenaar, C. M., Stratigraphy and depositional history of Upper Cretaceous rocks of the San Juan Basin area, New Mexico and Colorado, with a note on economic resources, *New Mexico Geological Society, Guidebook 28th Field Conference*, 159-166, 1977.

Murphy, E. M., J. A. Schramke, J. K. Fredrickson, H. W. Bledsoe, A. J. Francis, D. S. Sklarew, and J. C. Linehan, The influence of microbial activity and sediment organic carbon on the isotope geochemistry of the Middendorf Aquifer, *Water Resour. Res., 28*, 723-740, 1992.

Nelson, P., Permeability-Porosity Relationships in Sedimentary Rocks, *The Log Analyst*, 38-62, 1994.

Neuzil, C., How permeable are clays and shales?, *Water Resour. Res.*, *30*, 145-150, 1994.

Pedersen, K., The deep subterranean biosphere, *Earth Science Reviews*, 34, 243-260, 1993.

Pegram, P., *An Isotopic Study of Ground-Water Flow Near Cerro Negro, New Mexico*, unpublished Hydrology Master's Thesis, 145 pp., New Mexico Institute of Mining and Technology, Socorro, NM, 1995.

Perry, F.V., W. S. Baldridge, D. J. DePaolo, and M. Shafiqullah, Evolution of a Magmatic System During Continental Extension: The Mount Taylor Volcanic Field, New Mexico, *J. Geophys.*, *95*, B12, 19327-19348, 1990.

Person, M., J. P. Raffensperger, S. Ge., and G. Garven, Basin-Scale Hydrogeological Modeling, *Rev. Geophys.*, *34*, 61-87, 1996.

Phelps, T. J., C. B. Fliermans, T. R. Garland, S. M. Pfiffner, and D. C. White, Method for recovery of deep terrestrial subsurface sediments for microbiological studies, *J. Microbiol. Methods, 9*, 267-279, 1989.

Phillips, F. M., L. A. Peeters, M. K. Tansey, and S. N. Davis, Paleoclimatic inferences from an isotopic investigation of groundwater in the central San Juan Basin, New Mexico*, Quaternary Research, 26*, 179-193, 1986.

Phillips, F. M., M. K. Tansey, L. A. Peeters, S. Cheng, A. Long, A., An Isotopic Investigation of Groundwater in the San Juan Basin New Mexico: Carbon 14 Dating as a Basis for Numerical Flow Modeling, *Water Resour. Res., 25,* 2259-2273, 1989.

Plummer, L.N., B. F. Jones, and A. H. Truesdell, WATEQF - A FORTRAN IV version of WATEQ, a computer program for calculating chemical equilibria of natural waters, *U.S. Geol.l Surv. Water Resour. Invest. Report 75-13*, 61 pp., 1976.

Plummer, L.N., E. C. Prestemon, and D. L. Parkhurst, An interactive code (NETPATH) for modeling net geochemical reaction along a flow path, *U.S. Geol. Surv. Water Resour. Invest. Report 91-4169*, 130 pp., 1994.

Risser, D. W., and F. P. Lyford, Water resources on the Pueblo of Laguna, West-Central New Mexico, *U. S. Geol. Surv. Water Resour. Invest. Report 83-4038*, 308 pp., 1983.

Reiter, M., C. L. Edwards, H. Hartman, C. Weidman, Terrestrial Heat Flow along the Rio Grande Rift, New Mexico and Southern Colorado, *Geol. Soc. Am. Bull., 86*, 811-818, 1975.

Reiter, M., and D. L. Jordan, Hydrogeothermal studies across the Pecos River Valley, southeastern New Mexico, *Geol. Soc. Amer. Bull., 108*, 747-756, 1996.

Schlee, J.S., and R. H. Moench, Geologic quadrangle map of the Moquino quadrangle, New Mexico, *U.S. Geol. Surv. Map GQ-209*, 1963.

Senger, R. K., and Fogg, G. E., Stream Functions and Equivalent Freshwater Heads for Modeling Regional Flow of Variable-Density Groundwater, 1. Review of Theory and Verification, *Water Resour. Res.*, *26*, 2089-2096, 1990.

Sibson, R.H., Crustal stress, faulting, and fluid flow in Geofluids in *Origin, Migration and Evolution of Fluids in Sedimentary Basins,* edited by J. Parnell, Special Publication no. 78, Geological Society, 69-84, 1994.

Smith, L., and D. S. Chapman, On the Thermal Effects of Groundwater Flow 1. Regional Scale Systems, *J. Geophys. Res.,* 88, B1, 593-608, 1983.

Stephens, D. B., Ground water flow and implications for groundwater contamination north of Prewitt, New Mexico, U.S.A., *J. Hydrol.*, *61*, 391-408, 1983.

Stetter, K.O., G. Fiala, G. Huber, R. Huber, and A. Segerer, Hyperthermophilic microorganisms, *FEMS Microbiol. Rev*., *75,* 117-124, 1990.

Stevens, T. O., J. P. McKinley, and J. K. Fredrickson, Bacteria associated with deep, alkaline, anaerobic groundwaters in southeast Washington, *Microb. Ecol.*, *25*, 35, 1993.

Stevens, T. O. and J. P. McKinley, Geochemically produced hydrogen supports microbial ecosystems in deep basalt aquifers, *Science, 270*, 450-454, 1995.

Stone, W. J., F. P. Lyford, P. F. Frenzel, N. H. Mizell, and E. T. Padgett, Hydrogeology and water resources of  San Juan Basin, New Mexico, *Hydrologic Report 6*, New Mexico Bureau of Mines and Mineral Resources, Socorro, NM, 70pp., 1983.

Stute, M., J. F. Clark, P. Schlosser, W. Broecker, and G. Bonani, A 30,000 yr continental paleotemperature record derived from noble gases dissolved in groundwater from the San Juan Basin, New Mexico, *Quaternary Research, 43*, 209-220, 1995.

Taylor, J. Z. and M. Person, Wellhead delineation on island aquifer systems, *Groundwater*,  (in press, 1998).

Vacquier, V., The origin of terrestrial heat flow, *Geophys. J. Int., 106,* 199-202, 1991.

Wagner, G. and P. van den Haute, *Fission-Track Dating,* Kluwer Academic Publishers, Dordrecht, pp. 285, 1992.

Ward, J. J., G. R. Walters, S. J. Alweis, G. J. Axen, H. W. Bentley, Effects of uranium mine dewatering on the water resources of the Pueblo of Laguna, New Mexico, prepared for the Pueblo of Laguna, Laguna, NM by Hydro Geo Chem, Inc., Tuscon, AZ, 250 pp., 1982.

Woodward, L. A. and J. F. Callender, Tectonic framework of the San Juan Basin, *New Mexico Geological Society Guidebook 28th Field Conference*, 209-212, 1977.

# APPENDIX A

<u>LIST OF CERRO NEGRO MICROBIAL ORIGINS PROJECT COLLABORATORS</u>

(*taken primarily from Pegram, 1995*)


GEOCHEMISTRY

| INVESTIGATOR(S) | AFFILIATED INSTITUTION | ANALYSES |
|---|---|---|
| J. McKinley | Pacific Northwest National Laboratory | groundwater geochemical analyses; whole sediment analyses for C, N, P, S, and Fe |
| T. C. Onstott, G. Gao | Princeton University | C, O, and S stable isotope analyses; argon dating; fluid inclusion and diagenetic cement analyses |
| P. Pegram, F. Phillips | New Mexico Tech | groundwater geochemical analyses and modeling; $^{14}$C groundwater dating |


GEOLOGY/ HYDROGEOLOGY

| INVESTIGATOR(S) | AFFILIATED INSTITUTION | ANALYSES |
|---|---|---|
| B. Bjornstad, P. Long, C. Murray | Pacific Northwest National Laboratory | core logging; stratigraphic interpretation; mesoscopic petrographic relationships; local fracture mapping |
| S. Rawson, C. Gullett | Pacific Northwest National Laboratory | sediment hydrologic property laboratory analyses; petrography |
| M. Walvoord, F. Phillips, M. Person | New Mexico Tech, University of MN | hydrogeologic modeling; fission-track analyses |

MICROBIOLOGY

| | | |
|---|---|---|
| D. Balkwill | Florida State University | culturable aerobes; preservation of aerobic cultures; 16S rRNA gene sequencing |
| D. Boone | Oregon Graduate Institute | culturable anaerobes; preservation of anaerobic cultures |
| D Caldwill | University of Saskatchewan | enrichment and preservation of microbial communities |
| W. Chesbro | University of New Hampshire | culturable aerobes; role of Tween and elevated $CO_2$ on growth; starvation characteristics of pure cultures |
| F. Colwell | Idaho National Engineering Laboratory | community-level substrate use patterns; enrichments for S and Fe lithotropes |
| M. Fletcher | University of Maryland | bacterial attachment and transport through core material |
| L. Forney | Michigan State University | effect of nutrient limitations on genetic rearrangement in subsurface bacteria |
| J. Fredrickson, F. Brockman, T. Stevens | Pacific Northwest National Laboratory | aerobic and anaerobic activities; enrichments and MPNs for selected aerobes and anaerobes |
| R. Griffiths | Oregon State University | aerobic metabolic and enzymatic activites; influence of salt |
| W. Holben | Agouron Institute | molecular analysis of whole community DNA based on %G+C fractionation |
| T. Kieft, P. Amy | New Mexico Tech, University of Nevada – Las Vegas | total microscopic counts; endogenous respiration; aerobic respiration of $^{14}$C-labeled organic compounds |
| A. Matin, T. Schmidt | Standford University, Michigan State University | starvation gene expression and role in survival of subsurface bacteria |

| R. Miller | Oklahoma State University | presence of bacterial viruses;  recA gene in subsurface bacteria |
|---|---|---|
| S. Nierzwicki-Bauer | Rensselaer Polytechnic Institute | characterization of community using phylogenetic group specific 16S rRNA-directed oligo probes |
| T. Phelps | Oak Ridge National Laboratory | anaerobic activities; enrichments and MPN's of select anaerobes |
| F. Roberto | Idaho National Engineering Laboratory | phylogenetic characterization of whole community DNA;  Fe lithotrophs |
| D. White, D. Ringelberg | University of Tennessee | lipid analysis for total biomass;  community structure;  nutritional status |

# APPENDIX B

METHODS FOR MICROBIOLOGICAL ACTIVITY MEASUREMENTS

Mineralization of $^{14}C$-labeled acetate to $^{14}CO_2$ was quantified in rock slurries essentially as described by Fredrickson *et al*. (1997). A 0.2 mL solution of sterile $[1-^{14}C]$ sodium acetate (74 kBq $\mu mol^{-1}$, >98% radiopurity, NEN Research Products, Boston, MA) was added along with 4.8 ml sterile artificial groundwater to 5.0 g homogenized rock in sterile 150-ml glass bottles. Artificial groundwater contained 3.8 mg NaF, 0.2 mg KBr, 7.2 mg KCl, 336.4 mg $CaCl_2.2H_2O$, 713 mg $Na_2SO_4$, 32.7 mg $MgCl_2.6H_2O$, 200.8 mg NaCl, 82.2 mg $Na_2SiO_3.9H_2O$, and 899.8 mg $NaHCO_3$ $L^{-1}$ deionized water. For anaerobic assays, rock material was handled in an anaerobic glove bag and all solutions were purged with $O_2$-free $N_2$. Slurries were incubated at 22°C. Labeled $CO_2$ in the headspace of the bottles was trapped in an alkaline solution consisting of 1 mL 0.3 M KOH. The KOH was transferred to liquid scintillation; radioactivity was quantified by liquid scintillation counting. Sterile subsurface samples (autoclaved on three successive days) served as controls.

Sulfate reducing activity was measured using $^{35}S$-labeled sulfate, as described by Fredrickson *et al.* (1997). Sterile artificial groundwater (as described above, but without the $Na_2SO_4$) (10 mL), a sterile solution containing 20 mM each of sodium benzoate, ammonium formate, sodium lactate, propionic acid, isobutyric acid, and sodium acetate (5 mL), and a $^{35}SO_4^{2-}$ solution (370 kBq, carrier-free, NEN Research Products) (1 mL)

was added to 10 g crushed rock in sterile Balsch tubes (Bellco, Vineland, NJ). All manipulations were performed in a sterile glove bag and all solutions were purged of $O_2$. Samples were incubated in the dark at room temperature for 14 days, after which Zn acetate was added and the samples were frozen. For analysis, samples were centrifuged and labeled sulfate was measured in the supernatant by liquid scintillation counting. Total reduced $^{35}S$ in sediments was quantified by chromium reduction (Canfield *et al.*, 1986) and liquid scintillation counting.

# APPENDIX C

FISSION-TRACK DATING

I.      Theory

A zone of damage forms when a radioisotope fissions, causing daughter fragments to travel at approximately 180° to each other within a mineral grain.  Several naturally occurring isotopes fission spontaneously, but only $^{238}$U has a sufficiently short fission half-life (8.2 x $10^{15}$ years) and is abundant enough in nature to produce significant numbers of spontaneous tracks over a time period of geologic interest.  Trace amounts of uranium occur in several common minerals, including apatite and zircon.  Based on the assumption that $^{238}$U fissions at a constant rate, fission-tracks can be used to date mineral grains.  An age is determined by comparing the number of fission-tracks on a polished surface of the mineral to the concentration of uranium (parent material) present in the mineral.  To estimate the parent isotopic abundance, the sample is irradiated in a nuclear reactor.  Thermal (slow) neutron irradiation induces fission in $^{235}$U, but not in $^{238}$U.  The abundance of $^{235}$U is related to the $^{238}$U concentration using the relationship of uranium isotope abundance in nature ($^{235}$U/$^{238}$U = 7.2527 x $10^{-3}$) (Wagner and van den Haute, 1992).  The determination of the parent and daughter abundance in fission-track analyses involves measuring and comparing the densities of induced and spontaneous fission-tracks within individual mineral grains.   Using a ratio eliminates the need to consider uranium concentration as a variable in the apparent age calculation.

Fission-tracks in apatite grains will anneal, partially (60°C - 140°C) or completely (>140°C), when subjected to elevated temperature for significant periods of geologic time. Fission-tracks in zircon grains will anneal, partially (210°C - 320°C) or completely (>320°C), when subjected to elevated temperature for significant periods of geologic time. Ions, previously displaced along the damage zone, migrate back into their original crystallographic positions in the mineral, thereby shortening, or completely repairing the fission-track. The progressive shortening, or disappearance, of spontaneous fission-tracks results in a younger *apparent* age determination for the grain. Unannealed, spontaneous apatite fission-tracks are about 14-15 microns in length. Unannealed, spontaneous zircon fission-tracks are about 11 microns in length. Shorter fission-track lengths reflect subjection to elevated temperatures. Annealing is a function of both time and temperature, which makes fission-track analysis a useful tool for discerning thermal histories of rock packages. Fission-track ages represent the time period of fission-track accumulation in a sample, and record absolute ages only if the rock has not been subjected to temperatures exceeding annealing temperatures. In the case of a rock that has been subjected to high temperatures and then rapidly cooled, the ages will closely correspond to the timing of cooling.

II.    Methods

  A.  Sample Preparation

Sandstone samples from the CNV-R borehole and the CNAR borehole were ground to a fine powder.  Mineral separation methods were performed on the powdered samples in order to retrieve apatite (mineral density = 3.1 – 3.35 $g/cm^3$) and zircon grains (mineral density = 4.6 – 4.7 $g/cm^3$).  First, a Wilfey table was used to separate felsic minerals with densities < 2.7 $g/cm^3$ from the mafic minerals with densities of  > 2.7 $g/cm^3$.   Then the mafic mineral fraction underwent further separation of magnetics and nonmagnetics using a large hand magnet and the Frantz magnetic separation machine.  Final separation required the use of heavy liquids, Lithium Metatungstate and Methylene Iodide.  The apatite grains and zircon grains for each sample were mounted in small squares of epoxy, which were ground on a polishing wheel to expose mineral grains.  The polished apatite mounts were etched using 5 M nitric acid for 25 seconds.  The polished zircon mounts were etched using a eutectic melt of NaOH and KOH at 230°C for 12-20 hours.  (Zircon etching time is age dependent: older samples require shorter etching times die to alpha decay damage through time).  The etching process preferentially enlarged the zones of damage enabling fission-tracks to be detected under a petrographic microscope.  Etched samples were fitted securely with muscovite covers and irradiated at the Texas A&M University Nuclear Reactor.  Samples were subjected to irradiation of thermal (slow) neutrons at a specified fluence to induce fission of $^{235}$U recorded in the muscovite covers. The specified fluences for the apatite and zircon samples were 1 x $10^{16}$ neutrons/ $cm^2$ and 1 x $10^{15}$ neutrons/ $cm^2$, respectively.   Grain mounts of known standards, Durango

113

apatites, Fish Canyon apatites and zircons, and Corning dosimeter glasses were included in the irradiation package in order to monitor the neutron flux and calibrate the analyses.

After irradiation, the muscovite covers were carefully separated from the samples, etched to display induced fission-tracks, and each muscovite cover/sample pair was mounted on a microscope slide.

B.  Sample Analysis

A dry lens objective on a petrographic Leitz microscope at 1000x was used for fission-track counting by the grain by grain method.  Analyses were conducted by the external detector method with muscovite as the external detector.  The induced track density reflected on the muscovite cover was measured on the same grain as the spontaneous track density.  Ideally, 20 grains were examined for each sample.  The poor quality and paucity of mineral grains in some samples, particularly the apatite samples, precluded the analyses of 20 grains per sample.  Of 21 total samples, 7 did not contain enough zircon for fission-track analyses.  None of the apatite samples yielded the recommended 20 grains suitable for fission-track analyses.  There are a few reasons for the analysis difficulties.  1) There was very little apatite present in most of the samples.  Units of the Dakota Sandstone in other localities have also shown to be sparse in apatite (S. Kelley, personal communication, 1996).  2)  Apatite and zircon grains in these sandstone samples are detrital, and presumably have been reworked for hundreds of millions of years. Grain clearness is very important for fission-track counting and measuring lengths.  Reworking

has made many of the zircon grains quite dark, cruddy and not datable by fission-track analysis.

The Chi-squared test was the statistical technique used for determining whether single grain ages belonged to the same population (or geologic event). A group of grain ages was considered to belong to a single population if the distribution passed the $\chi^2$ test at the > 5% probability level. If the individual grains passed the $\chi^2$ test, then an apparent age was estimated using the sum of the spontaneous and induced track counts for all the grains in the sample. Ages were calculated using the zeta calibration method (Green, 1985), and errors were calculated by the conventional method (Green, 1981).

III. Results

Information and results from the remaining 14 samples are listed in the following data table. Grain count sheets for each of the 14 samples are also included (p. 119 – 132). Sample names that begin with A represent those taken from CNA-R, the angled borehole, and samples names that begin with V represent those taken from CNV, the vertical borehole. The apparent ages for samples A-10 and A-12, which were collected closest to the intrusion and basaltic stringers, are notably younger than all other samples, including samples from the same unit in the vertical borehole (V-20 and V-21). These results suggest that sediments out to at least 55 m beyond the main plug were heated by the intrusion at Cerro Negro.

## SUMMARY OF ZIRCON FISSION TRACK ANALYSES

| Sample | Unit | Borehole Distance (m) | Depth (m) | Distance from Center of Intrusion (m) | Number of Grains Counted | Apparent FT Age (Ma) | Age Standard Deviation (m) | Chi Squared Probability (%) |
|---|---|---|---|---|---|---|---|---|
| A-2 | Two Wells SS | 251.3 | 131.3 | 215.7 | 20 | 423 | 12.8 | 55.12 |
| A-4 | Two Wells SS | 298.5 | 158.2 | 176.9 | 20 | 441 | 17.0 | 43.61 |
| A-5 | Paguate Sandstone | 332.6 | 176.3 | 148.0 | 20 | 431 | 16.6 | 25.70 |
| A-6 | Paguate Sandstone | 356.3 | 196.1 | 132.5 | 20 | 382 | 16.1 | 72.00 |
| A-8 | Cubero Sandstone | 384.3 | 212.0 | 109.5 | 20 | 417 | 12.4 | 87.27 |
| A-1 | Cubero Sandstone | 392.9 | 219.0 | 103.5 | 20 | 435 | 17.3 | 16.14 |
| A-9 | Cubero Sandstone | 402.2 | 226.0 | 96.1 | 20 | 364 | 13.8 | 62.43 |
| A-10 | Oak Canyon Mb | 426.5 | 236.6 | 75.2 | 20 | 243 | 10.7 | 79.60 |
| A-12 | Oak Canyon Mb | 438.4 | 246.4 | 67.4 | 20 | 252 | 11.0 | 70.10 |
| V-13 | Two Wells SS | 126.0 | 126.0 | 1200 | 20 | 415 | 13.7 | 49.42 |
| V-17 | Cubero Sandstone | 186.9 | 186.9 | 1200 | 15 | 379 | 15.3 | 28.41 |
| V-18 | Cubero Sandstone | 191.0 | 191.0 | 1200 | 20 | 413 | 14.2 | 22.13 |
| V-20 | Oak Canyon Mb | 214.0 | 214.0 | 1200 | 18 | 428 | 15.5 | 19.01 |
| V-21 | Oak Canyon Mb | 221.3 | 221.3 | 1200 | 20 | 395 | 13.4 | 32.59 |

Zircon fission-track core samples collected from the CNA-R ("A" series) and CNV ("V" series) boreholes near Cerro Negro.
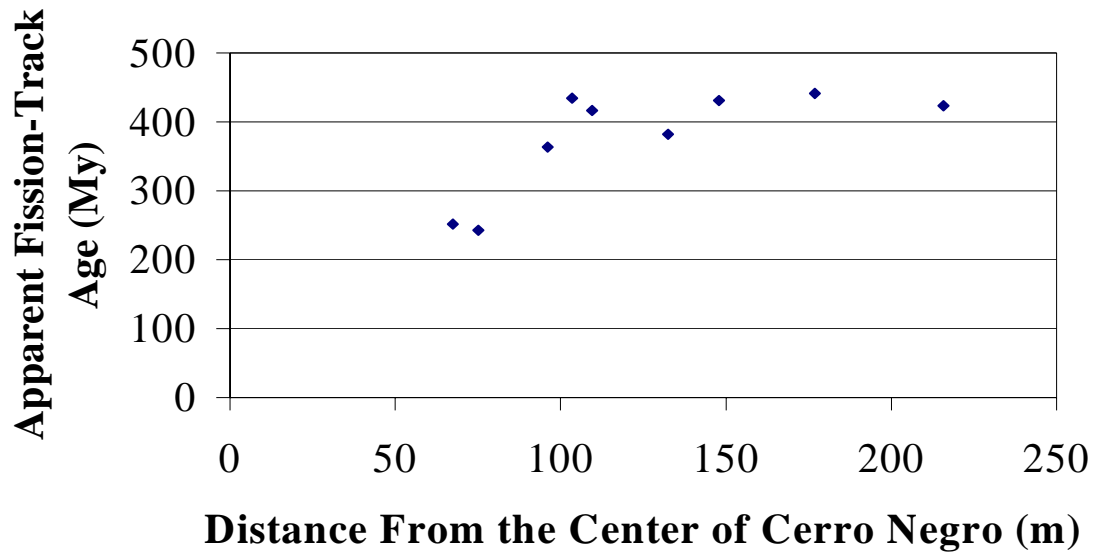
The above graph displays apparent zircon fission-track ages in relation to distance from the center of Cerro Negro. The intrusion is approximately 38 m in diameter. All samples represented above were taken from the angled borehole, CNA-R. Samples from the vertical borehole, located 1.2 km from the intrusion, ranged from 380 – 430 My.

# FISSION TRACK AGE DATA

| | | | |
|---|---|---|---|
| **PROJECT:** | CERRO NEGRO | **DATE:** March, 1997 | **FT AGE:** 434.8 Ma |
| **SAMPLE #:** | A-1 | **BOREHOLE DISTANCE (m):** 392.9 | |
| **LAB:** | NMT | **ELEVATION (M):** 219 | |
| **REACTOR RUN:** | RR-12-13-96Z2 | **DISTANCE FROM CN (M):** 103.5 | **STD ERR:** 17.30 Ma |
| **RHO D** | 2.981E+05 | **MICROSCOPE:** LEITZ | **C. COEFF:** 0.962 |
| **# TRACKS (FLUX)** | 2745 | **MAGNIFICATION:** 1000 X | **CHI²:** 16.142 |
| **ZETA** | 7330 | **ROCK TYPE:** Cubero Sandstone | **AVG. AGE:** 440.2 Ma |
| **# OF GRAINS:** | 20 | **MINERAL:** Zircon | **STD. ERR:** 15.7 |

| GRAIN # | AREA USED (SQ. CM) | Ns | RHO(S) (/CM²) | Ni | RHO(I) (/CM²) | RATIO (Ns/Ni) | AGE (MA) | STD.DEV. (MA) |
|---|---|---|---|---|---|---|---|---|
| 1. Ss | 1.6E-05 | 38 | 2.375E+06 | 94 | 1.175E+07 | 0.40 | 427.2 | 82.5 |
| 2. Ss | 1.6E-05 | 49 | 3.063E+06 | 122 | 1.525E+07 | 0.40 | 424.5 | 72.3 |
| 3. Ss | 1.6E-05 | 59 | 3.688E+06 | 136 | 1.700E+07 | 0.43 | 457.4 | 71.8 |
| 4. Ss | 1.6E-05 | 51 | 3.188E+06 | 129 | 1.613E+07 | 0.40 | 418.1 | 69.6 |
| 5. Ss | 1.6E-05 | 61 | 3.813E+06 | 108 | 1.350E+07 | 0.56 | 589.3 | 95.1 |
| 6. Ss | 1.6E-05 | 46 | 2.875E+06 | 85 | 1.063E+07 | 0.54 | 565.7 | 104.1 |
| 7. Ss | 1.6E-05 | 24 | 1.500E+06 | 61 | 7.625E+06 | 0.39 | 416.1 | 100.6 |
| 8. Ss | 1.6E-05 | 57 | 3.563E+06 | 140 | 1.750E+07 | 0.41 | 430.1 | 68.1 |
| 9. Ss | 1.6E-05 | 50 | 3.125E+06 | 132 | 1.650E+07 | 0.38 | 401.1 | 67.0 |
| 10. Ss | 1.6E-05 | 83 | 5.188E+06 | 190 | 2.375E+07 | 0.44 | 460.4 | 61.2 |
| 11. Ss | 1.6E-05 | 70 | 4.375E+06 | 159 | 1.988E+07 | 0.44 | 463.9 | 67.1 |
| 12. Ss | 1.6E-05 | 47 | 2.938E+06 | 118 | 1.475E+07 | 0.40 | 421.1 | 73.1 |
| 13. Ss | 1.6E-05 | 107 | 6.688E+06 | 236 | 2.950E+07 | 0.45 | 477.2 | 56.4 |
| 14. Ss | 1.6E-05 | 48 | 3.000E+06 | 162 | 2.025E+07 | 0.30 | 315.9 | 52.3 |
| 15. Ss | 1.6E-05 | 42 | 2.625E+06 | 109 | 1.363E+07 | 0.39 | 407.8 | 74.5 |
| 16. Ss | 1.6E-05 | 55 | 3.438E+06 | 107 | 1.338E+07 | 0.51 | 538.5 | 89.9 |
| 17. Ss | 1.6E-05 | 30 | 1.875E+06 | 89 | 1.113E+07 | 0.34 | 358.1 | 75.9 |
| 18. Ss | 1.6E-05 | 36 | 2.250E+06 | 95 | 1.188E+07 | 0.38 | 401.3 | 78.9 |
| 19. Ss | 1.6E-05 | 51 | 3.188E+06 | 125 | 1.563E+07 | 0.41 | 431.0 | 72.1 |
| 20. Ss | 1.6E-05 | 154 | 9.625E+06 | 416 | 5.200E+07 | 0.37 | 392.3 | 37.8 |
| | 3.2E-04 | 1158 | 3.619E+06 | 2813 | 1.758E+07 | 0.41 | | |

# FISSION TRACK AGE DATA

| | | | |
|---|---|---|---|
| **PROJECT:** Cerro Negro | **DATE:** MARCH,1997 | **FT AGE:** 423.4 Ma | |
| **SAMPLE #:** A-2 | **BOREHOLE DISTANCE (m):** 251.3 | | |
| **LAB:** NMT | **ELEVATION (M):** 131.3 | | |
| **REACTOR RUN:** RR-12-13-96Z2 | **DISTANCE TO CN (m):** 215.7 | **STD ERR:** 12.84 Ma | |
| **RHO D** 2.981E+05 | **MICROSCOPE:** LEITZ | **C. COEFF:** 0.973 | |
| **# TRACKS (FLUX)** 2745 | **MAGNIFICATION:** 1000 X | **CHI²:** 55.120 | |
| **ZETA** 7330 | **ROCK TYPE:** Two Wells Sandstone | **AVG. AGE:** 436.0 Ma | |
| **# OF GRAINS:** 20 | **MINERAL:** Zircon | **STD. ERR:** 20.5 | |

| GRAIN # | AREA USED (SQ. CM) | Ns | RHO(S) (/CM²) | Ni | RHO(I) (/CM²) | RATIO (Ns/Ni) | AGE (MA) | STD.DEV. (MA) |
|---|---|---|---|---|---|---|---|---|
| 1. Ss | 1.6E-05 | 82 | 5.125E+06 | 239 | 2.988E+07 | 0.34 | 364.4 | 47.1 |
| 2. Ss | 1.6E-05 | 44 | 2.750E+06 | 187 | 2.338E+07 | 0.24 | 252.1 | 42.5 |
| 3. Ss | 1.6E-05 | 101 | 6.313E+06 | 268 | 3.350E+07 | 0.38 | 399.1 | 47.2 |
| 4. Ss | 1.6E-05 | 122 | 7.625E+06 | 282 | 3.525E+07 | 0.43 | 456.1 | 50.2 |
| 5. Ss | 1.6E-05 | 130 | 8.125E+06 | 277 | 3.463E+07 | 0.47 | 493.4 | 53.3 |
| 6. Ss | 1.6E-05 | 142 | 8.875E+06 | 303 | 3.788E+07 | 0.47 | 492.7 | 51.0 |
| 7. Ss | 1.6E-05 | 249 | 1.556E+07 | 805 | 1.006E+08 | 0.31 | 329.4 | 24.7 |
| 8. Ss | 1.6E-05 | 205 | 1.281E+07 | 476 | 5.950E+07 | 0.43 | 454.1 | 38.9 |
| 9. Ss | 1.6E-05 | 53 | 3.313E+06 | 159 | 1.988E+07 | 0.33 | 354.3 | 56.6 |
| 10. Ss | 1.6E-05 | 50 | 3.125E+06 | 87 | 1.088E+07 | 0.57 | 599.2 | 106.9 |
| 11. Ss | 1.6E-05 | 85 | 5.313E+06 | 238 | 2.975E+07 | 0.36 | 378.8 | 48.4 |
| 12. Ss | 1.6E-05 | 72 | 4.500E+06 | 189 | 2.363E+07 | 0.38 | 403.3 | 56.4 |
| 13. Ss | 1.6E-05 | 65 | 4.063E+06 | 140 | 1.750E+07 | 0.46 | 488.3 | 73.9 |
| 14. Ss | 1.6E-05 | 89 | 5.563E+06 | 171 | 2.138E+07 | 0.52 | 544.9 | 72.0 |
| 15. Ss | 1.6E-05 | 85 | 5.313E+06 | 195 | 2.438E+07 | 0.44 | 459.5 | 60.4 |
| 16. Ss | 1.6E-05 | 196 | 1.225E+07 | 403 | 5.038E+07 | 0.49 | 510.6 | 45.5 |
| 17. Ss | 1.6E-05 | 467 | 2.919E+07 | 1186 | 1.483E+08 | 0.39 | 416.5 | 24.1 |
| 18. Ss | 1.6E-05 | 105 | 6.563E+06 | 197 | 2.463E+07 | 0.53 | 557.5 | 68.2 |
| 19. Ss | 1.6E-05 | 122 | 7.625E+06 | 320 | 4.000E+07 | 0.38 | 403.6 | 43.6 |
| 20. Ss | 1.6E-05 | 58 | 3.625E+06 | 175 | 2.188E+07 | 0.33 | 352.3 | 53.8 |
| – | – | –––– | – | – | – | – | – | – |
| | 3.2E-04 | 2522 | 7.881E+06 | 6297 | 3.936E+07 | 0.40 | | |

# FISSION TRACK AGE DATA

| | | | | |
|---|---|---|---|---|
| **PROJECT:** | Cerro Negro | **DATE:** | March, 1997 | **FT AGE:** 441.5 Ma |
| **SAMPLE:** | A-4 | **BOREHOLE DISTANCE (m):** | 298.5 | |
| **LAB:** | NMT | **ELEVATION (M):** | 158.2 | |
| **REACTOR RUN:** | RR-12-13-96Z2 | **DISTANCE TO CN (m):** | 176.9 | **STD ERR:** 16.97 Ma |
| **RHO D** | 2.981E+05 | **MICROSCOPE:** | LEITZ | **C. COEFF:** 0.854 |
| **# TRACKS (FLUX)** | 2745 | **MAGNIFICATION:** | 1000 X | **CHI²:** 43.606 |
| **ZETA** | 7330 | **ROCK TYPE:** | Two Wells Sandstone | **AVG. AGE:** 461.6 Ma |
| **# OF GRAINS:** | 20 | **MINERAL:** | Zircon | **STD. ERR:** 24.2 |

| GRAIN # | AREA USED (SQ. CM) | Ns | RHO(S) (/CM²) | Ni | RHO(I) (/CM²) | RATIO (Ns/Ni) | AGE (MA) | STD.DEV. (MA) |
|---|---|---|---|---|---|---|---|---|
| 1. Ss | 1.6E-05 | 19 | 1.188E+06 | 47 | 5.875E+06 | 0.40 | 427.2 | 116.4 |
| 2. Ss | 1.6E-05 | 32 | 2.000E+06 | 61 | 7.625E+06 | 0.52 | 549.1 | 120.3 |
| 3. Ss | 1.6E-05 | 78 | 4.875E+06 | 135 | 1.688E+07 | 0.58 | 602.2 | 86.4 |
| 4. Ss | 1.6E-05 | 69 | 4.313E+06 | 128 | 1.600E+07 | 0.54 | 563.6 | 84.9 |
| 5. Ss | 1.6E-05 | 38 | 2.375E+06 | 71 | 8.875E+06 | 0.54 | 559.7 | 113.0 |
| 6. Ss | 1.6E-05 | 46 | 2.875E+06 | 209 | 2.613E+07 | 0.22 | 236.1 | 38.7 |
| 7. Ss | 1.6E-05 | 36 | 2.250E+06 | 90 | 1.125E+07 | 0.40 | 422.8 | 83.8 |
| 8. Ss | 1.6E-05 | 76 | 4.750E+06 | 193 | 2.413E+07 | 0.39 | 416.5 | 57.0 |
| 9. Ss | 1.6E-05 | 59 | 3.688E+06 | 181 | 2.263E+07 | 0.33 | 346.6 | 52.4 |
| 10. Ss | 1.6E-05 | 37 | 2.313E+06 | 58 | 7.250E+06 | 0.64 | 661.8 | 139.8 |
| 11. Ss | 1.6E-05 | 109 | 6.813E+06 | 256 | 3.200E+07 | 0.43 | 449.2 | 52.1 |
| 12. Ss | 1.6E-05 | 75 | 4.688E+06 | 190 | 2.375E+07 | 0.39 | 417.5 | 57.5 |
| 13. Ss | 1.6E-05 | 82 | 5.125E+06 | 205 | 2.563E+07 | 0.40 | 422.8 | 55.8 |
| 14. Ss | 1.6E-05 | 119 | 7.438E+06 | 226 | 2.825E+07 | 0.53 | 551.0 | 63.3 |
| 15. Ss | 1.6E-05 | 80 | 5.000E+06 | 226 | 2.825E+07 | 0.35 | 375.6 | 49.4 |
| 16. Ss | 1.6E-05 | 39 | 2.438E+06 | 79 | 9.875E+06 | 0.49 | 518.0 | 101.9 |
| 17. Ss | 1.6E-05 | 67 | 4.188E+06 | 148 | 1.850E+07 | 0.45 | 476.5 | 70.8 |
| 18. Ss | 1.6E-05 | 74 | 4.625E+06 | 197 | 2.463E+07 | 0.38 | 397.9 | 54.8 |
| 19. Ss | 1.6E-05 | 95 | 5.938E+06 | 214 | 2.675E+07 | 0.44 | 467.6 | 58.3 |
| 20. Ss | 1.6E-05 | 44 | 2.750E+06 | 132 | 1.650E+07 | 0.33 | 354.3 | 62.0 |
| | 3.2E-04 | 1274 | 3.981E+06 | 3046 | 1.904E+07 | 0.42 | | |

# FISSION TRACK AGE DATA

| | | | | | |
|---|---|---|---|---|---|
| **PROJECT:** | Cerro Negro | **DATE:** | March, 1997 | **FT AGE:** | 430.8 Ma |
| **SAMPLE:** | A-5 | **BOREHOLE DISTANCE (m):** | 332.6 | | |
| **LAB:** | NMT | **ELEVATION (M):** | 176.3 | | |
| **REACTOR RUN:** | RR-12-13-96Z2 | **DISTANCE FROM CN (m):** | 148.0 | **STD ERR:** | 16.62 Ma |
| **RHO D** | 2.981E+05 | **MICROSCOPE:** | LEITZ | **C. COEFF:** | 0.988 |
| **# TRACKS (FLUX)** | 2745 | **MAGNIFICATION:** | 1000 X | **CHI²:** | 25.697 |
| **ZETA** | 7330 | **ROCK TYPE:** | Paguate Sandstone | **AVG. AGE:** | 442.0 Ma |
| **# OF GRAINS:** | 20 | **MINERAL:** | Zircon | **STD. ERR:** | 20.3 |

| GRAIN # | AREA USED (SQ. CM) | Ns | RHO(S) (/CM²) | Ni | RHO(I) (/CM²) | RATIO (Ns/Ni) | AGE (MA) | STD.DEV. (MA) |
|---|---|---|---|---|---|---|---|---|
| 1. Ss | 1.6E-05 | 241 | 1.506E+07 | 618 | 7.725E+07 | 0.39 | 412.6 | 32.3 |
| 2. Ss | 1.6E-05 | 39 | 2.438E+06 | 118 | 1.475E+07 | 0.33 | 351.3 | 65.2 |
| 3. Ss | 1.6E-05 | 48 | 3.000E+06 | 82 | 1.025E+07 | 0.59 | 609.8 | 111.4 |
| 4. Ss | 1.6E-05 | 30 | 1.875E+06 | 63 | 7.875E+06 | 0.48 | 500.3 | 111.4 |
| 5. Ss | 1.6E-05 | 83 | 5.188E+06 | 145 | 1.813E+07 | 0.57 | 596.9 | 82.9 |
| 6. Ss | 1.6E-05 | 44 | 2.750E+06 | 121 | 1.513E+07 | 0.36 | 385.5 | 68.3 |
| 7. Ss | 1.6E-05 | 37 | 2.313E+06 | 110 | 1.375E+07 | 0.34 | 357.4 | 68.3 |
| 8. Ss | 1.6E-05 | 29 | 1.813E+06 | 84 | 1.050E+07 | 0.35 | 366.6 | 79.3 |
| 9. Ss | 1.6E-05 | 83 | 5.188E+06 | 146 | 1.825E+07 | 0.57 | 593.0 | 82.3 |
| 10. Ss | 1.6E-05 | 241 | 1.506E+07 | 662 | 8.275E+07 | 0.36 | 386.0 | 30.0 |
| 11. Ss | 1.6E-05 | 12 | 7.500E+05 | 31 | 3.875E+06 | 0.39 | 409.6 | 139.5 |
| 12. Ss | 1.6E-05 | 25 | 1.563E+06 | 62 | 7.750E+06 | 0.40 | 426.1 | 101.3 |
| 13. Ss | 1.6E-05 | 47 | 2.938E+06 | 103 | 1.288E+07 | 0.46 | 480.2 | 85.0 |
| 14. Ss | 1.6E-05 | 35 | 2.188E+06 | 81 | 1.013E+07 | 0.43 | 455.6 | 92.6 |
| 15. Ss | 1.6E-05 | 72 | 4.500E+06 | 180 | 2.250E+07 | 0.40 | 422.8 | 59.5 |
| 16. Ss | 1.6E-05 | 18 | 1.125E+06 | 58 | 7.250E+06 | 0.31 | 330.4 | 89.4 |
| 17. Ss | 1.6E-05 | 61 | 3.813E+06 | 152 | 1.900E+07 | 0.40 | 424.2 | 64.8 |
| 18. Ss | 1.6E-05 | 18 | 1.125E+06 | 50 | 6.250E+06 | 0.36 | 381.8 | 105.2 |
| 19. Ss | 1.6E-05 | 43 | 2.688E+06 | 85 | 1.063E+07 | 0.51 | 530.3 | 99.7 |
| 20. Ss | 1.6E-05 | 46 | 2.875E+06 | 119 | 1.488E+07 | 0.39 | 409.1 | 71.4 |
| – | – | —— | – | – | – | – | – | – |
| | 3.2E-04 | 1252 | 3.913E+06 | 3070 | 1.919E+07 | 0.41 | | |

# FISSION TRACK AGE DATA

| | | |
|---|---|---|
| **PROJECT:** Cerro Negro | **DATE:** April, 1997 | **FT AGE:** 382.3 Ma |
| **SAMPLE:** A-6 | **BOREHOLE DISTANCE (m):** 356.3 | |
| **LAB:** NMT | **ELEVATION (M):** 196.1 | |
| **REACTOR RUN:** RR-12-12-96Z2 | **DISTANCE TO CN (m):** 132.5 | **STD ERR:** 16.06 Ma |
| **RHO D** 2.981E+05 | **MICROSCOPE:** LEITZ | **C. COEFF:** 0.803 |
| **# TRACKS (FLUX)** 2745 | **MAGNIFICATION:** 1000 X | **CHI²:** 71.999 |
| **ZETA** 7330 | **ROCK TYPE:** Paguate Sandstone | **AVG. AGE:** 376.5 Ma |
| **# OF GRAINS:** 20 | **MINERAL:** zircon | **STD. ERR:** 27.6 |

| GRAIN # | AREA USED (SQ. CM) | Ns | RHO(S) (/CM²) | Ni | RHO(I) (/CM²) | RATIO (Ns/Ni) | AGE (MA) | STD.DEV. (MA) |
|---|---|---|---|---|---|---|---|---|
| 1.  Ss | 1.6E-05 | 15 | 9.375E+05 | 42 | 5.250E+06 | 0.36 | 378.8 | 114.2 |
| 2.  Ss | 1.6E-05 | 112 | 7.000E+06 | 196 | 2.450E+07 | 0.57 | 595.9 | 71.5 |
| 3.  Ss | 1.6E-05 | 60 | 3.750E+06 | 223 | 2.788E+07 | 0.27 | 287.5 | 42.2 |
| 4.  Ss | 1.6E-05 | 41 | 2.563E+06 | 152 | 1.900E+07 | 0.27 | 288.2 | 51.0 |
| 5.  Ss | 1.6E-05 | 39 | 2.438E+06 | 88 | 1.100E+07 | 0.44 | 466.9 | 90.3 |
| 6.  Ss | 1.6E-05 | 18 | 1.125E+06 | 56 | 7.000E+06 | 0.32 | 341.9 | 92.9 |
| 7.  Ss | 1.6E-05 | 72 | 4.500E+06 | 128 | 1.600E+07 | 0.56 | 587.0 | 87.2 |
| 8.  Ss | 1.6E-05 | 48 | 3.000E+06 | 193 | 2.413E+07 | 0.25 | 266.1 | 43.2 |
| 9.  Ss | 1.6E-05 | 12 | 7.500E+05 | 58 | 7.250E+06 | 0.21 | 222.2 | 70.6 |
| 10. Ss | 1.6E-05 | 48 | 3.000E+06 | 202 | 2.525E+07 | 0.24 | 254.5 | 41.2 |
| 11. Ss | 1.6E-05 | 108 | 6.750E+06 | 235 | 2.938E+07 | 0.46 | 483.5 | 57.0 |
| 12. Ss | 1.6E-05 | 43 | 2.688E+06 | 94 | 1.175E+07 | 0.46 | 481.4 | 89.1 |
| 13. Ss | 1.6E-05 | 53 | 3.313E+06 | 161 | 2.013E+07 | 0.33 | 350.0 | 55.8 |
| 14. Ss | 1.6E-05 | 15 | 9.375E+05 | 44 | 5.500E+06 | 0.34 | 362.1 | 108.5 |
| 15. Ss | 1.6E-05 | 19 | 1.188E+06 | 78 | 9.750E+06 | 0.24 | 260.8 | 66.9 |
| 16. Ss | 1.6E-05 | 28 | 1.750E+06 | 135 | 1.688E+07 | 0.21 | 222.7 | 46.4 |
| 17. Ss | 1.6E-05 | 92 | 5.750E+06 | 210 | 2.625E+07 | 0.44 | 461.7 | 58.4 |
| 18. Ss | 1.6E-05 | 67 | 4.188E+06 | 140 | 1.750E+07 | 0.48 | 502.7 | 75.3 |
| 19. Ss | 1.6E-05 | 55 | 3.438E+06 | 186 | 2.325E+07 | 0.30 | 315.2 | 48.8 |
| 20. Ss | 1.6E-05 | 27 | 1.688E+06 | 75 | 9.375E+06 | 0.36 | 381.8 | 86.0 |
| | 3.2E-04 | 972 | 3.038E+06 | 2696 | 1.685E+07 | 0.36 | | |

# FISSION  TRACK  AGE
## DATA

| | | | | |
|---|---|---|---|---|
| **PROJECT:** | Cerro Negro | **DATE:** | April, 97 | **FT AGE:** 416.9 Ma |
| **SAMPLE:** | A-8 | **BOREHOLE DISTANCE (m)** | 384.3 | |
| **LAB:** | NMT | **ELEVATION (M):** | 212 | |
| **REACTOR RUN:** | RR-12-13-96Z2 | **Distance from CN (m)** | 109.5 | **STD ERR:** 12.41 Ma |
| **RHO D** | 2.981E+05 | **MICROSCOPE:** | LEITZ | **C. COEFF:** 0.941 |
| **# TRACKS (FLUX)** | 2745 | **MAGNIFICATION:** | 1000 X | **CHI²:** 87.270 19 |
| **ZETA** | 7330 | **ROCK TYPE:** | Cubero Sandstone | **AVG. AGE:** 405.5 Ma |
| **# OF GRAINS:** | 20 | **MINERAL:** | Zircon | **STD. ERR:** 21.0 |

| GRAIN # | AREA USED (SQ. CM) | Ns | RHO(S) (/CM²) | Ni | RHO(I) (/CM²) | RATIO (Ns/Ni) | AGE (MA) | STD.DEV. (MA) |
|---|---|---|---|---|---|---|---|---|
| 1. Ss | 1.6E-05 | 179 | 1.119E+07 | 382 | 4.775E+07 | 0.47 | 492.6 | 45.6 |
| 2. Ss | 1.6E-05 | 88 | 5.500E+06 | 305 | 3.813E+07 | 0.29 | 307.8 | 37.7 |
| 3. Ss | 1.6E-05 | 98 | 6.125E+06 | 345 | 4.313E+07 | 0.28 | 303.1 | 35.2 |
| 4. Ss | 1.6E-05 | 67 | 4.188E+06 | 241 | 3.013E+07 | 0.28 | 296.8 | 41.4 |
| 5. Ss | 1.6E-05 | 65 | 4.063E+06 | 208 | 2.600E+07 | 0.31 | 332.7 | 47.7 |
| 6. Ss | 1.6E-05 | 114 | 7.125E+06 | 291 | 3.638E+07 | 0.39 | 414.4 | 46.5 |
| 7. Ss | 1.6E-05 | 50 | 3.125E+06 | 203 | 2.538E+07 | 0.25 | 263.6 | 41.9 |
| 8. Ss | 1.6E-05 | 86 | 5.375E+06 | 255 | 3.188E+07 | 0.34 | 358.3 | 45.2 |
| 9. Ss | 1.6E-05 | 72 | 4.500E+06 | 151 | 1.888E+07 | 0.48 | 501.0 | 72.4 |
| 10. Ss | 1.6E-05 | 206 | 1.288E+07 | 471 | 5.888E+07 | 0.44 | 461.0 | 39.5 |
| 11. Ss | 1.6E-05 | 94 | 5.875E+06 | 318 | 3.975E+07 | 0.30 | 315.1 | 37.5 |
| 12. Ss | 1.6E-05 | 189 | 1.181E+07 | 620 | 7.750E+07 | 0.30 | 324.7 | 27.7 |
| 13. Ss | 1.6E-05 | 83 | 5.188E+06 | 231 | 2.888E+07 | 0.36 | 381.1 | 49.3 |
| 14. Ss | 1.6E-05 | 170 | 1.063E+07 | 342 | 4.275E+07 | 0.50 | 521.4 | 49.9 |
| 15. Ss | 1.6E-05 | 41 | 2.563E+06 | 108 | 1.350E+07 | 0.38 | 402.0 | 74.1 |
| 16. Ss | 1.6E-05 | 76 | 4.750E+06 | 195 | 2.438E+07 | 0.39 | 412.3 | 56.3 |
| 17. Ss | 1.6E-05 | 211 | 1.319E+07 | 408 | 5.100E+07 | 0.52 | 541.6 | 47.1 |
| 18. Ss | 1.6E-05 | 352 | 2.200E+07 | 780 | 9.750E+07 | 0.45 | 475.1 | 31.8 |
| 19. Ss | 1.6E-05 | 109 | 6.813E+06 | 225 | 2.813E+07 | 0.48 | 508.7 | 60.2 |
| 20. Ss | 1.6E-05 | 320 | 2.000E+07 | 695 | 8.688E+07 | 0.46 | 484.4 | 34.0 |
| – | – | —— | – | – | – | – | – | – |
| | 3.2E-04 | 2670 | 8.344E+06 | 6774 | 4.234E+07 | 0.39 | | |

# FISSION TRACK AGE DATA

| PROJECT: | Cerro Negro | DATE: | April, 1997 | FT AGE: | 395.2 Ma |
|---|---|---|---|---|---|
| SAMPLE: | A-9 | BOREHOLE DISTANCE (m) | 402.2 | | |
| LAB : | NMT | ELEVATION (m) | 226 | | |
| REACTOR RUN: | RR-12-13-96Z2 | DISTANCE FROM CN (m) | 96.1 | STD ERR: | 15.13 Ma |
| RHO D | 2.981E+05 | MICROSCOPE: | LEITZ | C. COEFF: | 0.928 |
| # TRACKS (FLUX) | 2745 | MAGNIFICATION: | 1000 X | CHI²: | 36.718 |
| ZETA | 7330 | ROCK TYPE: | Cubero Sandstone | AVG. AGE: | 399.7 Ma |
| # OF GRAINS: | 20 | MINERAL: | ZIRCON | STD. ERR: | 19.1 |

| GRAIN # | AREA USED (SQ. CM) | Ns | RHO(S) (/CM²) | Ni | RHO(I) (/CM²) | RATIO (Ns/Ni) | AGE (MA) | STD.DEV. (MA) |
|---|---|---|---|---|---|---|---|---|
| 1. Ss | 1.6E-05 | 15 | 9.375E+05 | 40 | 5.000E+06 | 0.38 | 397.2 | 120.5 |
| 2. Ss | 1.6E-05 | 48 | 3.000E+06 | 107 | 1.338E+07 | 0.45 | 472.4 | 82.6 |
| 3. Ss | 1.6E-05 | 29 | 1.813E+06 | 68 | 8.500E+06 | 0.43 | 449.9 | 100.1 |
| 4. Ss | 1.6E-05 | 39 | 2.438E+06 | 141 | 1.763E+07 | 0.28 | 295.3 | 53.7 |
| 5. Ss | 1.6E-05 | 34 | 2.125E+06 | 66 | 8.250E+06 | 0.52 | 539.6 | 114.4 |
| 6. Ss | 1.6E-05 | 62 | 3.875E+06 | 113 | 1.413E+07 | 0.55 | 573.2 | 91.2 |
| 7. Ss | 1.6E-05 | 62 | 3.875E+06 | 212 | 2.650E+07 | 0.29 | 311.9 | 45.4 |
| 8. Ss | 1.6E-05 | 12 | 7.500E+05 | 37 | 4.625E+06 | 0.32 | 344.9 | 114.8 |
| 9. Ss | 1.6E-05 | 85 | 5.313E+06 | 256 | 3.200E+07 | 0.33 | 352.9 | 44.7 |
| 10. Ss | 1.6E-05 | 42 | 2.625E+06 | 109 | 1.363E+07 | 0.39 | 407.8 | 74.5 |
| 11. Ss | 1.6E-05 | 64 | 4.000E+06 | 241 | 3.013E+07 | 0.27 | 283.8 | 40.3 |
| 12. Ss | 1.6E-05 | 110 | 6.875E+06 | 288 | 3.600E+07 | 0.38 | 404.3 | 46.0 |
| 13. Ss | 1.6E-05 | 55 | 3.438E+06 | 133 | 1.663E+07 | 0.41 | 436.7 | 70.5 |
| 14. Ss | 1.6E-05 | 71 | 4.438E+06 | 208 | 2.600E+07 | 0.34 | 362.5 | 50.3 |
| 15. Ss | 1.6E-05 | 67 | 4.188E+06 | 207 | 2.588E+07 | 0.32 | 344.3 | 48.8 |
| 16. Ss | 1.6E-05 | 66 | 4.125E+06 | 189 | 2.363E+07 | 0.35 | 370.7 | 53.5 |
| 17. Ss | 1.6E-05 | 46 | 2.875E+06 | 152 | 1.900E+07 | 0.30 | 322.4 | 54.6 |
| 18. Ss | 1.6E-05 | 78 | 4.875E+06 | 192 | 2.400E+07 | 0.41 | 429.2 | 58.2 |
| 19. Ss | 1.6E-05 | 60 | 3.750E+06 | 171 | 2.138E+07 | 0.35 | 372.4 | 56.3 |
| 20. Ss | 1.6E-05 | 202 | 1.263E+07 | 413 | 5.163E+07 | 0.49 | 513.4 | 45.2 |
| | 3.2E-04 | 1247 | 3.897E+06 | 3343 | 2.089E+07 | 0.37 | | |

# FISSION TRACK AGE DATA

| | | | | | |
|---|---|---|---|---|---|
| **PROJECT:** | Cerro Negro | **DATE:** | April, 1997 | **FT AGE:** | 243.1 Ma |
| **SAMPLE:** | A-10 | **BOREHOLE DEPTH (M):** | 426.5 | | |
| **LAB:** | NMT | **ELEVATION (M):** | 236.6 | | |
| **REACTOR RUN:** | RR-12-13-96Z2 | **DISTANCE FROM (CN):** | 75.2 | **STD ERR:** | 10.68 Ma |
| **RHO D** | 2.981E+05 | **MICROSCOPE:** | LEITZ | **C. COEFF:** | 0.809 |
| **# TRACKS (FLUX)** | 2745 | **MAGNIFICATION:** | 1000 X | **CHI²:** | 79.547 |
| **ZETA** | 7330 | **ROCK TYPE:** | Oak Canyon Member Sandstone | **AVG. AGE:** | 255.9 Ma |
| **# OF GRAINS:** | 20 | **MINERAL:** | Zircon | **STD. ERR.** | 21.9 |

| GRAIN # | AREA USED (SQ. CM) | Ns | RHO(S) (/CM²) | Ni | RHO(I) (/CM²) | RATIO (Ns/Ni) | AGE (MA) | STD.DEV. (MA) |
|---|---|---|---|---|---|---|---|---|
| 1. Ss | 1.0E-04 | 48 | 4.800E+05 | 157 | 3.140E+06 | 0.31 | 325.7 | 54.1 |
| 2. Ss | 1.6E-05 | 17 | 1.063E+06 | 65 | 8.125E+06 | 0.26 | 279.6 | 76.4 |
| 3. Ss | 1.6E-05 | 51 | 3.188E+06 | 275 | 3.438E+07 | 0.19 | 199.5 | 30.7 |
| 4. Ss | 1.6E-05 | 42 | 2.625E+06 | 196 | 2.450E+07 | 0.21 | 230.0 | 39.3 |
| 5. Ss | 1.6E-05 | 43 | 2.688E+06 | 254 | 3.175E+07 | 0.17 | 182.4 | 30.3 |
| 6. Ss | 1.6E-05 | 33 | 2.063E+06 | 197 | 2.463E+07 | 0.17 | 180.5 | 34.1 |
| 7. Ss | 1.6E-05 | 20 | 1.250E+06 | 94 | 1.175E+07 | 0.21 | 228.4 | 56.4 |
| 8. Ss | 1.6E-05 | 14 | 8.750E+05 | 64 | 8.000E+06 | 0.22 | 234.7 | 69.4 |
| 9. Ss | 1.6E-05 | 89 | 5.563E+06 | 221 | 2.763E+07 | 0.40 | 425.6 | 54.0 |
| 10. Ss | 1.6E-05 | 79 | 4.938E+06 | 311 | 3.888E+07 | 0.25 | 271.7 | 34.6 |
| 11. Ss | 1.6E-05 | 36 | 2.250E+06 | 241 | 3.013E+07 | 0.15 | 161.2 | 29.0 |
| 12. Ss | 1.6E-05 | 44 | 2.750E+06 | 332 | 4.150E+07 | 0.13 | 143.2 | 23.1 |
| 13. Ss | 1.6E-05 | 15 | 9.375E+05 | 65 | 8.125E+06 | 0.23 | 247.3 | 71.0 |
| 14. Ss | 1.6E-05 | 29 | 1.813E+06 | 122 | 1.525E+07 | 0.24 | 254.6 | 52.8 |
| 15. Ss | 1.6E-05 | 18 | 1.125E+06 | 89 | 1.113E+07 | 0.20 | 217.3 | 56.3 |
| 16. Ss | 1.6E-05 | 95 | 5.938E+06 | 446 | 5.575E+07 | 0.21 | 228.6 | 26.2 |
| 17. Ss | 1.6E-05 | 50 | 3.125E+06 | 116 | 1.450E+07 | 0.43 | 454.5 | 77.4 |
| 18. Ss | 1.6E-05 | 12 | 7.500E+05 | 63 | 7.875E+06 | 0.19 | 204.8 | 64.6 |
| 19. Ss | 1.6E-05 | 9 | 5.625E+05 | 56 | 7.000E+06 | 0.16 | 173.2 | 62.3 |
| 20. Ss | 1.6E-05 | 39 | 2.438E+06 | 89 | 1.113E+07 | 0.44 | 461.8 | 89.1 |
| | 4.0E-04 | 783 | 1.938E+06 | 3453 | 1.709E+07 | 0.23 | | |

# FISSION TRACK AGE DATA

| PROJECT: | Cerro Negro | DATE: | | April, 1997 | FT AGE: | 252.1 | Ma |
|---|---|---|---|---|---|---|---|
| SAMPLE: | A-12 | BOREHOLE DISTANCE (m): | | 438.4 | | | |
| LAB: | NMT | ELEVATION (M): | | 246.4 | | | |
| REACTOR RUN: | RR-12-13-96Z2 | DISTANCE TO CN (m): | | 67.4 | STD ERR: | 10.96 | Ma |
| RHO D | 2.98E+05 | MICROSCOPE: | | LEITZ | C. COEFF: | 0.939 | |
| # TRACKS (FLUX) | 2745 | MAGNIFICATION: | | 1000 X | CHI²: | 70.777 | |
| ZETA | 7330 | ROCK TYPE: | | Oak Canyon Member sandstone | AVG. AGE: | 234.1 | Ma |
| # OF GRAINS: | 20 | MINERAL: | | Zircon | STD. ERR: | 16.67521 | |

| GRAIN # | AREA USED (SQ. CM) | Ns | RHO(S) (/CM²) | Ni | RHO(I) (/CM²) | RATIO (Ns/Ni) | AGE (MA) | STD.DEV. (MA) |
|---|---|---|---|---|---|---|---|---|
| 1. Ss | 1.6E-06 | 28 | 1.750E+07 | 98 | 1.225E+08 | 0.29 | 304.8 | 65.6 |
| 2. Ss | 1.6E-06 | 44 | 2.750E+07 | 159 | 1.988E+08 | 0.28 | 295.5 | 50.6 |
| 3. Ss | 1.6E-06 | 41 | 2.563E+07 | 160 | 2.000E+08 | 0.26 | 274.1 | 48.3 |
| 4. Ss | 1.6E-06 | 33 | 2.063E+07 | 205 | 2.563E+08 | 0.16 | 173.5 | 32.7 |
| 5. Ss | 1.6E-06 | 18 | 1.125E+07 | 112 | 1.400E+08 | 0.16 | 173.2 | 44.1 |
| 6. Ss | 1.6E-06 | 64 | 4.000E+07 | 248 | 3.100E+08 | 0.26 | 276.0 | 39.0 |
| 7. Ss | 1.6E-06 | 22 | 1.375E+07 | 107 | 1.338E+08 | 0.21 | 220.8 | 51.9 |
| 8. Ss | 1.6E-06 | 68 | 4.250E+07 | 248 | 3.100E+08 | 0.27 | 292.8 | 40.5 |
| 9. Ss | 1.6E-06 | 168 | 1.050E+08 | 426 | 5.325E+08 | 0.39 | 417.1 | 38.8 |
| 10. Ss | 1.6E-06 | 29 | 1.813E+07 | 159 | 1.988E+08 | 0.18 | 196.3 | 39.8 |
| 11. Ss | 1.6E-06 | 24 | 1.500E+07 | 142 | 1.775E+08 | 0.17 | 182.1 | 40.3 |
| 12. Ss | 1.6E-06 | 52 | 3.250E+07 | 191 | 2.388E+08 | 0.27 | 290.8 | 45.8 |
| 13. Ss | 1.6E-06 | 16 | 1.000E+07 | 114 | 1.425E+08 | 0.14 | 151.5 | 40.6 |
| 14. Ss | 1.6E-06 | 32 | 2.000E+07 | 128 | 1.600E+08 | 0.25 | 267.5 | 53.1 |
| 15. Ss | 1.6E-06 | 37 | 2.313E+07 | 183 | 2.288E+08 | 0.20 | 217.2 | 39.4 |
| 16. Ss | 1.6E-06 | 17 | 1.063E+07 | 97 | 1.213E+08 | 0.18 | 188.7 | 49.7 |
| 17. Ss | 1.6E-06 | 40 | 2.500E+07 | 154 | 1.925E+08 | 0.26 | 277.7 | 49.6 |
| 18. Ss | 1.6E-06 | 23 | 1.438E+07 | 182 | 2.275E+08 | 0.13 | 136.6 | 30.3 |
| 19. Ss | 1.6E-06 | 37 | 2.313E+07 | 187 | 2.338E+08 | 0.20 | 212.6 | 38.5 |
| 20. Ss | 1.6E-06 | 16 | 1.000E+07 | 138 | 1.725E+08 | 0.12 | 125.4 | 33.2 |
| | 3.2E-05 | 809 | 2.528E+07 | 3438 | 2.149E+08 | 0.24 | | |

# FISSION TRACK AGE DATA

| | | | | |
|---|---|---|---|---|
| **PROJECT:** | Cerro Negro | **DATE:** | April, 1997 | **FT AGE:** 414.5 Ma |
| **SAMPLE:** | V-13 | | | |
| **LAB:** | NMT | **DEPTH (M):** | 126.0 | |
| **REACTOR RUN:** | RR-12-13-96Z2 | **DISTANCE TO CN (m):** | 1200.0 | **STD ERR:** 13.73 Ma |
| **RHO D** | 2.981E+05 | **MICROSCOPE:** | LEITZ | **C. COEFF:** 0.907 |
| **# TRACKS (FLUX)** | 2745 | **MAGNIFICATION:** | 1000 X | **CHI²:** 49.421 |
| **ZETA** | 7330 | **ROCK TYPE:** | Two Wells Sandstone | **AVG. AGE:** 415.0 Ma |
| **# OF GRAINS:** | 20 | **MINERAL:** | Zircon | **STD. ERR:** 18.5 |

| GRAIN # | AREA USED (SQ. CM) | Ns | RHO(S) (/CM²) | Ni | RHO(I) (/CM²) | RATIO (Ns/Ni) | AGE (MA) | STD.DEV. (MA) |
|---|---|---|---|---|---|---|---|---|
| 1. Ss | 1.6E-05 | 54 | 3.375E+06 | 189 | 2.363E+07 | 0.29 | 304.8 | 47.4 |
| 2. Ss | 1.6E-05 | 81 | 5.063E+06 | 206 | 2.575E+07 | 0.39 | 415.9 | 55.1 |
| 3. Ss | 1.6E-05 | 60 | 3.750E+06 | 156 | 1.950E+07 | 0.38 | 407.1 | 62.3 |
| 4. Ss | 1.6E-05 | 125 | 7.813E+06 | 269 | 3.363E+07 | 0.46 | 488.7 | 53.7 |
| 5. Ss | 1.6E-05 | 75 | 4.688E+06 | 277 | 3.463E+07 | 0.27 | 289.2 | 38.1 |
| 6. Ss | 1.6E-05 | 55 | 3.438E+06 | 166 | 2.075E+07 | 0.33 | 352.2 | 55.2 |
| 7. Ss | 1.6E-05 | 198 | 1.238E+07 | 612 | 7.650E+07 | 0.32 | 344.1 | 28.9 |
| 8. Ss | 1.6E-05 | 59 | 3.688E+06 | 143 | 1.788E+07 | 0.41 | 435.7 | 67.9 |
| 9. Ss | 1.6E-05 | 161 | 1.006E+07 | 274 | 3.425E+07 | 0.59 | 612.0 | 61.9 |
| 10. Ss | 1.6E-05 | 88 | 5.500E+06 | 205 | 2.563E+07 | 0.43 | 452.7 | 58.3 |
| 11. Ss | 1.6E-05 | 43 | 2.688E+06 | 150 | 1.875E+07 | 0.29 | 305.8 | 53.2 |
| 12. Ss | 1.6E-05 | 134 | 8.375E+06 | 303 | 3.788E+07 | 0.44 | 465.9 | 49.1 |
| 13. Ss | 1.6E-05 | 51 | 3.188E+06 | 123 | 1.538E+07 | 0.41 | 437.8 | 73.4 |
| 14. Ss | 1.6E-05 | 93 | 5.813E+06 | 202 | 2.525E+07 | 0.46 | 484.3 | 61.4 |
| 15. Ss | 1.6E-05 | 77 | 4.813E+06 | 184 | 2.300E+07 | 0.42 | 441.7 | 60.5 |
| 16. Ss | 1.6E-05 | 196 | 1.225E+07 | 503 | 6.288E+07 | 0.39 | 412.3 | 35.6 |
| 17. Ss | 1.6E-05 | 89 | 5.563E+06 | 211 | 2.638E+07 | 0.42 | 445.1 | 56.9 |
| 18. Ss | 1.6E-05 | 119 | 7.438E+06 | 267 | 3.338E+07 | 0.45 | 469.4 | 52.5 |
| 19. Ss | 1.6E-05 | 51 | 3.188E+06 | 160 | 2.000E+07 | 0.32 | 339.2 | 54.9 |
| 20. Ss | 1.6E-05 | 89 | 5.563E+06 | 244 | 3.050E+07 | 0.36 | 386.7 | 48.4 |
| | 3.2E-04 | 1898 | 5.931E+06 | 4844 | 3.028E+07 | 0.39 | | |

# FISSION TRACK AGE DATA

| | | | | | |
|---|---|---|---|---|---|
| **PROJECT:** | Cerro Negro | **DATE:** | April, 1997 | **FT AGE:** | 379.0 Ma |
| **SAMPLE:** | V-17 | | | | |
| **LAB:** | NMT | **DEPTH (M):** | 186.9 | | |
| **REACTOR RUN:** | RR-12-13-96Z2 | **DISTANCE TO CN (m):** | 1200.0 | **STD ERR:** | 15.32 Ma |
| **RHO D** | 2.981E+05 | **MICROSCOPE:** | LEITZ | **C. COEFF:** | 0.962 |
| **# TRACKS (FLUX)** | 2745 | **MAGNIFICATION:** | 1000 X | **CHI²:** | 28.405 |
| **ZETA** | 7330 | **ROCK TYPE:** | Cubero Sandstone | **AVG. AGE:** | 288.0 Ma |
| **# OF GRAINS:** | 20 | **MINERAL:** | Zircon | **STD. ERR:** | 24.7 |

| GRAIN # | AREA USED (SQ. CM) | Ns | RHO(S) (/CM²) | Ni | RHO(I) (/CM²) | RATIO (Ns/Ni) | AGE (MA) | STD.DEV. (MA) |
|---|---|---|---|---|---|---|---|---|
| 1. Ss | 1.6E-05 | 91 | 5.688E+06 | 226 | 2.825E+07 | 0.40 | 425.6 | 53.5 |
| 2. Ss | 1.6E-05 | 32 | 2.000E+06 | 103 | 1.288E+07 | 0.31 | 330.8 | 67.2 |
| 3. Ss | 1.6E-05 | 77 | 4.813E+06 | 223 | 2.788E+07 | 0.35 | 366.6 | 49.0 |
| 4. Ss | 1.6E-05 | 111 | 6.938E+06 | 313 | 3.913E+07 | 0.35 | 376.3 | 42.2 |
| 5. Ss | 1.6E-05 | 46 | 2.875E+06 | 127 | 1.588E+07 | 0.36 | 384.1 | 66.5 |
| 6. Ss | 1.6E-05 | 60 | 3.750E+06 | 179 | 2.238E+07 | 0.34 | 356.2 | 53.6 |
| 7. Ss | 1.6E-05 | 40 | 2.500E+06 | 129 | 1.613E+07 | 0.31 | 330.2 | 60.1 |
| 8. Ss | 1.6E-05 | 59 | 3.688E+06 | 168 | 2.100E+07 | 0.35 | 372.7 | 56.8 |
| 9. Ss | 1.6E-05 | 161 | 1.006E+07 | 425 | 5.313E+07 | 0.38 | 401.1 | 37.9 |
| 10. Ss | 1.6E-05 | 54 | 3.375E+06 | 149 | 1.863E+07 | 0.36 | 384.3 | 61.5 |
| 11. Ss | 1.6E-05 | 39 | 2.438E+06 | 202 | 2.525E+07 | 0.19 | 207.6 | 36.5 |
| 12. Ss | 1.6E-05 | 90 | 5.625E+06 | 298 | 3.725E+07 | 0.30 | 321.8 | 39.2 |
| 13. Ss | 1.6E-05 | 76 | 4.750E+06 | 165 | 2.063E+07 | 0.46 | 484.6 | 67.8 |
| 14. Ss | 1.6E-05 | 81 | 5.063E+06 | 159 | 1.988E+07 | 0.51 | 533.9 | 73.6 |
| 15. Ss | 1.6E-05 | 52 | 3.250E+06 | 126 | 1.575E+07 | 0.41 | 435.8 | 72.3 |
| | 2.4E-04 | 1069 | 4.454E+06 | 2992 | 2.493E+07 | 0.36 | | |

# FISSION  TRACK  AGE DATA

| PROJECT: | Cerro Negro | DATE: | April, 1997 | FT AGE: | 413.2 | Ma |
| SAMPLE: | V-18 | | | | | |
| LAB: | NMT | DEPTH (M): | 191.0 | | | |
| REACTOR RUN: | RR-12-13-96Z2 | DISTANCE TO CN (m): | 1200.0 | STD ERR: | 14.17 | Ma |
| RHO D | 2.981E+05 | MICROSCOPE: | LEITZ | C. COEFF: | 0.964 | |
| # TRACKS (FLUX) | 2745 | MAGNIFICATION: | 1000 X | CHI²: | 22.132 | |
| ZETA | 7330 | ROCK TYPE: | Cubero Sandstone | AVG. AGE: | 415.0 | Ma |
| # OF GRAINS: | 20 | MINERAL: | Zircon | STD. ERR: | 13.6 | |

| GRAIN # | AREA USED (SQ. CM) | Ns | RHO(S) (/CM²) | Ni | RHO(I) (/CM²) | RATIO (Ns/Ni) | AGE (MA) | STD.DEV. (MA) |
|---|---|---|---|---|---|---|---|---|
| 1. Ss | 1.6E-05 | 126 | 7.875E+06 | 367 | 4.588E+07 | 0.34 | 364.6 | 38.3 |
| 2. Ss | 1.6E-05 | 57 | 3.563E+06 | 169 | 2.113E+07 | 0.34 | 358.3 | 55.3 |
| 3. Ss | 1.6E-05 | 84 | 5.250E+06 | 203 | 2.538E+07 | 0.41 | 436.9 | 57.3 |
| 4. Ss | 1.6E-05 | 206 | 1.288E+07 | 504 | 6.300E+07 | 0.41 | 431.8 | 36.6 |
| 5. Ss | 1.6E-05 | 23 | 1.438E+06 | 59 | 7.375E+06 | 0.39 | 412.4 | 101.7 |
| 6. Ss | 1.6E-05 | 72 | 4.500E+06 | 166 | 2.075E+07 | 0.43 | 457.3 | 65.1 |
| 7. Ss | 1.6E-05 | 63 | 3.938E+06 | 120 | 1.500E+07 | 0.53 | 549.5 | 86.1 |
| 8. Ss | 1.6E-05 | 94 | 5.875E+06 | 268 | 3.350E+07 | 0.35 | 372.2 | 45.2 |
| 9. Ss | 1.6E-05 | 159 | 9.938E+06 | 365 | 4.563E+07 | 0.44 | 459.2 | 44.5 |
| 10. Ss | 1.6E-05 | 46 | 2.875E+06 | 139 | 1.738E+07 | 0.33 | 351.8 | 60.2 |
| 11. Ss | 1.6E-05 | 82 | 5.125E+06 | 171 | 2.138E+07 | 0.48 | 503.7 | 68.3 |
| 12. Ss | 1.6E-05 | 27 | 1.688E+06 | 64 | 8.000E+06 | 0.42 | 445.2 | 102.5 |
| 13. Ss | 1.6E-05 | 93 | 5.813E+06 | 241 | 3.013E+07 | 0.39 | 408.4 | 50.5 |
| 14. Ss | 1.6E-05 | 168 | 1.050E+07 | 364 | 4.550E+07 | 0.46 | 485.5 | 46.2 |
| 15. Ss | 1.6E-05 | 75 | 4.688E+06 | 192 | 2.400E+07 | 0.39 | 413.2 | 56.8 |
| 16. Ss | 1.6E-05 | 91 | 5.688E+06 | 299 | 3.738E+07 | 0.30 | 324.2 | 39.3 |
| 17. Ss | 1.6E-05 | 56 | 3.500E+06 | 148 | 1.850E+07 | 0.38 | 400.7 | 63.3 |
| 18. Ss | 1.6E-05 | 98 | 6.125E+06 | 285 | 3.563E+07 | 0.34 | 365.1 | 43.3 |
| 19. Ss | 1.6E-05 | 43 | 2.688E+06 | 120 | 1.500E+07 | 0.36 | 380.1 | 67.9 |
| 20. Ss | 1.6E-05 | 49 | 3.063E+06 | 139 | 1.738E+07 | 0.35 | 374.1 | 62.6 |
| | 3.2E-04 | 1712 | 5.350E+06 | 4383 | 2.739E+07 | 0.39 | | |

# FISSION TRACK AGE DATA

| | | | | | |
|---|---|---|---|---|---|
| **PROJECT:** | Cerro Negro | **DATE:** | April, 1997 | **FT AGE:** | 427.7 Ma |
| **SAMPLE:** | V-20 | | | | |
| **LAB:** | NMT | **DEPTH (M):** | 221.3 | | |
| **REACTOR RUN:** | RR-12-13-96Z2 | **DISTANCE TO CN (m):** 1200.0 | | **STD ERR:** | 15.46 Ma |
| **RHO D** | 2.981E+05 | **MICROSCOPE:** | LEITZ | **C. COEFF:** | 0.975 |
| **# TRACKS (FLUX)** | 2745 | **MAGNIFICATION:** | 1000 X | **CHI²:** | 19.086 |
| **ZETA** | 7330 | **ROCK TYPE:** | Oak Canyon Mb Sandstone | **AVG. AGE:** | 376.0 Ma |
| **# OF GRAINS:** | 20 | **MINERAL:** | Zircon | **STD. ERR:** | 14.7 |

| GRAIN # | AREA USED (SQ. CM) | Ns | RHO(S) (/CM²) | Ni | RHO(I) (/CM²) | RATIO (Ns/Ni) | AGE (MA) | STD.DEV. (MA) |
|---|---|---|---|---|---|---|---|---|
| 1. Ss | 1.6E-05 | 48 | 3.000E+06 | 120 | 1.500E+07 | 0.40 | 422.8 | 72.7 |
| 2. Ss | 1.6E-05 | 79 | 4.938E+06 | 204 | 2.550E+07 | 0.39 | 409.8 | 54.9 |
| 3. Ss | 1.6E-05 | 155 | 9.688E+06 | 360 | 4.500E+07 | 0.43 | 454.0 | 44.5 |
| 4. Ss | 1.6E-05 | 134 | 8.375E+06 | 355 | 4.438E+07 | 0.38 | 399.7 | 41.2 |
| 5. Ss | 1.6E-05 | 169 | 1.056E+07 | 360 | 4.500E+07 | 0.47 | 493.5 | 47.0 |
| 6. Ss | 1.6E-05 | 59 | 3.688E+06 | 160 | 2.000E+07 | 0.37 | 390.8 | 60.0 |
| 7. Ss | 1.6E-05 | 55 | 3.438E+06 | 147 | 1.838E+07 | 0.37 | 396.3 | 63.1 |
| 8. Ss | 1.6E-05 | 31 | 1.938E+06 | 76 | 9.500E+06 | 0.41 | 430.9 | 92.2 |
| 9. Ss | 1.6E-05 | 20 | 1.250E+06 | 48 | 6.000E+06 | 0.42 | 439.9 | 117.4 |
| 10. Ss | 1.6E-05 | 81 | 5.063E+06 | 188 | 2.350E+07 | 0.43 | 454.3 | 61.0 |
| 11. Ss | 1.6E-05 | 143 | 8.938E+06 | 350 | 4.375E+07 | 0.41 | 431.6 | 43.6 |
| 12. Ss | 1.6E-05 | 64 | 4.000E+06 | 165 | 2.063E+07 | 0.39 | 410.4 | 60.9 |
| 13. Ss | 1.6E-05 | 28 | 1.750E+06 | 79 | 9.875E+06 | 0.35 | 376.0 | 83.0 |
| 14. Ss | 1.6E-05 | 96 | 6.000E+06 | 290 | 3.625E+07 | 0.33 | 351.9 | 42.0 |
| 15. Ss | 1.6E-05 | 33 | 2.063E+06 | 95 | 1.188E+07 | 0.35 | 368.8 | 74.8 |
| 16. Ss | 1.6E-05 | 185 | 1.156E+07 | 356 | 4.450E+07 | 0.52 | 544.1 | 50.4 |
| 17. Ss | 1.6E-05 | 61 | 3.813E+06 | 189 | 2.363E+07 | 0.32 | 343.3 | 51.0 |
| 18. Ss | 1.6E-05 | 50 | 3.125E+06 | 142 | 1.775E+07 | 0.35 | 373.7 | 61.9 |
| | 2.9E-04 | 1491 | 5.177E+06 | 3684 | 2.558E+07 | 0.40 | | |

# FISSION  TRACK  AGE DATA

| | | | | |
|---|---|---|---|---|
| **PROJECT:** | Cerro Negro | **DATE:** | April, 1997 | **FT AGE:** 394.6 Ma |
| **SAMPLE:** | V-21 | | | |
| **LAB:** | NMT | **DEPTH (M):** | 221.3 | |
| **REACTOR RUN:** | RR-12-13-96Z2 | **DISTANCE TO CN (m):** 1200.0 | | **STD ERR:** 13.42 Ma |
| **RHO D** | 2.981E+05 | **MICROSCOPE:** | LEITZ | **C. COEFF:** 0.953 |
| **# TRACKS (FLUX)** | 2745 | **MAGNIFICATION:** | 1000 X | **CHI²:** 32.593 |
| **ZETA** | 7330 | **ROCK TYPE:** | Oak Canyon Mb Sandstone | **AVG. AGE:** 392.4 Ma |
| **# OF GRAINS:** | 20 | **MINERAL:** | Zircon | **STD. ERR:** 14.9 |

| GRAIN # | AREA USED (SQ. CM) | Ns | RHO(S) (/CM²) | Ni | RHO(I) (/CM²) | RATIO (Ns/Ni) | AGE (MA) | STD.DEV. (MA) |
|---|---|---|---|---|---|---|---|---|
| 1. Ss | 1.6E-05 | 36 | 2.250E+06 | 80 | 1.000E+07 | 0.45 | 473.8 | 95.5 |
| 2. Ss | 1.6E-05 | 59 | 3.688E+06 | 147 | 1.838E+07 | 0.40 | 424.2 | 65.9 |
| 3. Ss | 1.6E-05 | 78 | 4.875E+06 | 246 | 3.075E+07 | 0.32 | 337.4 | 44.3 |
| 4. Ss | 1.6E-05 | 195 | 1.219E+07 | 491 | 6.138E+07 | 0.40 | 419.9 | 36.4 |
| 5. Ss | 1.6E-05 | 91 | 5.688E+06 | 240 | 3.000E+07 | 0.38 | 401.5 | 50.0 |
| 6. Ss | 1.6E-05 | 28 | 1.750E+06 | 98 | 1.225E+07 | 0.29 | 304.8 | 65.6 |
| 7. Ss | 1.6E-05 | 57 | 3.563E+06 | 192 | 2.400E+07 | 0.30 | 316.5 | 48.1 |
| 8. Ss | 1.6E-05 | 61 | 3.813E+06 | 157 | 1.963E+07 | 0.39 | 411.1 | 62.5 |
| 9. Ss | 1.6E-05 | 84 | 5.250E+06 | 307 | 3.838E+07 | 0.27 | 292.2 | 36.4 |
| 10. Ss | 1.6E-05 | 154 | 9.625E+06 | 375 | 4.688E+07 | 0.41 | 433.7 | 42.3 |
| 11. Ss | 1.6E-05 | 167 | 1.044E+07 | 344 | 4.300E+07 | 0.49 | 509.7 | 49.0 |
| 12. Ss | 1.6E-05 | 25 | 1.563E+06 | 70 | 8.750E+06 | 0.36 | 378.8 | 88.6 |
| 13. Ss | 1.6E-05 | 63 | 3.938E+06 | 202 | 2.525E+07 | 0.31 | 332.0 | 48.3 |
| 14. Ss | 1.6E-05 | 90 | 5.625E+06 | 310 | 3.875E+07 | 0.29 | 309.6 | 37.5 |
| 15. Ss | 1.6E-05 | 188 | 1.175E+07 | 485 | 6.063E+07 | 0.39 | 410.2 | 36.1 |
| 16. Ss | 1.6E-05 | 53 | 3.313E+06 | 130 | 1.625E+07 | 0.41 | 430.7 | 70.7 |
| 17. Ss | 1.6E-05 | 60 | 3.750E+06 | 158 | 1.975E+07 | 0.38 | 402.1 | 61.5 |
| 18. Ss | 1.6E-05 | 84 | 5.250E+06 | 179 | 2.238E+07 | 0.47 | 493.3 | 65.9 |
| 19. Ss | 1.6E-05 | 97 | 6.063E+06 | 253 | 3.163E+07 | 0.38 | 405.8 | 49.1 |
| 20. Ss | 1.6E-05 | 62 | 3.875E+06 | 186 | 2.325E+07 | 0.33 | 354.3 | 52.4 |
| | 3.2E-04 | 1732 | 5.413E+06 | 4650 | 2.906E+07 | 0.37 | | |

# APPENDIX D

WATER TABLE TEMPERATURE CALCULATIONS

To determine a local lapse rate for the study area, published mean annual temperature data were cumulated from 19 various locations in Valencia and Cibola counties.

## VALENCIA AND CIBOLA COUNTY TEMPERATURE DATA

(Compiled from Gabin and Lesperance, 1977; Kunkel, 1984)

| Location | Latitude | Longitude | Elevation (m) | Reported Mean Annual Air Temperature (°C) |
|---|---|---|---|---|
| Acomita CAA Airport | 35°03' | 107°43' | 2004 | 10.7 |
| Belen* | 34°40' | 106°46' | 1463 | 13.6 |
| Bluewater 3WSW | 35°15' | 108°02' | 2073 | 8.8 |
| Diener | 35°11' | 108°08' | 2438 | 5.5 |
| El Morro CAA | 35°01' | 108°25' | 2170 | 7.6 |
| El Morro Nat. Mon.* | 35°03' | 108°21' | 2202 | 8.6 |
| Fence Lake | 34°37' | 108°43' | 2200 | 9.7 |
| Fence Lake A* | 34°39' | 108°40' | 2150 | 8.5 |
| Floyd Lee Ranch | 35°21' | 107°40' | 2195 | 8.8 |
| Grants | 35°10' | 107°52' | 1981 | 11.1 |
| Grants Airport* | 35°10' | 107°54' | 1987 | 9.5 |
| IX-XI Ranch A | 34°59' | 107°57' | 2201 | 8.8 |

| | | | | |
|---|---|---|---|---|
| Laguna* | 35°02' | 107°24' | 1768 | 11.8 |
| Los Lunas | 34°43' | 106°46' | 1469 | 12.4 |
| Los Lunas A | 34°48' | 106°44' | 1489 | 12.9 |
| Los Lunas 3 SSW* | 34°46' | 106°45' | 1475 | 12.4 |
| San Fidel | 35°06' | 107°36' | 1878 | 10.8 |
| San Mateo* | 35°20' | 107°39' | 2210 | 9.6 |
| San Rafael | 35°07' | 107°53' | 1981 | 10.7 |

* Climatological Data Station

The mean annual temperature values were plotted against elevation for each of the 19 reporting locations in Valencia County and what is presently referred to as Cibola County. The linear regression found to best fit the data indicated a lapse rate of a 6.3°C temperature decrease per 1000 m gain in elevation. The calculated lapse rate is consistent with the -5.3 °C/km lapse rate in the southeastern reported by Reiter and Jordan (1996).



**LAPSE RATE**
**based on 19 temperature stations in Valencia and Cibola Counties**

slope = -0.0063 deg C/m
intercept = 22.4 deg C
$R^2 = 0.8523$
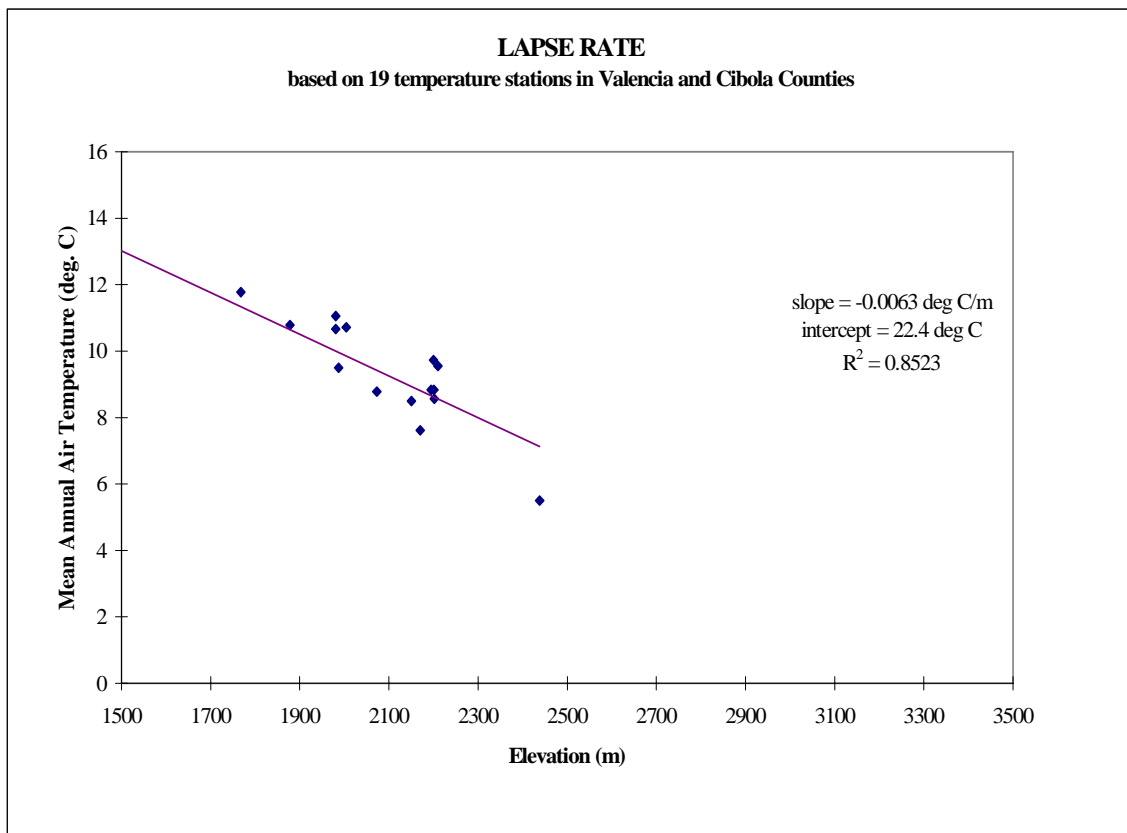
The following equations and estimated constants were used to solve for the water table

temperature at each top boundary node of the finite element mesh:

$$T_s = (z_0 - z) * LR + T_0$$

$$\Delta T_v = d_v * GTG_v$$

$$T_{wt} = T_s + \Delta T_v$$

where,

$d_v =$ thickness of vadose zone (or depth to water table)  (m)

$GTG_v =$ geothermal gradient of the vadose zone  (°C/ m)

$LR =$ local lapse rate (°C/ m)

$T_0 =$ reference mean annual surface temperature  (°C)

$T_s =$ mean annual surface temperature  (°C)

$T_{wt} =$ temperature at the water table  (°C)

$\Delta T_v =$ change in temperature in the vadose zone, (or difference in temperature from the surface to the water table)  (°C)

$z =$ surface elevation (m)

$z_0 =$ reference surface elevation (m)

| Constants | $GTG_v$ | LR | $T_0$ * | $Z_0$ * |
| --- | --- | --- | --- | --- |
| | 0.09 °C/m | 0.0063 °C/m | 11.8 °C | 1768 m |

*The climatological station at Laguna, NM is closest to the study area and was therefore

used as the reference location.  Data obtained from Gabin and Lesperance, 1977.

| Node in Mesh | Depth to Water Table (m) | Surface Elevation (m) | Mean Annual Surface Temperature (°C) | Δ Temperature (from Top to Bottom of the Vadose Zone) (°C) | Calculated Temperature @ the Water Table (°C) |
|---|---|---|---|---|---|
| 21 | 550 | 3350 | 1.8 | 49.5 | 25◊ |
| 42 | 510 | 3298 | 2.2 | 45.9 | 25◊ |
| 63 | 475 | 3250 | 2.5 | 42.8 | 25◊ |
| 84 | 450 | 3203 | 2.8 | 40.5 | 25◊ |
| 105 | 270 | 3000 | 4.1 | 24.3 | 25◊ |
| 126 | 250 | 2955 | 4.3 | 22.5 | 25◊ |
| 147 | 200 | 2870 | 4.9 | 18.0 | 22.9 |
| 168 | 155 | 2800 | 5.3 | 14.0 | 19.3 |
| 189 | 140 | 2750 | 5.6 | 12.6 | 18.2 |
| 210 | 150 | 2745 | 5.7 | 13.5 | 19.2 |
| 231 | 150 | 2720 | 5.8 | 13.5 | 19.3 |
| 252 | 140 | 2700 | 5.9 | 12.6 | 18.5 |
| 273 | 135 | 2685 | 6.0 | 12.2 | 18.2 |
| 294 | 130 | 2668 | 6.1 | 11.7 | 17.8 |
| 315 | 125 | 2645 | 6.3 | 11.3 | 17.6 |
| 336 | 120 | 2600 | 6.6 | 10.8 | 17.4 |
| 357 | 110 | 2550 | 6.9 | 9.9 | 16.8 |
| 378 | 100 | 2530 | 7.0 | 9.0 | 16.0 |
| 399 | 90 | 2510 | 7.1 | 8.1 | 15.2 |
| 420 | 80 | 2490 | 7.3 | 7.2 | 14.5 |
| 441 | 70 | 2470 | 7.4 | 6.3 | 13.7 |
| 462 | 60 | 2458 | 7.5 | 5.4 | 12.9 |
| 483 | 50 | 2445 | 7.5 | 4.5 | 12.0 |
| 504 | 50 | 2443 | 7.6 | 4.5 | 12.1 |
| 525 | 40 | 2430 | 7.6 | 3.6 | 11.2 |
| 546 | 40 | 2428 | 7.7 | 3.6 | 11.3 |
| 567 | 40 | 2425 | 7.7 | 3.6 | 11.3 |
| 588 | 40 | 2423 | 7.7 | 3.6 | 11.3 |
| 609 | 40 | 2420 | 7.7 | 3.6 | 11.3 |
| 630 | 40 | 2405 | 7.8 | 3.6 | 11.4 |
| 651 | 50 | 2395 | 7.9 | 4.5 | 12.4 |
| 671 | 60 | 2380 | 8.0 | 5.4 | 13.4 |
| 710 | 60 | 2340 | 8.2 | 5.4 | 13.6 |
| 728 | 60 | 2310 | 8.4 | 5.4 | 13.8 |
| 745 | 60 | 2270 | 8.7 | 5.4 | 14.1 |
| 762 | 60 | 2230 | 8.9 | 5.4 | 14.3 |
| 778 | 60 | 2205 | 9.1 | 5.4 | 14.5 |
| 793 | 60 | 2175 | 9.2 | 5.4 | 14.6 |
| 807 | 60 | 2115 | 9.6 | 5.4 | 15.0 |
| 820 | 60 | 2070 | 9.9 | 5.4 | 15.3 |
| 832 | 60 | 2045 | 10.1 | 5.4 | 15.5 |
| 844 | 60 | 2025 | 10.2 | 5.4 | 15.6 |
| 856 | 60 | 2005 | 10.3 | 5.4 | 15.7 |
| 868 | 60 | 1960 | 10.6 | 5.4 | 16.0 |
| 880 | 60 | 1940 | 10.7 | 5.4 | 16.1 |

| | | | | | |
|---|---|---|---|---|---|
| 892 | 60 | 1930 | 10.8 | 5.4 | 16.2 |
| 904 | 60 | 1920 | 10.9 | 5.4 | 16.3 |
| 916 | 60 | 1910 | 10.9 | 5.4 | 16.3 |
| 928 | 60 | 1905 | 10.9 | 5.4 | 16.3 |
| 940 | 60 | 1900 | 11.0 | 5.4 | 16.4 |
| 952 | 60 | 1895 | 11.0 | 5.4 | 16.4 |
| 964 | 65 | 1895 | 11.0 | 5.9 | 16.9 |
| 976 | 65 | 1895 | 11.0 | 5.9 | 16.9 |
| 988 | 70 | 1900 | 11.0 | 6.3 | 17.3 |
| 1000 | 70 | 1900 | 11.0 | 6.3 | 17.3 |
| 1012 | 70 | 1900 | 11.0 | 6.3 | 17.3 |
| 1024 | 70 | 1900 | 11.0 | 6.3 | 17.3 |
| 1036 | 70 | 1900 | 11.0 | 6.3 | 17.3 |
| 1048 | 70 | 1900 | 11.0 | 6.3 | 17.3 |
| 1060 | 70 | 1900 | 11.0 | 6.3 | 17.3 |
| 1071 | 70 | 1900 | 11.0 | 6.3 | 17.3 |
| 1082 | 70 | 1900 | 11.0 | 6.3 | 17.3 |
| 1093 | 70 | 1900 | 11.0 | 6.3 | 17.3 |
| 1104 | 70 | 1900 | 11.0 | 6.3 | 17.3 |
| 1115 | 70 | 1900 | 11.0 | 6.3 | 17.3 |
| 1126 | 70 | 1900 | 11.0 | 6.3 | 17.3 |
| 1137 | 70 | 1900 | 11.0 | 6.3 | 17.3 |
| 1148 | 70 | 1900 | 11.0 | 6.3 | 17.3 |
| 1159 | 70 | 1900 | 11.0 | 6.3 | 17.3 |
| 1170 | 70 | 1900 | 11.0 | 6.3 | 17.3 |
| 1181 | 70 | 1900 | 11.0 | 6.3 | 17.3 |
| 1192 | 70 | 1900 | 11.0 | 6.3 | 17.3 |
| 1203 | 70 | 1900 | 11.0 | 6.3 | 17.3 |
| 1214 | 70 | 1900 | 11.0 | 6.3 | 17.3 |
| 1225 | 70 | 1900 | 11.0 | 6.3 | 17.3 |
| 1236 | 70 | 1897 | 11.0 | 6.3 | 17.3 |
| 1247 | 70 | 1896 | 11.0 | 6.3 | 17.3 |
| 1258 | 70 | 1895 | 11.0 | 6.3 | 17.3 |
| 1269 | 70 | 1894 | 11.0 | 6.3 | 17.3 |
| 1280 | 70 | 1893 | 11.0 | 6.3 | 17.3 |
| 1290 | 70 | 1892 | 11.0 | 6.3 | 17.3 |
| 1300 | 70 | 1891 | 11.0 | 6.3 | 17.3 |
| 1310 | 70 | 1890 | 11.0 | 6.3 | 17.3 |
| 1320 | 70 | 1889 | 11.1 | 6.3 | 17.4 |
| 1330 | 70 | 1888 | 11.1 | 6.3 | 17.4 |
| 1340 | 70 | 1887 | 11.1 | 6.3 | 17.4 |
| 1350 | 70 | 1886 | 11.1 | 6.3 | 17.4 |
| 1360 | 70 | 1885 | 11.1 | 6.3 | 17.4 |
| 1369 | 70 | 1884 | 11.1 | 6.3 | 17.4 |
| 1378 | 70 | 1883 | 11.1 | 6.3 | 17.4 |
| 1387 | 70 | 1882 | 11.1 | 6.3 | 17.4 |
| 1396 | 70 | 1881 | 11.1 | 6.3 | 17.4 |
| 1405 | 70 | 1880 | 11.1 | 6.3 | 17.4 |
| 1414 | 70 | 1879 | 11.1 | 6.3 | 17.4 |
| 1423 | 70 | 1878 | 11.1 | 6.3 | 17.4 |
| 1432 | 70 | 1877 | 11.1 | 6.3 | 17.4 |

| | | | | | |
|---|---|---|---|---|---|
| 1440 | 70 | 1876 | 11.1 | 6.3 | 17.4 |
| 1448 | 70 | 1875 | 11.1 | 6.3 | 17.4 |
| 1456 | 70 | 1874 | 11.1 | 6.3 | 17.4 |
| 1464 | 70 | 1873 | 11.2 | 6.3 | 17.5 |
| 1472 | 70 | 1872 | 11.2 | 6.3 | 17.5 |
| 1480 | 70 | 1871 | 11.2 | 6.3 | 17.5 |
| 1488 | 70 | 1870 | 11.2 | 6.3 | 17.5 |
| 1495 | 70 | 1869 | 11.2 | 6.3 | 17.5 |
| 1502 | 70 | 1868 | 11.2 | 6.3 | 17.5 |
| 1509 | 70 | 1867 | 11.2 | 6.3 | 17.5 |
| 1516 | 70 | 1866 | 11.2 | 6.3 | 17.5 |
| 1523 | 70 | 1865 | 11.2 | 6.3 | 17.5 |
| 1530 | 70 | 1864 | 11.2 | 6.3 | 17.5 |

◊  Temperature values of 25°C were estimated, rather than calculated.  Due to the steep change and considerable thickness of the vadose zone beneath the peak of Mount Taylor, calculated values would be unreasonably high and would not reflect mixing that would presumably subdue the water table temperature directly beneath the peak.

# APPENDIX E

MATHMATICAL EQUATIONS USED IN THE NUMERICAL MODEL

Expression for the equivalent freshwater head:

$$h = \frac{p}{\rho_0 g} + z$$

Steady-state groundwater flow equation for a single phase fluid through a homogeneous, anisotropic porous media in 2-dimensions:

(expressed in terms of h),

$$\frac{\partial}{\partial x}\left(K_x \frac{\partial h}{\partial x}\right) + \frac{\partial}{\partial z}\left(K_z \frac{\partial h}{\partial z}\right) = 0$$

(and expressed in terms of ψ),

$$\frac{\partial}{\partial x}\left(\frac{1}{K_x} \frac{\partial \psi}{\partial x}\right) + \frac{\partial}{\partial z}\left(\frac{1}{K_z} \frac{\partial \psi}{\partial z}\right) = 0$$

The heat transfer equation for a homogeneous fluid and porous media:

$$\frac{\partial}{\partial x}\left[\lambda_s \frac{\partial T}{\partial x} + \lambda_s \frac{\partial T}{\partial z}\right] - q_x \rho_f c_f \frac{\partial T}{\partial x} + \frac{\partial}{\partial z}\left[\lambda_s \frac{\partial T}{\partial x} + \lambda_s \frac{\partial T}{\partial z}\right]$$

$$- q_x \rho_f c_f \frac{\partial T}{\partial z} = 0$$

$c_f$ = specific heat capacity of the fluid phase (J/°C- kg)

$c_s$ = specific heat capacity of the solid phase (J/°C- kg)

$g$ = gravitational acceleration (m/s$^2$)

$h$ = hydraulic head (m)

$K_x$ = horizontal hydraulic conductivity (m/s)

$K_z$ = vertical hydraulic conductivity (m/s)

$\lambda_f$ = thermal conductivity of the fluid phase (W/°C – m)

$\lambda_s$ = thermal conductivity of the solid phase (W/°C – m)

$p$ = pressure (N/m$^2$)

$q_x$ = horizontal Darcy velocity (m/s)

$q_z$ = vertical Darcy velocity (m/s)

$\rho_f$ = density of the fluid (kg/m$^3$)

$\rho_o$ = reference density (kg/m$^3$)

$T$ = temperature (°C)

$x$ = horizontal spatial coordinate (m)

$\Psi$ = stream function (m$^2$/s)

$z$ = vertical spatial coordinate, elevation head (m)

# APPENDIX F

BOREHOLE TEMPERATURE PROFILING

    I.  Methods

An In-Situ TXD 200 Temperature Probe connected to an In-Situ Hermit SE 1000C Data

Logger was used to measure groundwater temperatures in the vertical borehole drilled

near Cerro Negro (CNV-R) from the top of the water table to 40 meters below the water

table in 2 meters intervals.  Temperatures ranged from 18.07°C - 20.27 °C at depths of 62

m - 101 m, respectively.

II. Results

CNV–R Borehole Temperature Profile

Water table elevation = 61.62 m

Measurements collected February 10, 1997

| Depth below WT (m) | Temperature (°C) |
| --- | --- |
| 0.38 | 18.07 |
| 2.38 | 18.15 |
| 4.38 | 18.24 |
| 6.38 | 18.35 |
| 8.38 | 18.47 |
| 10.38 | 18.59 |
| 12.38 | 18.71 |
| 14.38 | 18.85 |
| 16.38 | 18.99 |
| 18.38 | 19.13 |
| 20.38 | 19.27 |
| 22.38 | 19.39 |
| 24.38 | 19.52 |
| 26.38 | 19.64 |
| 28.38 | 19.76 |
| 30.38 | 19.86 |
| 32.38 | 19.96 |
| 34.38 | 20.06 |
| 36.38 | 20.17 |
| 39.38 | 20.27 |